Partnership for AiR Transportation
Noise and Emissions Reduction
An FAA/NASA/Transport Canada-
sponsored Center of Excellence

Uncertainty Quantification of Aviation Fuel Burn Performance

A PARTNER Project 48 report

prepared by
Sergio Amaral, Elena de la Rosa Blanco,
Douglas Allaire, Karen E. Willcox

September 2016

REPORT NO. PARTNER-COE-2016-003

Uncertainty Quantification of Aviation Fuel Burn Performance

A PARTNER Project 48 Report

Sergio Amaral, Elena de la Rosa Blanco, Douglas Allaire, Karen E. Willcox

PARTNER-COE-2016-003

September 2016

This work was funded by the US Federal Aviation Administration Office of Environment and Energy. The project was managed by James Skalecky of the FAA.

The Partnership for AiR Transportation Noise and Emissions Reduction — PARTNER — is a cooperative aviation research organization, and an FAA/NASA/Transport Canada-sponsored Center of Excellence. PARTNER fosters breakthrough technological, operational, policy, and workforce advances for the betterment of mobility, economy, national security, and the environment. The organization's operational headquarters is at the Massachusetts Institute of Technology.

The Partnership for AiR Transportation Noise and Emissions Reduction
Massachusetts Institute of Technology, 77 Massachusetts Avenue, 33-240
Cambridge, MA 02139 USA
partner.aero

Uncertainty Quantification of Aviation Fuel Burn Performance

Author:

Sergio Amaral

Project Supervisors:

Elena de la Rosa Blanco

Douglas Allaire

Karen E. Willcox

Summary

Estimating future aircraft fuel burn performance is essential when setting aviation standards and efficiency goals for future commercial aviation. Changes in fuel efficiency may result from aviation technology enhancements and/or adjustments in aviation operations. In order to support effective decision-making, it is important that fuel burn estimates come with an assessment of the associated uncertainties. This report presents a quantitative approach to evaluating the uncertainty of aircraft fuel burn performance and determining which factors in aircraft technologies or design operations cause the greatest variation in the fuel burn performance. The report investigates varying aircraft configurations using a conventional Boeing 737-800 aircraft and an unconventional configuration MIT D8 (Double Bubble) aircraft. We also investigate varying aviation technologies with the D8 configuration using current technologies and advanced technologies.

Aircraft flight performance in relation to aircraft technologies, design operations, and their interactions is modeled using the software tool Transport Aviation Systems Optimization (TASOpt). The software TASOpt allows users to evaluate future aircraft with potentially unconventional airframe, aerodynamic, engine, or operational parameters. The aircraft designed in TASOpt are then imported into the FAA software package Aviation Environmental Design Tool Version 2a (AEDT 2a) to evaluate the aircrafts fuel burn performance. The coupling of TASOpt and AEDT into a system-level analysis tool allows one to model the interdependencies between aircraft technology and design operation of conventional aircraft as well as unconventional aircraft.

The coupling of TASOpt and AEDT into a system-level analysis tool requires compiling approximately one hundred AEDT aircraft performance parameters and coefficients using the TASOpt aircraft flight performance output. The connection between TASOpt and AEDT is shown to be accurate in regards to total fuel burn performance to within 5% relative uncertainty over similar flight scenarios, where uncertainty refers to the difference between TASOpt and AEDT estimations of the fuel burn. The discrepancy between TASOpt and AEDT fuel burn performance is typically observed near the departure and arrival segments. In particular, the TASOpt and AEDT fuel burn performance in the approach segment, from cruise to airport arrival, has an approximately 15% relative uncertainty due to the varying methodologies between TASOpt and AEDT. The TASOpt to AEDT fuel burn performance for cruise varies with the worst case being approximately 3% relative uncertainty due to the differences in initial takeoff weight.

For the Boeing 737-800 fuel burn performance, which is evaluated using the fuel energy consumption per payload range (PFEI), has the largest expectation and variance of the three aircraft configurations. The 737-800's PFEI variation is attributed to two main sources; uncertainties in the aircraft's design cruising altitude and the aircraft's wing cap yield stress technological variable. The D8 with standard technology has a lower expected PFEI mean and variance than the Boeing 737-800. That is, for the scenarios studied, the unconventional D8 aircraft configuration reduces the variability in fuel burn performance. The D8 with standard technology PFEI variation is susceptible to multiple aircraft technology uncertainties and operational uncertainties, whereas the Boeing 737-800 has only two important factors contributing to variability in its fuel burn performance. Finally, the D8 with advanced technology has the lowest PFEI mean and variance of the three aircraft configurations. Furthermore, the D8 with advanced technology has only two significant contributing uncertainties to PFEI uncertainty; turbine inlet gas temperature and aircraft design Mach number. These results indicate that large variations in aircraft configuration and technology substantially modify the research prioritization efforts.

The report also presents a new approach to evaluating the system-level uncertainty quantification using a decomposition-based methodology. The decomposition-based uncertainty quantification approach has multiple benefits in comparison to a standard all-at-once system-level uncertainty quantification approach. The decomposition-based uncertainty quantification approach breaks the system-level analysis into manageable components which can be individually analyzed by the respective component experts using local resources. However, the decomposition-based uncertainty quantification approach is challenging when the interface between two components in a system contains a large number of variables as this problem does. This report presents our current findings on decomposition-based uncertainty quantification of a large scale system. The results show great potential for decomposition-based uncertainty quantification. But, further research is required to accurately and rigorously perform the decomposition-based uncertainty quantification on large-scale systems.

The report contains a step-by-step procedure and necessary scripts for initializing TASOpt, AEDT, and integrating the two modules. In this report we have addressed the following key issues: analyzing non-conventional and other unrepresented aircraft in AEDT, assessing how uncertainties in aircraft technologies and design operations impact fuel burn performance, assessing how fuel burn performance is impacted by aircraft configurations and aviation technology enhancements, and demonstrating the decomposition-based uncertainty quantification on a large-scale application problem.

Table of Contents

List of Figures

List of Tables

Nomenclature

Abbreviations

AEDT	Aviation & Environmental Design Tool
ASIF	AEDT Standard Input File
B738	Boeing 737-8000 Aircraft Configuration
BADA	Base of Aircraft Data
CAS	Calibrated Airspeed
CAEP	Committee for Environmental Protection
CR	Cruise
D8	Double Bubble Aircraft Configuration
DE	Descent
GHG	Greenhouse Gas
GSA	Global Sensitivity Analysis
IC	Initial Climb
ICAO	International Civil Aviation Organization
ISA	International Standard Atmosphere
MCS	Monte Carlo Simulation
MSI	Main Sensitivity Index
MSL	Mean Sea Level
MTOW	Maximum Takeoff Weight
MLW	Maximum Landing Weight
LD	Landing
TAS	True Airspeed
TASOpt	Transport Aircraft System OPTimization
TO	Takeoff
TOW	Takeoff Weight
TSFC	Thrust Specific Fuel Consumption
TSI	Total Sensitivity Index
UQ	Uncertainty Quantification
X_Y	Unit Conversion from X to Y

Notations

C_D	Coefficient of Drag	[-]
C_f	Initial-climb calibrated airspeed coefficient	[-]
C_L	Coefficient of Lift	[-]
$C_{L,max}$	Maximum Coefficient of Lift	[-]
B_f	Takeoff ground-roll coefficient	[-]
D_f	Landing Speed coefficient	[-]
$\varepsilon_{pol,lc}$	Low Pressure Compressor Polytrophic Efficiency	[-]
$\varepsilon_{pol,hc}$	High Pressure Compressor Polytrophic Efficiency	[-]
$\varepsilon_{pol,lt}$	Low Pressure Turbine Polytrophic Efficiency	[-]

$\varepsilon_{pol,ht}$	High Pressure Turbine Polytrophic Efficiency	[-]
E_{cap}	Airfoil Cap Modulus of Elasticity	
E_{strut}	Airfoil Strut Modulus of Elasticity	
FPR	Fan Pressure Ratio	[-]
h	Altitude	[ft]
M	Mach Number	
$\dot{m}$	Fuel Flow	[kg/sec]
n_{eng}	Number of Engines Supplying Thrust	
OPR	Operating Pressure Ratio	[-]
P_o	Pressure at MSL	[Pa]
P	Pressure at Engine Inlet	[Pa]
σ_{skin}	Aircraft Skin Yield Stress	[MPa]
σ_{bend}	Bend Yield Stress	[MPa]
σ_{cap}	Airfoil Cap Yield Stress	[MPa]
τ_{web}	Web Shear Yield Stress	[MPa]
σ_{strut}	Airfoil Strut Yield Stress	[MPa]
R	Range	[nmi]
ρ_{skin}	Aircraft Skin Yield Stress	[MPa]
ρ_{bend}	Bend Yield Stress	[MPa]
ρ_{cap}	Airfoil Cap Yield Stress	[MPa]
ρ_{web}	Yield Stress	[MPa]
ρ_{strut}	Airfoil Strut Yield Stress	[MPa]
St_c	Stanton Number	[-]
T_o	Temperature at Airport Altitude	[K]
T	Temperature at Engine Inlet	[K]
T_{metal}	Allowable Metal Temperature	[K]
$T_{o,TO}$	Takeoff Temperature at Engine Inlet and Airport Altitude	[K]
$TT_{4,TO}$	Turbine Inlet (Stage 4) Gas Temperature at Takeoff	[K]
$TT_{4,CR}$	Turbine Inlet (Stage 4) Gas Temperature at Cruise	[K]
ΔT	Temperature deviation from ISA at Airport Altitude	[K]
V	Aircraft Velocity	[knts]
λ	Temperature Variation with Altitude = -0.0065	[K/m]
θ_f	Film cooling effectiveness	[-]

Section 1

Introduction

As part of the tool development effort the Federal Aviation Administration (FAA) Office of Environment and Energy (AEE) is conducting research to evaluate how uncertainties in input parameters and assumptions affect the outputs of the analytical tools that comprise the aviation environmental tool suite. As part of this work, AEE is interested in performing a system-level uncertainty quantification (UQ) analysis. This system-level assessment will quantify how uncertainties in aircraft technologies and design operation parameters propagate onto aircraft performance uncertainties and finally uncertainty in total fuel burn and overall policy outcomes. The following section will outline the motivation and objectives of the work as well as describe the standard system-level Monte Carlo simulation (MCS) and the decomposition-based UQ methodologies.

Motivation

The aviation sector is believed to be one of the fastest growing anthropogenic GHG emissions. In 2005, aircraft emissions increased 45% from 1992 and accounted for approximately 2.5% of anthropogenic CO_2 emissions and 3.5% of historical manmade radiative forcing (Lee, et al., 2009). Left unconstrained, aircraft emissions could quadruple by 2050 (2010a, 2010). As a measure to manage the climate impact of aviation, the Committee for Environmental Protection (CAEP) under the International Civil Aviation Organization (ICAO), adopted an aspirational 2% annual efficiency improvement goal for aviation through 2050 (2010b, 2010). To reduce its CO_2 emissions, aviation is pursuing significant enhancements to aviation technology, sustainable fuels with low CO_2 emissions, and efficient operational procedures (Rutherford & Mazyar, 2009).

To meet these demanding requirements, CAEP assembled a panel of independent experts with varying backgrounds to establish long-term technology goals for aviation fuel burn (Cumpsty, et al., 2010). Their study investigated future aviation technology scenarios, which represented varying regulatory pressure to reduce fuel burn. The future aircraft technology scenarios were then applied in analysis tools as “technology packages” to assess the technology improvement on aircraft fuel burn. Due to resource limitations the independent experts were unable to address the following issues:

- The impact of uncertainties in aviation technology development on fuel burn performance and implications on policy assessment.
- The lack in modeling of integration interdependencies between technologies which could not be handled by conceptual-level tools.

In this report, we will address these challenges along with the following:

- The impact of uncertainties in aircraft technology and design operations on predictability of fuel burn performance and implications on policy assessment.

These tasks are accomplished by performing a system-level uncertainty quantification using a conceptual-level aircraft design tool and an aviation environmental design tool. This report will assist in understanding how the uncertainties in aircraft technologies and design operations integrate into the uncertainty in the aircraft fuel burn performance while considering the impacts of aircraft configurations and aviation technological developments.

Methodology

The objective of this effort is to perform a system-level uncertainty quantification (UQ) analysis on a toolset consisting of the Transport Aircraft System OPTimization (TASOpt) (Drela, Simultaneous Optimization of the Airframe, Powerplant, and Operation of Transport Aircraft., 2010) and the Aviation Environment Design Tool (AEDT) Version 2a (Roof, et al., 2007) as depicted in Figure 1 using the standard system-level MCS UQ and novel decomposition-based UQ approaches.

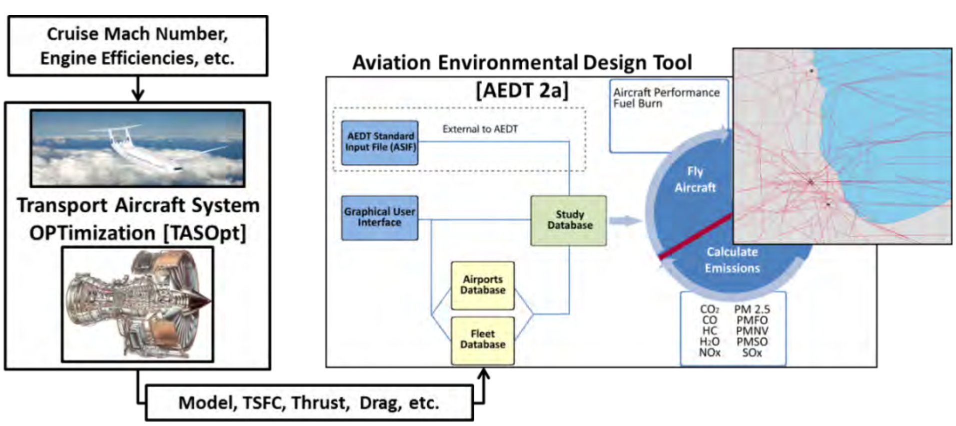

Figure 1: System-level UQ of the toolset consists of quantifying how uncertainty in aircraft technology and design operations impacts the uncertainty in the outputs of interest (e.g., fuel burn).

The intent of the UQ analysis is to characterize the system outputs of interest (e.g., fuel burn and emissions) distributions due to uncertainties in system inputs (e.g., aircraft technologies and design operation parameters) as well as identify which inputs have the greatest impact on the outputs of interest, while accounting for aviation technology development and aircraft configuration. The results of this analysis could be used, for example, to assist manufacturers and designers by prioritizing their research efforts in reducing uncertainty in specific aircraft technologies or design mission parameter. Our analysis will investigate three aircraft configurations: the Boeing 737-800 and the MIT Double Bubble (D8) design with standard and advanced technologies (Drela, Development of the D8 Transport Configuration, 2010). Further, the UQ analysis is performed using the new decomposition-based approach developed at MIT (Amaral, Allaire, & Willcox, 2012) and the standard all-at-once MCS UQ approach. The specific research tasks are listed below:

1. Define the aircraft configurations: Boeing 737-800, D8 (Standard), and D8 (Advance).
2. Characterize aircraft technology and design operation uncertainty distributions using historical trends and engineering judgment.
3. Develop a mapping from TASOpt aircraft performance to AEDT aircraft metrics.
4. Perform the system-level MCS uncertainty quantification analysis.
5. Perform the decomposition-based uncertainty quantification analysis.

The results will characterize the outputs of interest distribution and identify the most significant sources of uncertainty across different aircraft configurations and technologies. Further, the results will compare the standard system-level MCS UQ approach and the decomposition-based UQ approach.

System-Level Uncertainty Quantification

The system-level MCS UQ approach is a standard approach to quantifying uncertainty in systems. The approach requires integrating all the components under one framework as shown in Figure 1, from which uncertainty and sensitivity analysis may be computed.

Uncertainty Analysis

The objective of uncertainty analysis is to answer the question, “How do uncertainties in model factors propagate to uncertainties in model outputs?”. Uncertainties in model outputs are characterized by statistics of interest such as model output mean, variance, and the probability of an event occurring. These quantitative representations of uncertainty in model outputs provide a means of comparing various policy scenarios and quantitatively evaluating the performance of the model relative to fidelity requirements. Uncertainty analysis can be carried out with several different methods, such as mean-value methods, analytic reliability methods, stochastic expansion methods (e.g., polynomial chaos expansion), and sampling-based techniques such as Monte Carlo simulation. The approach we selected for this work is the sampling-based Monte Carlo simulation technique as shown in Figure 2.

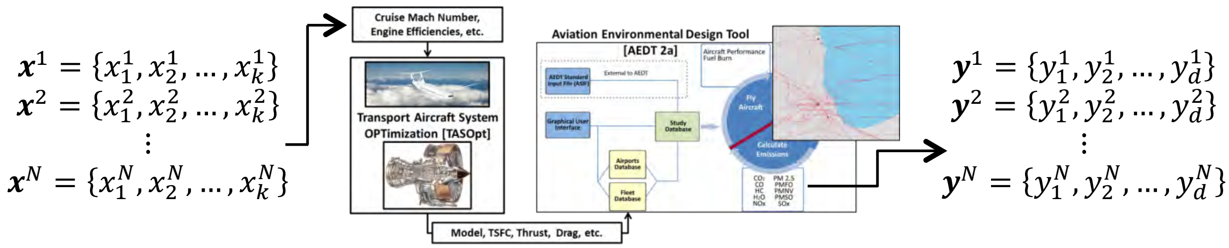

Figure 2: System-level uncertainty analysis using the sampling-based technique (e.g., MCS)

The TASOpt-AEDT system maps a k-dimensional input vector $\boldsymbol{x}$ (e.g., $\boldsymbol{x}$ = {Engine Efficiencies, Cruise Altitude, … }) into a d-dimensional output vector $\boldsymbol{y}$ (e.g., $\boldsymbol{y}$ = {Fuel Burn, CO2, … }). Let the sequence $\{\boldsymbol{x}^1, \boldsymbol{x}^2, \dots, \boldsymbol{x}^N\}$ be an independent identically distributed set of realizations from the input distribution where $\boldsymbol{x}^i$ represents the i^{th} realization. An expectation of $\boldsymbol{y}$ evaluated using N realizations is defined as,

$$\boldsymbol{\mu} = \frac{1}{N}\sum_{i=1}^{N} \boldsymbol{y}^i. \qquad \textbf{Eq. 1}$$

By the strong law of large numbers, $\boldsymbol{\mu}$ weakly converges to $\mathbb{E}_{\boldsymbol{y}}[\boldsymbol{y}]$ as $N \to \infty$. By the Central Limit Theorem, the convergence rate of $\boldsymbol{\mu}$ to the expected value of $\mathbb{E}_{\boldsymbol{y}}[\boldsymbol{y}]$ is given by $O\left(1/\sqrt{\mathrm{N}}\right)$. Variance and other quantities of interest can similarly be estimated using MCS.

Sampling Methods

There are several approaches to draw realizations of the random vector $\boldsymbol{x}$. The most common approaches are pseudo-random sampling and quasi-random sampling. Pseudo-random sampling uses a computer's pseudo-random number generator to draw realization as shown on the left of Figure 3. Quasi-random sampling selects samples deterministically using a low-discrepancy sequence, which attempts to draw realizations from a space uniformly as shown on the right of Figure 3. For the uncertainty analysis, quasi-random sampling was selected since its convergence rate is $O\left(\log(\mathrm{N})^{\mathrm{k}}/\mathrm{N}\right)$, where k is the number of input dimensions (Niederreiter, 1992).

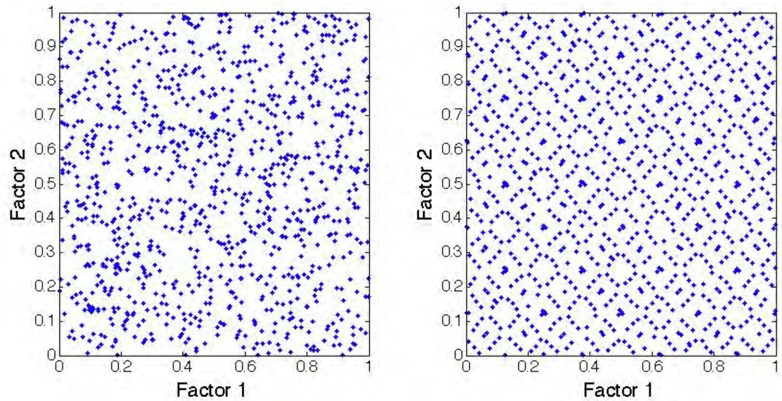

Figure 3: Uniform sampling (Left: Pseudo-Random) (Right: Quasi-Random)

Global Sensitivity Analysis

The second component of uncertainty quantification is global sensitivity analysis (GSA). The motivation for GSA is to prioritize research and to simplify the model (Andrea Saltelli, 2008).

- Prioritize research: Which factors are most deserving of further analysis?
- Model simplification: Can some factors of the model be fixed?

The GSA method selected for our analysis is a variance based method. Variance based methods decompose the output variance into contributions from individual model parameters and the interactions between parameters as shown in Figure 4. Variance based methods calculate an averaged global contribution to output variance from each factor, which includes all interaction effects among the different factors. That is, it includes any effects that occur by two or more factors directly affecting each other. For this assessment, the Sobol' method, discussed in Appendix A, is used to compute the expected global contribution represented as the total sensitivity index (TSI). The TSI quantifies the impact an input and the distribution assigned to that input have on the variance of a specific output. TSI is defined as the output variance caused by a given factor and its interactions, divided by the total output variance. Therefore, the larger a factor's TSI, the larger impact it has on the variance of the output. Main sensitivity indices (MSI) quantify the impact the input without interaction effects and the distribution assigned to that input have on the variance of a specific output. Therefore, MSI is always less than or equal to TSI and both values are less than or equal to one.

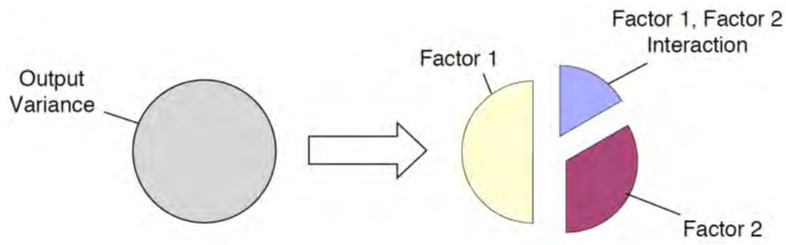

Figure 4: Global sensitivity analysis variance decomposition (Allaire, 2009)

The outcome of a global sensitivity analysis is to identify and rank the factors' influence on the output variance. This information allows the user to prioritize their future research efforts and perform factor fixing. Understanding which inputs have the largest influence on the output variance would guide future research efforts in reducing the input variance through stricter analysis or improved understanding. Factor fixing allows the user to reduce the complexity of the model inputs by identifying those factors that once fixed have negligible impact on output variance and can therefore be treated as deterministic.

Decomposition-Based Uncertainty Quantification

In some scenarios it may be challenging to conduct UQ of systems comprising multiple components. In such cases, the models may be developed by different groups and run on different computational platforms. In addition, the models may not be seamlessly integrated in an automated fashion. Existing UQ methods typically involve coupling the models and performing a system-level MCS uncertainty and sensitivity analysis. This approach, while adequate in some situations, emphasizes joining multiple models under one group, which is undesirable and even infeasible in many cases. In this work we propose to develop a different approach for system UQ that involves decomposition of the UQ task, performing UQ on the respective models individually, and reassembling model-level information to quantify uncertainty at the system level. Our approach enables a new view to system UQ, through decomposition of the system-level UQ into a set of manageable model-level UQ analyses followed by synthesizing the information at the system level in a provably convergent manner.

Uncertainty Analysis

In the case of uncertainty analysis, the decomposition-based approach is composed to two main procedures: **(1) Local uncertainty analysis**: perform a local Monte Carlo uncertainty analysis on each discipline over their respective *proposal* input distributions; and **(2) Global**

compatibility satisfaction: reweight the individual discipline Monte Carlo proposal samples such that the reweighted samples approximate the *target* input distributions to satisfy global compatibility constraints. We use the terms *proposal distribution* to refer to the input distribution assumed at the local level for each discipline, and *target distribution* to refer to the actual input distribution when system compatibility constraints are satisfied (e.g., the target distribution might be specified through the output distribution of an upstream discipline). Through these two steps it is possible to propagate input uncertainties from the system inputs to system outputs of interest in a manner that is provably convergent. The idea of the approach is illustrated in Figure 5 [9].

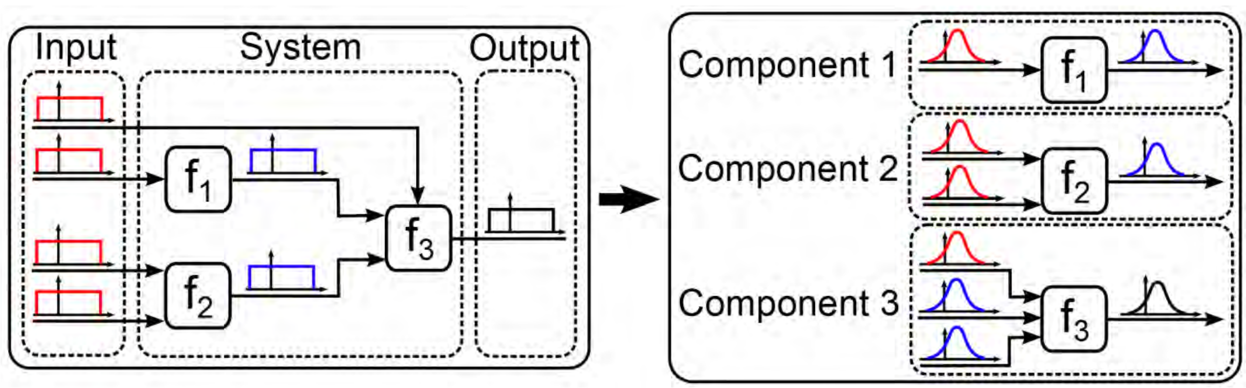

Figure 5: The proposed method of multicomponent uncertainty analysis decomposes the problem into manageable components; similar to decomposition-based approaches used in multidisciplinary analysis and optimization, and synthesize the system uncertainty analysis without needing to evaluate the system in its entirety.

Sensitivity Analysis

The decomposition-based global sensitivity analysis, illustrated in Figure 6, resolves the *main sensitivity indices* of the system by building upon the decomposition-based uncertainty analysis results. Future research efforts include assessing 2nd and higher order sensitivity indices by a decomposition-based approach.

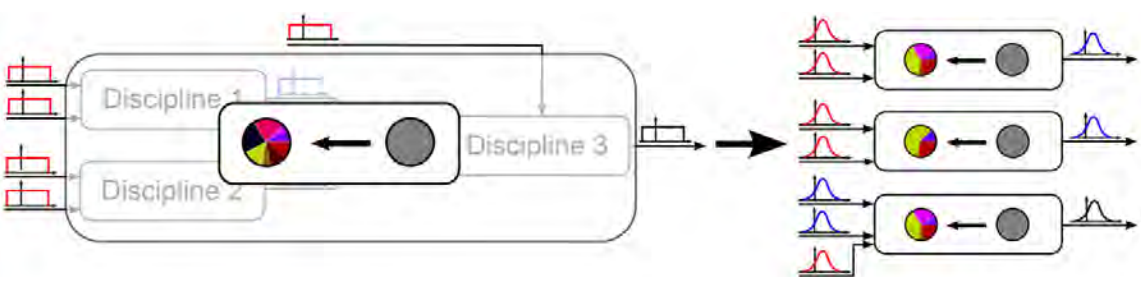

Figure 6: Illustration of the proposed method for decomposition-based global sensitivity analysis.

Section 2

TASOpt

The TASOpt module is an aircraft performance tool developed by Prof. Mark Drela at MIT. TASOpt allows users to evaluate future aircraft with potentially unconventional airframe, aerodynamic, engine, or operation parameters using low-order physical models implementing fundamental structural, aerodynamic, and thermodynamic theory. It uses historical based correlations only when necessary, in particular only for some of the secondary structure and aircraft equipment. The TASOpt module takes as input aircraft technology and operational parameters and can optimize an aircraft over a given set of constraints or resize an aircraft to meet the desired mission requirements.

Source Code Modifications

The TASOpt module required slight modifications to the source code in order to integrate it with the AEDT module. These modifications are discussed below.

Mission Inputs

To extract the AEDT aircraft performance metrics from the TASOpt aircraft performance metrics requires simulating a particular aircraft design over multiple mission scenarios. Therefore, the source codes getval.f and getparam.f are modified so that TASOpt may simulate up to 100 mission scenarios. The source file getparam.f was modified to include cutback sight angle, cutback climb angle, top descent angle, bottom descent angle, cruise coefficient of lift, and cruise Mach number as extra mission parameters.

Airport Temperature

The AEDT module contains aircraft performance correlations that are a function of change in temperature from ISA. Therefore, the TASOpt input file (e.g., *.tas) was modified such that the temperature at the airport is a change in temperature from ISA instead of an absolute temperature at the airport. For example, a $\mathrm{T}_{0,TO} = 0\ [K]$ is equivalent to ISA conditions at the airport altitude and $\mathrm{T}_{0,TO} = 10\ [K]$ is equivalent to ISA conditions at the airport altitude plus $10\ [K]$.

Atmospheric Conditions

The source code atmos.f was modified so that the atmospheric conditions are equivalent to the AEDT 2a atmospheric conditions (Manual, 2012). The code was also modified to account for a change in temperature from ISA conditions at the airport altitude as shown,

$$T(h) = \frac{(T_o - \lambda \cdot 3280.84 \cdot h)}{1.8} + \Delta T, \qquad \text{Eq. 2}$$

$$P(h) = P_o \cdot \left(\frac{(1 - \lambda \cdot 3280.84 \cdot h)}{518.67}\right)^{5.256} \cdot \frac{1}{0.0393701} \cdot \frac{101.325}{760.0} \cdot 1000. \qquad \text{Eq. 3}$$

The source codes which call atmos.f were modified to take in the variable ΔT. The source codes modified include: fusebl.f, getparm.f, mission.f, output.f, tasopt.f, woper.f, and wsize.f.

Cruise Flight

The source file misson.f was modified so that the first cruise point is evaluated with respect to its current altitude and atmospheric conditions. The atmospheric conditions at the first cruise point are then used to initialize the engine variables as is done for the last cruise point.

Initialize Engine

The source code woper.f was modified so that was engine parameters are initialized to the design engine parameters before initializing to the known operating conditions.

Performance Output

The source code output.f was modified to print out a custom output file which simplified the TASOpt and AEDT integration. This output file contains the necessary aircraft performance metrics and is formatted as shown in Table 1.

Table 1: Custom TASOpt output file (e.g., *.dat) required for TASOpt-AEDT modules integration.

MTOW	= 185810.8	lb						
Wempty	= 93909.8	lb						
WfuelM	= 64103.2	lb						
S	= 1476.9	ft^2						
Fmax	= 127.86	kN						
Mission	Profile	1						
		R [nmi]	h [ft]	⋯	Feng [kN]	mdotf [kg/sec]	⋯	Mach
ST	1	0.0	0.0	⋯	127.86	2.794	⋯	0.000
TO	1	0.0	0.0	⋯	103.66	2.855	⋯	0.258
⋮	⋮	⋮	⋮	⋮	⋮	⋮	⋮	⋮
D5	1	3000.0	0.0	⋯	6.64	0.238	⋯	0.225
Mission	Profile	2						
		R [nmi]	h [ft]	⋯	Feng [kN]	mdotf [kg/sec]	⋯	Mach
ST	2	0.0	105.0	⋯	125.83	2.753	⋯	0.000
⋮	⋮	⋮	⋮	⋮	⋮	⋮	⋮	⋮

Aircraft Configuration

The aircraft configurations selected for this study are the Boeing 737-800 and MIT D8. The MIT D8 is a concept aircraft designed at MIT by Prof. Mark Drela (Drela, Development of the D8 Transport Configuration, 2010). The MIT D8 aircraft was developed to operate in the short- to medium range while seating 180 passengers similar to the Boeing 737-800. The aircraft configurations are shown for comparison in Figure 7.

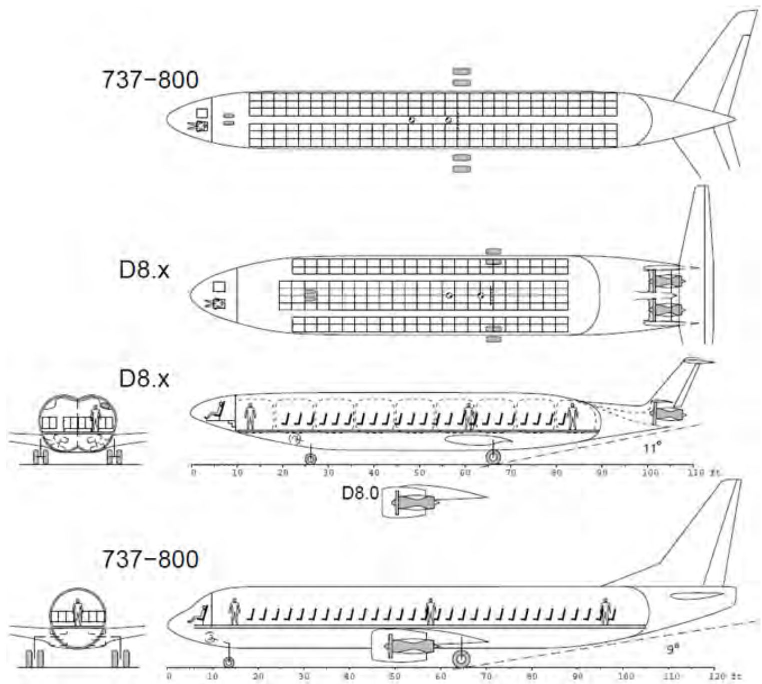

Figure 7: Boeing 737-800 and MIT D8 airframe configurations [6]

This study also considers the impacts of aviation technology enhancements using the MIT D8 configuration. Future technology enhancements include improved aircraft engine efficiencies, aircraft engine materials, and light-weight carbon fiber components. For each aircraft configuration, we first use the TASOpt module to optimize the aircrafts over their respective set of variables for a mission consisting of a 3000 [nmi] range with a payload weight of 40,500 [lb] at ISA conditions. The resulting optimal aircraft configuration then becomes the design aircraft from which the UQ study is performed. The optimal design aircraft TASOpt input files (e.g., B737.tas) are given in Appendix B. These TASOpt input files represent the optimal configuration and contain place holders for the uncertain parameters. Given realizations from the uncertain parameter distributions, the TASOpt input file is populated; afterwards TASOpt sizes the aircraft beginning from the optimal uncertain configuration to meet the desired mission scenarios.

TASOpt Input Parameters

This section will describe the 27 uncertain parameters including their respective distributions. The section will also present the mission parameter sweep required to extract the AEDT aircraft performance metrics from the TASOpt aircraft performance metrics.

Uncertainty Distributions

The following uncertain distributions are the 27 uncertain parameters selected for the UQ study. A realization from these distributions populates the first mission which TASOpt uses to appropriately size the aircraft. This random aircraft is then flown over multiple missions to extract the desired information required by AEDT.

Engine Metal Temperature (T_{metal})

The engine metal temperature determines the temperature the engine blade material can withstand on average. For example, a high metal temperature engine requires less coolant then a low metal temperature engine and therefore is more efficient. Figure 8 illustrates the temperature capacity of materials commonly used in aircraft engines (Kyprianidis, 2011). While the standard technology aircraft metal temperatures are reasonable, the D8 advanced technology would require a significant improvement in technology to obtain a 1500 [K] metal temperature. The uncertainty in engine metal temperature capacity represents our uncertainty in material properties and measurements.

Table 2: Engine metal temperature distribution

Name	Units	Distribution	Boeing 737-800	Standard D8	Advanced D8
T_{metal}	[K]	U[-50, 50]	1222	1200	1500

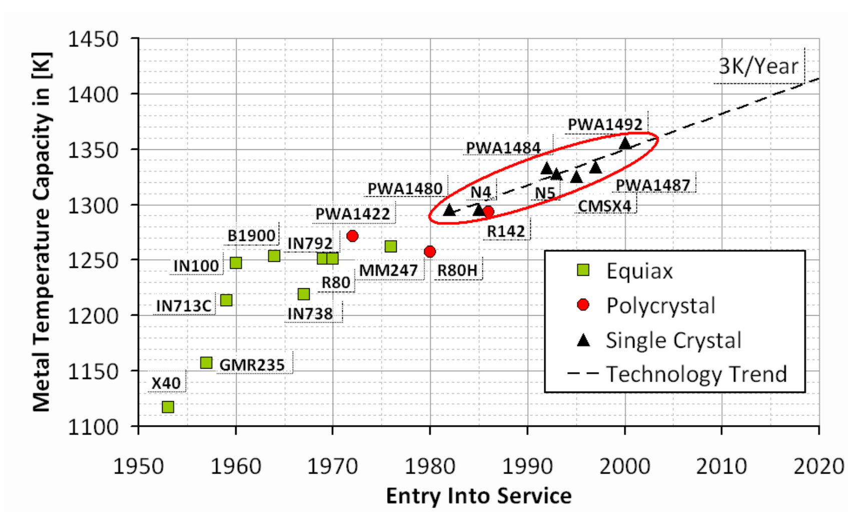

Figure 8: Historical trends for engine metal temperature capacity (Kyprianidis, 2011)

Film Effectiveness (θ_f)

The film effectiveness is defined as follows,

$$\theta_f = \frac{T_g - T_{faw}}{T_g - T_{co}}, \qquad \textbf{Eq. 4}$$

where θ_f is the film effectiveness, T_g is the hot gas fluid temperature, T_{co} is the cool gas fluid temperature exiting the film hole, and T_{faw} is the hypothetical adiabatic wall temperature. If $\theta_f = 1$, the cooling fluid covers the blade and if $\theta_f = 0$, the cooling flow is absent. The uncertainty in film effectiveness represents our uncertainty in manufacturing cooling holes and the supply and dump pressures.

Table 3: Film cooling effectiveness

Name	Units	Distribution	Boeing 737-800	Present D8	Future D8
θ_f	[-]	U[-0.005, 0.005]	0.32	0.30	0.4

Stanton Number (St_c)

The Stanton number is defined as follows,

$$\eta = \frac{T_{co} - T_{ci}}{T_m - T_{ci}} = 1 - exp\left(-\frac{A_{cs}}{A_c}St_c\right) \cong 0.7, \qquad \textbf{Eq. 5}$$

where η is the cooling efficiency, St_c is the Stanton number, T_m is the metal temperature, T_{ci} is the cool gas fluid temperature entering the film hole, A_c is the cooling flow area, and A_{cs} is the cooling hole heat transfer area. A low Stanton number indicates a better film cooling technology which draws more cool air to the hot surface. The uncertainty in Stanton number represents our uncertainties in manufacturing film cooling holes and the supply and dump pressures.

Table 4: Film cooling effectiveness

Name	Units	Distribution	Boeing 737-800	Present D8	Future D8
St_c	[-]	U[-0.001, 0.001]	0.095	0.09	0.065

Compressor Polytrophic Efficiency ($\varepsilon_{pol,lc}/\varepsilon_{pol,hc}$)

The compressor polytrophic efficiency accounts for the non-isentropic compression process. A high compressor polytrophic efficiency results in a more efficient engine. The uncertainty in compressor polytrophic efficiencies represents our uncertainty attributed to measuring compressor efficiency while in operation and component manufacturing.

Table 5: Compressor polytrophic efficiency distribution

Name	Units	Distribution	Boeing 737-800	Present D8	Future D8
$\varepsilon_{pol,lc}$	[-]	U[-0.001, 0.001]	0.937	0.92	0.93
$\varepsilon_{pol,hc}$	[-]	U[-0.001, 0.001]	0.904	0.89	0.9

Turbine Polytrophic Efficiency ($\varepsilon_{pol,lt}/\varepsilon_{pol,ht}$)

The turbine polytrophic efficiency similar to the compressor polytrophic efficiency accounts for the non-isentropic process but for the turbine section of the engine.

Table 6: Turbine polytrophic efficiency distribution

Name	Units	Distribution	Boeing 737-800	Present D8	Future D8
$\varepsilon_{pol,lt}$	[-]	U[-0.001, 0.001]	0.871	0.91	0.925
$\varepsilon_{pol,ht}$	[-]	U[-0.001, 0.001]	0.876	0.92	0.93

Turbine Entry Temperature ($TT_{4,TO}$/ $TT_{4,CR}$)

The turbine entry temperature defines the gas temperature entering the turbine component of the aircraft engine. Figure 9 shows the historical and the extrapolated turbine inlet gas temperatures. The uncertainty associated to turbine entry temperatures are measurement uncertainties and variability in upstream components.

Table 7: Turbine entry total temperature distribution

Name	Units	Distribution	Boeing 737-800	Present D8	Future D8
$TT_{4,TO}$	[K]	U[-50, 50]	1833	1576	1709
$TT_{4,CR}$	[K]	U[-50, 50]	1591.5	1335	1506

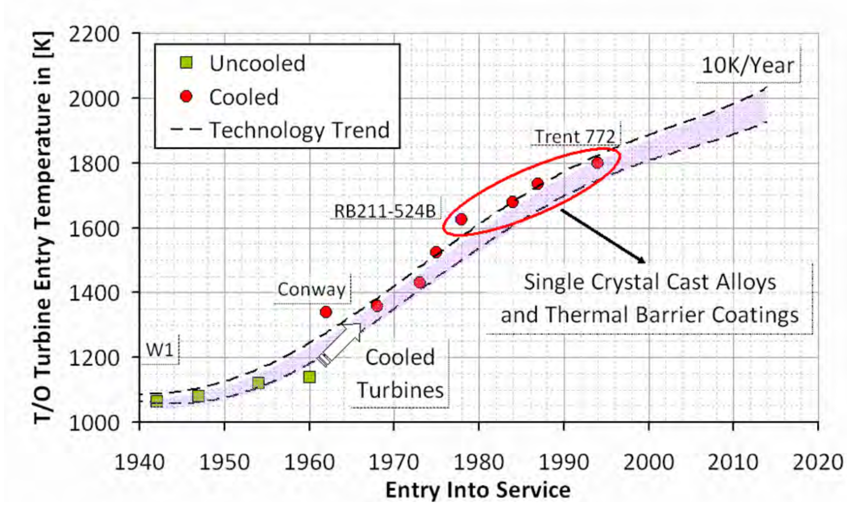

Figure 9: Historical trends for turbine entry total temperature (Kyprianidis, 2011)

Overall Pressure Ratio (OPR)

The overall pressure ratio corresponds to the pressure ratio between the exit of the high pressure compressor and the atmospheric pressure. Figure 10 shows the historical overall pressure ratio in relation to entry of service. The uncertainty associated to the overall pressure ratio represents our uncertainty in measurement and variability in manufacturing components.

Table 8: Overall pressure ratio distribution

Name	Units	Distribution	Boeing 737-800	Present D8	Future D8
OPR	[-]	U[-2.0, 2.0]	26.2	35	50

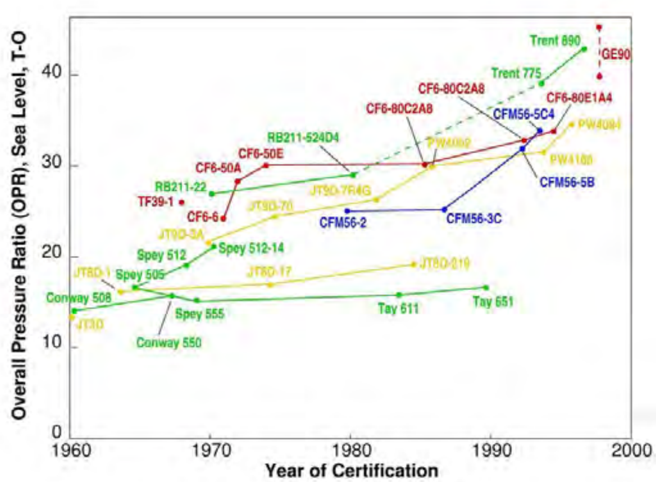

Figure 10: Historical trends for engine overall pressure ratio (Gunston, 1998)

Fan Pressure Ratio (FPR)

The fan pressure ratio is equal to the pressure ratio between the outlet of the fan and the atmospheric pressure. The standard technology configurations use conventional direct drive turbofan whereas the advanced technology configuration would use a geared turbofan which allows for a lower fan pressure ratio and higher propulsive efficiency. The uncertainty associated to the fan pressure ratio is our uncertainty in measurement and variability in manufacturing components.

Table 9: Fan Pressure ratio distribution

Name	Units	Distribution	Boeing 737-800	Present D8	Future D8
FPR	[-]	U[-0.001, 0.001]	1.61	1.6108	1.39262

Material Stress Properties ($\sigma_{skin}, \sigma_{bend}, \sigma_{cap}, \tau_{web}, \sigma_{strut}$)

The material stress properties are the fuselage pressurization skin stress (σ_{skin}), fuselage bending skin and stringer stress (σ_{bend}), wing/tail bending caps (σ_{cap}), wing/tail webs shear stress (τ_{web}), and strut stress (σ_{strut}). These uncertainties are associated to measurement accuracy.

Table 10: Material stress properties distribution

Name	Units	Distribution	Boeing 737-800	Present D8	Future D8
σ_{skin}	[psi]	U[-5%, 5%]	15000	15000	29800
σ_{bend}	[psi]	U[-5%, 5%]	30000	30000	49500
σ_{cap}	[psi]	U[-5%, 5%]	30000	30000	39700
τ_{web}	[psi]	U[-5%, 5%]	20000	20000	21300
σ_{strut}	[psi]	U[-5%, 5%]	30000	30000	66000

Material Modulus of Elasticity Properties (E_{cap}, E_{strut})

The material modulus of elasticity properties are the wing spar cap modulus of elasticity (E_{cap}) and strut modulus of elasticity (E_{strut}). These uncertainties are associated to measurement accuracy.

Table 11: Material stress properties distribution

Name	Units	Distribution	Boeing 737-800	Present D8	Future D8
E_{cap}	[psi]	U[-5%, 5%]	10e6	10e6	18.2e6
E_{strut}	[psi]	U[-5%, 5%]	10e6	10e6	7.5e6

Material Density Properties ($\rho_{skin}, \rho_{bend}, \rho_{cap}, \rho_{web}, \rho_{strut}$)

The material density properties are the fuselage skin density (ρ_{skin}), fuselage bending skin+stringer density (ρ_{bend}), wing/tail bending cap density (ρ_{cap}), wing/tail web density (ρ_{web}), and strut density (ρ_{strut}). These uncertainties are associated to measurement accuracy.

Table 12: Material stress properties distribution

Name	Units	Distribution	Boeing 737-800	Present D8	Future D8
ρ_{skin}	[psi]	U[-1%, 1%]	2698.8	2698.8	1550.1
ρ_{bend}	[psi]	U[-1%, 1%]	2698.8	2698.8	1550.1
ρ_{cap}	[psi]	U[-1%, 1%]	2698.8	2698.8	1550.1
ρ_{web}	[psi]	U[-1%, 1%]	2698.8	2698.8	1550.1
ρ_{strut}	[psi]	U[-1%, 1%]	2698.8	2698.8	1550.1

Operational Uncertainties (h_{CR}, $C_{L,max}$, C_L, M)

The operational parameters include the cruise altitude, maximum coefficient of lift, coefficient of lift at cruise, and cruise Mach number. These uncertainties represent the uncertainty a designer would have in the design of an aircraft for a typical flight operation scenario.

Table 13: Aircraft operational distribution

Name	Units	Distribution	Boeing 737-800	Present D8	Future D8
h_{CR}	[ft]	U[-1000, 1000]	35000	39911	42838
$C_{L,max}$	[-]	U[-0.05, 0.05]	2.25	2.15	2.5
C_L	[-]	U[-0.01, 0.01]	0.57714	0.6945	0.70476
M	[-]	U[-0.01, 0.01]	0.78	0.72	0.74

Mission Parameters

After obtaining a single realization vector from the 27 input distributions, the remaining 99 missions are generated using a design of experiments. A Latin hypercube sampling scheme provides the remaining 99 missions in order to quantify the aircraft performance under multiple mission scenarios. The mission parameters selected along with their respective parameter sweeps are given in Table 14. For a particular variable (e.g., R), Eq. 6 describes how the variable varies given the center, span, and Latin hypercube value for the variable, $\mathrm{X}_i \in [0,1]$. For example, the range variable is expected to sweep from 750 [nmi] to 3250 [nmi].

$$Value = Center + (\mathrm{X} - 0.5) \cdot Span. \qquad \text{Eq. 6}$$

Table 14: Aircraft Operational Distribution

Name	Units	Center [Boeing 737-800/D8]	Span
R	[nmi]	2000	2500
W_{pax}	[lb]	215	100
h_{TO}	[ft]	0.0	8000
ΔT	[K]	0.0	25
h_{CR}	[ft]	Random Variable	8000
$C_{l,max}$	[-]	Random Variable	0.1
Θ_{TO}	[deg]	40.0	2.0
Θ_{IC}	[deg]	3.0	0.4
$\Theta_{DE,1}$	[deg]	[-3.0/ -2.0]	0.4
$\Theta_{DE,5}$	[deg]	[-3.0/ -2.5]	0.4
C_l	[-]	Random Variable	0.05
M	[-]	Random Variable	0.04

The TASOpt module steps are shown in Figure 11. Starting from the optimal aircraft configuration (e.g., blue aircraft), 27 temporary place holders located in the 1st mission are replaced by 27 realizations each drawn from their respective uncertain distributions. These 27 random variables describe a new aircraft configuration which is similar to the optimal aircraft configuration but characterizes our lack of knowledge regarding the 27 input variables. TASOpt then resizes the new aircraft configuration to meet the first mission which is common among all aircraft configurations (e.g., red aircraft). The remaining 99 missions, described by the Latin Hypercube, use the resized aircraft from the first mission. The results produced by TASOpt over these 100 missions are transformed into AEDT performance coefficients in order to generate a similar aircraft in AEDT.

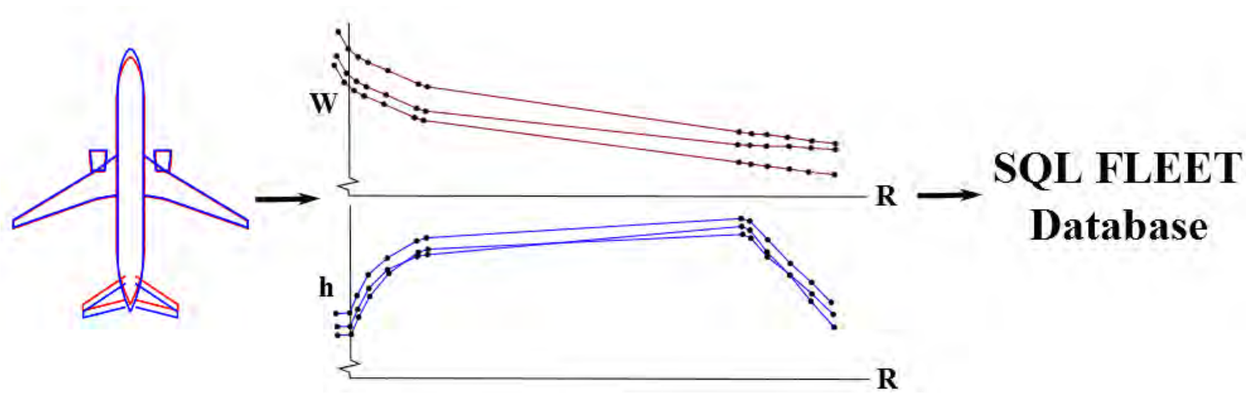

Figure 11: Starting from the optimal aircraft configuration (blue aircraft) we incorporate uncertainties to characterize the lack of knowledge in aircraft technology and design operations. The new (uncertain realization) aircraft is resized to meet the desired first mission flight specification (red aircraft). The (red) aircraft is then flown over multiple mission scenarios to extra the aircraft flight performance. This in turn is then imported into the AEDT SQL FLEET Database to create an equivalent aircraft in AEDT.

Section 3

AEDT

The Aviation Environmental Design Tool (AEDT) models aircraft performance in space and time to estimate fuel consumption, emissions, and noise. AEDT also provides users with the ability to assess the interdependencies among aviation-produced fuel consumption, emissions, and noise. Here we use the AEDT Version 2a. This study will focus on fuel consumption which for cruise conditions relies on the EUROCONTROL's Base of Aircraft Data (BADA) version 3.10 (BADA, 2012). The BADA fuel consumption model uses an energy-balance thrust model and Thrust Specific Fuel Consumption (TSFC) modeled as a function of airspeed. The BADA fuel consumption model has been shown to work well in cruise, with differences from airplane reported fuel consumption of about 5%. For terminal conditions (e.g., departure/ arrival flights until 10,000 [ft] above ground level), AEDT 2a derived a new set of energy-balance equations to support a higher level of fidelity in fuel consumption modeling.

AEDT Fleet Database

To improve the computational runtime of the AEDT module it is necessary to evaluate multiple aircraft realizations at a given time. To do this will recommend creating 1000 temporary aircrafts in the AEDT SQL Fleet database. This step involves identifying the fleet database tables used by AEDT to represent a unique aircraft. The SQL FLEET database tables including unique identifiers required to create unique aircraft are listed in Table 15.

To populate 1000 temporary aircraft the recommended approach is to extract from the SQL FLEET database the tables listed in Table 15 belonging to an aircraft which is similar to the desired temporary aircraft (e.g., Boeing 737-800). Using a software package similar to Microsoft Excel, each table is duplicated 1000 times and modified to have unique identifiers so that the aircraft does not duplicate an existing aircraft identifier while being sure that the aircraft's interconnecting identifiers are consistent. With the tables properly populated, each individual table, which now includes 1000 aircraft, are saved as a comma separated values file and named according to their respective SQL FLEET database table (e.g., FLT_ACTYPES.csv). Appendix C provides the scripts necessary to import the comma separated value files into the SQL FLEET databases. With the aircraft properly populated in the SQL FLEET database, the user may use any of the temporary aircraft in their AEDT simulations.

Table 15: AEDT SQL FLEET database entries for temporary TASOpt aircraft.

FLEET Database Table Name	Identifier	Type
[dbo].[FLT_REF_ICAO_ACTYPES]	ZZ000 – ZZ999	ACTYPE
[dbo].[FLT_ACTYPES]	ZZ000 – ZZ999	ACTYPE
[dbo].[FLT_AIRFRAMES]	1000-1999	AIRFRAME_ID
[dbo].[FLT_REF_ACCODES]	ZZ000-1 –ZZ999-1	ACCODE
[dbo].[FLT_AIRFRAME_ACTYPE_MAP]	ZZ000 – ZZ999	ACTYPE
[dbo].[FLT_BADA_ACFT]	ZZ000 – ZZ999	BADA_ID
[dbo].[FLT_ANP_AIRPLANES]	MIT0 – MIT999	ACFT_ID
[dbo].[FLT_EQUIPMENT]	5000 – 5999	EQUIP_ID
[dbo].[FLT_DEFAULT_ENGINES]	10000 – 10999	DEF_ENG_ID
[dbo].[FLT_FLEET]	60000 – 60999	FLEET_ID
[dbo].[FLT_DISPERSION]	5000 –5999	DISPERSION_ID
[dbo].[FLT_BADA_CONFIG]	ZZ000 – ZZ999	BADA_ID
[dbo].[FLT_BADA_FUEL]	ZZ000 – ZZ999	BADA_ID
[dbo].[FLT_BADA_APF]	ZZ000 – ZZ999	BADA_ID
[dbo].[FLT_BADA_ALTITUDE_DISTRIBUTION]	ZZ000 – ZZ999	BADA_ID
[dbo].[FLT_BADA_THRUST]	ZZ000 – ZZ999	BADA_ID
[dbo].[FLT_ANP_AIRPLANE_FLAPS]	MIT0 – MIT999	ACFT_ID
[dbo].[FLT_ANP_AIRPLANE_PROFILES]	MIT0 – MIT999	ACFT_ID
[dbo].[FLT_ANP_AIRPLANE_PROCEDURES]	MIT0 – MIT999	ACFT_ID
[dbo].[FLT_ANP_AIRPLANE_PROCEDURES_EXT]	MIT0 – MIT999	ACFT_ID
[dbo].[FLT_ANP_AIRPLANE_THRUST_JET]	MIT0 – MIT999	ACFT_ID
[dbo].[FLT_ANP_AIRPLANE_TSFC_COEFFICIENTS]	MIT0 – MIT999	ACFT_ID
[dbo].[FLT_ACTYPE_CARRIER]	ZZ000 – ZZ999	ACTYPE
[dbo].[FLT_REF_ANP_EQUIPMENT_DEFAULT]	MIT0 – MIT999	ANP_AIRPLANE_ID
[dbo].[FLT_ANP_BADA_ENERGYSHARE]	MIT0 – MIT999	ANP_AIRPLANE_ID

Flight Trajectory

To compare the uncertainty quantification results with one another, deterministic AEDT flight trajectories were selected and used for all the scenarios flown in the AEDT module. The flight trajectories were selected from a 2006 representative day flight scenario database (Administration, 2013). Using the representative day, the flights associated with the Boeing 737-700 aircraft were extracted as possible flight trajectories since the Boeing 737-800 was not comprehensively represented in the 2006 day flight scenario database. Of the 900 possible flight trajectories (e.g., departure – arrival airport combinations), for computational resource purposes, only 20 flight trajectories were selected. The 20 flight trajectories are given in Table 16 and shown in Figure 12. For simplification purposes, these flight trajectories are approximated using a great circle path from the departure airport to the arrival airport.

Table 16: UQ study AEDT flight trajectories

Flight	Depart Airport	Depart Runway	Arrival Airport	Arrival Runway	Range [nmi]
1	KDTW	04L	KPVD	23	535
2	KIAH	26L	KLAX	24L	1197
3	KLGA	22	KMEM	27	835
4	KDTW	04L	KSFO	28R	1801
5	KPDX	28R	KLAX	24L	725
6	KMIA	08L	KDEN	35R	1482
7	KPDX	28L	KABQ	08	964
8	KJFK	31R	KLGB	16L	2138
9	KIAD	01R	KORD	28	511
10	KPHX	26	KMSP	35	1106
11	KBWI	28	KFLL	09L	806
12	KPHX	26	KFLL	09L	1710
13	KMCO	35L	KDCA	01	662
14	KIAH	26L	KBOS	27	1387
15	KMCO	17R	KMKE	07R	928
16	KSJC	30R	KIAD	19L	2082
17	KSFO	28L	KPHX	25L	565
18	KDFW	35L	KSFO	28R	1270
19	KPHL	09R	KFLL	09L	864
20	KCLE	24L	KSFO	28R	1874

The flight procedure used in this study was the AEDT sensor path flight procedure. A sensor path flight procedure requires the aircraft's latitude, longitude, altitude, and true airspeed along the flight path from departure airport to arrival airport. Using the TASOpt module and respective optimal aircraft configurations, the sensor path data points were generated by flying each optimal aircraft in TASOpt over the ranges specified in Table 16. The resulting TASOpt output which included distance, altitude, and true airspeed are converted to sensor path data points and formatted into an AEDT Standard Input File (ASIF). With the ASIF, shown in Appendix C, an AEDT Study can be created and initialized. When an AEDT Study is generated so are the SQL databases belonging to the AEDT Study. Therefore, a user may now modify existing aircraft in the AEDT Study by manipulating the SQL databases. For computational purposes, the ASIF shown in Appendix C only imports a single aircraft (e.g., MIT0). However, the goal is to simulate 1000 aircraft simultaneously in AEDT. Therefore, the operations belonging to the single aircraft (e.g., MIT0) are duplicated 999 times for the remaining aircraft (e.g., MIT1 – MIT999). To duplicate the operations two update SQL scripts are required; one script updates [TEST].[dbo].[AIR_OPERATION_AIRCRAFT] and another script updates [TEST].[dbo].[AIR_OPERATION] as described in Appendix D.

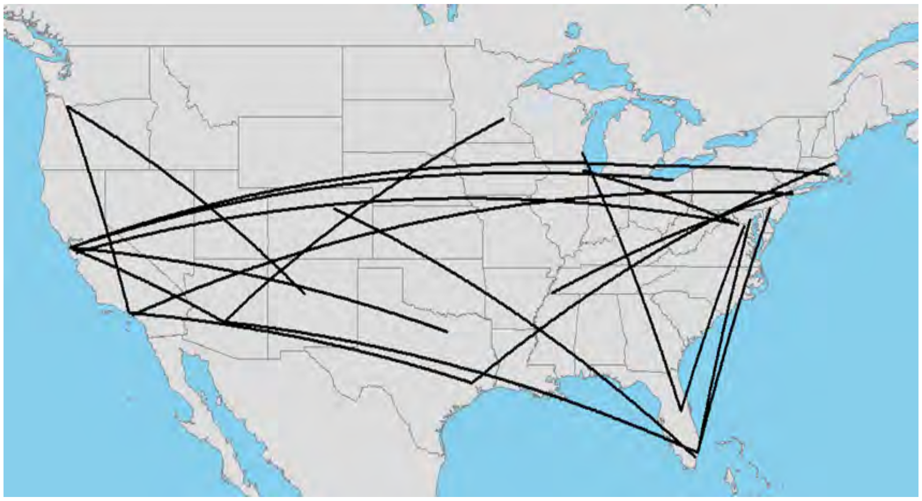

Figure 12: AEDT UQ 20 great circle flight trajectories

AEDT Run Study

At this point in the analysis the AEDT Study contains 1000 unique aircraft configurations and 20 flight trajectories which will result in 20,000 individual flights. With the AEDT study loaded in the SQL database all other operations regarding pre-processing, simulation, and post-processing can be performed without the AEDT graphical user interface. For propose of demonstration we will assume the AEDT study is named “B738”.

Before executing the AEDT study, we would need to modify the 1000 aircraft configurations currently in the AEDT study fleet database to represent 1000 aircraft configuration realizations from the UQ results. Modifying these aircraft requires generating the individual AEDT coefficients which would represent the aircraft, followed by importing the data into the appropriate place holders in the AEDT study FLEET database. To import data into the AEDT Study FLEET database in batch mode requires the following command,

```
sqlcmd -E -S B738 -i DATA.sql
```

where “B738” is the SQL database server name, automatically named after the AEDT study, and “DATA.sql” is the SQL file information regarding the 1000 aircraft realizations. The process of generating these AEDT aircraft realizations is discussed in Section 2.

Prior to running AEDT in batch mode the AEDT results, if they exist, need to be deleted. This is done using the following command while in the AEDT folder (e.g., C:/AEDT).

```
./FAA.AEE.AEDT.RemoveResults.exe NAME B738 ALL
```

To run the AEDT study in batch mode, use the following command while in the AEDT_RunStudy folder (e.g., C:/AEDT_RunStudy).

./FAA.AEE.AEDT.RunStudy B738 /a=C:/AEDT

To read the AEDT output data in the AEDT SQL databases requires converting the results from binary to text using a post-processing command while in the AEDT folder (e.g., C:/AEDT).

./FAA.AEE.AEDT.DeserializeEmissions.exe B738 1

Finally, to extract the text results out of the AEDT SQL database requires the following SQL script.

```
SET NOCOUNT ON;
SELECT s.[CASE_ID], e.[mode], e.[FUEL_BURN], e.[CO2], e.[CO], e.[NOX]
FROM [B738].[dbo].[RSLT_EMISSIONS] e
JOIN [B738].[dbo].[EVENT_RESULTS_SOURCE] s
ON e.EVENT_RESULTS_SOURCE_ID = s.EVENT_RESULTS_SOURCE_ID
JOIN [B738].[dbo].[AIR_OPERATION] o
ON s.AIR_OP_ID = o.AIR_OP_ID
JOIN [B738].[dbo].[AIR_OPERATION_AIRCRAFT] a
ON o.AIRCRAFT_ID = a.AIRCRAFT_ID
JOIN [B738].[dbo].[FLT_EQUIPMENT] f
ON a.EQUIPMENT_ID = f.EQUIP_ID
WHERE s.JOB_ID = 1
AND e.EMISSIONS_TYPE = 53
AND f.ANP_AIRPLANE_ID = 'MITXXX'
```

Here ‘MITXXX’ represents an aircraft of interest selected out of the 1000 aircraft realizations simulated by AEDT. A user may also extract the text results from the SQL database in batch mode using a similar command to that used for importing 1000 aircraft configurations into the AEDT Study FLEET database.

Section 4

TASOpt-AEDT Connection

This chapter presents the process of transferring the TASOpt aircraft performance outputs to AEDT aircraft performance inputs. The first section discusses the format of the TASOpt output and AEDT input. The second section will derive the relationship between TASOpt outputs and AEDT inputs. The final section validates the transformation by comparing the results obtained from TASOpt and AEDT over similar flight paths.

Data Format

The TASOpt output was previously shown in Table 1. The output file contains the following vector which defines the aircraft structure,

$$\mathbf{A} = \begin{Bmatrix} MTOW\ [lb] \\ W_{empty}\ [lb] \\ W_{max,fuel}\ [lb] \\ S\ [ft^2] \\ F_{max}\ [kN] \end{Bmatrix}. \qquad \text{Eq. 7}$$

The output file also contains a matrix with 1500 rows (100 missions by 15 flight segments) by 12 columns. The 15 flight segments consist of 3 takeoff segments, 5 climb segments, 2 cruise segments, and 5 descent segments as shown in Figure .

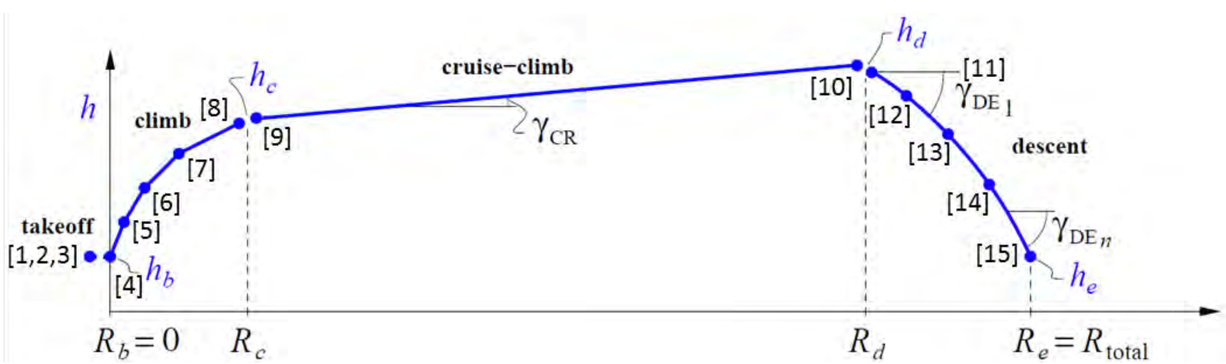

Figure 13: TASOpt flight segment breakdown.

For a given mission M (e.g., 100 possible flight missions) and flight segment S (e.g., 15 possible flight segments) the column entries of the matrix are given by the following vector,

$$\mathbf{B}(i,:) = \left\{ \begin{array}{c} R\ [nmi] \\ h\ [ft] \\ V_{TAS}\ [knts] \\ M\ [-] \\ C_L\ [-] \\ \dfrac{C_L}{C_D}\ [-] \\ \dfrac{W}{MTOW}\ [-] \\ F_{eng}\ [kN] \\ \dot{m}_f\ [kg\ sec^{-1}] \\ Angle\ [deg] \\ T_O\ [K] \\ P_O [Pa] \end{array} \right\}^T . \qquad \text{Eq. 8}$$

For example, $\mathbf{B}(M \cdot 15 + S,:)$ represents the aircraft performance at mission M and flight segment S. The first 50 missions are flown under ISA conditions (e.g., $T_{O,TO} = 0$) and the remaining 50 missions are flown under non-ISA conditions (e.g., $T_{O,TO} \neq 0$).

The AEDT inputs are the SQL FLEET database tables given in Table 15. The objective is to determine the appropriate coefficient in the SQL FLEET database tables that would accurately represent the aircraft flight performance computed by TASOpt. Using these SQL FLEET database tables, a user may import this information into AEDT and fly an aircraft in AEDT which was designed in TASOpt. The next section will look at each individual table and transform the data in $\mathbf{A}$ and $\mathbf{B}$ into the necessary table entries.

Transformation

The following section presets the transformation from TASOpt output to AEDT input. The discussion assumes FLEET_ID is 60000, BADA_ID is 'ZZ000', and the SQL database name is FLEET. The section will first introduce each AEDT table along with the description of the AEDT table followed by a TASOpt transformation table describing the variables in the AEDT table. The transformations were obtained using engineering judgment while attempting to duplicate the AEDT Boeing 737-800 aircraft coefficients from TASOpt flight performance outputs.

FLT_FLEET

```
UPDATE [FLEET].[dbo].[FLT_FLEET] SET
[MAX_TAKEOFF_WGT]                       = Var1,
[MAX_LANDING_WGT]                       = Var2,
[ENG_PRESSURE_RATIO]                    = Var3,
[ENG_MAX_RATED_THRUST]                  = Var4,
[AEDT_OPERATING_EMPTY_WEIGHT_LBS]       = Var5,
[MAX_PAYLOAD]                           = Var6,
[FUEL_CAPACITY_US_GALS_FLOAT]           = Var7
WHERE [FLEET_ID] = 60000
```

Name	Description	Unit	TASOpt
Var1	MTOW	[kg]	$\mathbf{A}(1) \cdot \mathrm{lb\_kg}$
Var2	Max Landing Weight	[kg]	$(\mathbf{A}(1) - \mathbf{A}(3) \cdot 0.85) \cdot \mathrm{lb\_kg}$
Var3	OPR	[-]	Random Variable
Var4	Engine Max Thrust	[kN]	$\mathbf{A}(5)$
Var5	Empty Weight	[kg]	$\mathbf{A}(2)$
Var6	Max Payload	[kg]	$215 \cdot 180 = 38{,}700 \cdot \mathrm{lb\_kg}$
Var7	Fuel Capacity	[gal]	$\mathbf{A}(3) \cdot \rho_{fuel}$

The fuel for this study is Kerosene which has a weight of 6.75 [lb] per gallon, $\rho_{fuel} = 1/6.75$.

FLT_BADA_THRUST

UPDATE [FLEET].[dbo].[FLT_BADA_THRUST] SET					
[COEFF_TC1]	=	$\boldsymbol{TC_{C1}}$,	[COEFF_TC2]	=	$\boldsymbol{TC_{C2}}$,
[COEFF_TC3]	=	$\boldsymbol{TC_{C3}}$,	[COEFF_TC4]	=	$\boldsymbol{TC_{C4}}$,
[COEFF_TC5]	=	$\boldsymbol{TC_{C5}}$,	[COEFF_TDL]	=	$\boldsymbol{TC_{D,LO}}$,
[COEFF_TDH]	=	$\boldsymbol{TC_{D,HI}}$,	[DES_ALT]	=	$\boldsymbol{h_{DES}}$,
[COEFF_TAPP]	=	$\boldsymbol{TC_{APP}}$,	[COEFF_TLD]	=	$\boldsymbol{TC_{LD}}$,
[DES_CAS]	=	$\boldsymbol{V_{D,CAS}}$,	[DES_MACH]	=	$\boldsymbol{M_{DES}}$
WHERE [BADA_ID] = **'ZZ000'**					

AEDT (3.6.3.14)

The maximum total net thrust [N] during climb in ISA conditions is given by:

$$F_{m,C_{ISA}} = TC_{C1} \cdot \left(1 - \frac{h}{TC_{C2}} + TC_{C3} \cdot h^2\right) \qquad \textbf{Eq. 9}$$

where

h	aircraft altitude above mean sea level [ft]
TC_{C1}	1st max climb thrust coefficient [N]
TC_{C2}	2nd max climb thrust coefficient [ft]
TC_{C3}	3rd max climb thrust coefficient [ft^2]

TASOpt

AEDT maximum net thrust is total aircraft thrust whereas TASOpt engine thrust output is per engine, therefore the TASOpt engine thrust must be multiplied by number of engines.

Mission	Segment	AEDT	TASOpt
[1:50]	[5:8]	$F_{m,C_{ISA}}$	$\mathbf{B}(M * 15 + S, 8) \cdot n_{eng} \cdot N\_kN$
[1:50]	[5:8]	h	$\mathbf{B}(M * 15 + S, 2)$

AEDT (3.6.3.14)

The maximum total net thrust [N] during climb for all weather contexts is given by:

$$F_{mC} = F_{m,C_{ISA}} \cdot \left(1 - TC_{C5} \cdot \Delta T_{ISA_{eff}}\right) \qquad \textbf{Eq. 10}$$

with

$$\Delta T_{ISA_{eff}} = \Delta T_{ISA} - TC_{C4}$$

and the limitations that

$$0.0 \leq TC_{C5} \cdot \Delta T_{ISA_{eff}} \leq 0.4$$

and

$$TC_{C5} \geq 0.0$$

where

ΔT_{ISA}	Atmospheric temperature deviation from ISA [K]
TC_{C4}	4^{th} thrust temperature coefficient [K]
TC_{C5}	5^{th} thrust temperature coefficient [K^{-1}]

TASOpt

Mission	Segment	AEDT	TASOpt
[51:100]	[2:7]	F_{mC}	$\mathbf{B}(M * 15 + S, 8) \cdot n_{eng} \cdot N\_kN$
[51:100]	[2:7]	ΔT_{ISA}	$\mathbf{B}(M * 15 + S, 10) - T_{ISA}(h)$
[51:100]	[2:7]	TC_{C5}	$\max(TC_{C5}, 0)$

AEDT (3.6.3.14)

The standard total net thrust [N] during descent is given by:

$$F_{mD} = \begin{cases} TC_{D,HI} \cdot F_{mC} \ (h > h_{DES}) \\ TC_{D,LO} \cdot F_{mC} \ (h \leq h_{DES}) \end{cases} \quad \textbf{Eq. 11}$$

$$F_{mD} = TC_{APP} \cdot F_{mC} \ (h \leq 1000\ [ft]) \quad \textbf{Eq. 12}$$

$$F_{mD} = TC_{LD} \cdot F_{mC} \ (h \leq 100\ [ft]) \quad \textbf{Eq. 13}$$

$$M_{DES} \quad \textbf{Eq. 14}$$

$$V_{D,CAS} \quad \textbf{Eq. 15}$$

where

h_{des}	Transition altitude for calculation of descent thrust [ft]
$TC_{D,HI}$	High altitude descent thrust coefficient [-]
$TC_{D,LO}$	Low altitude descent thrust coefficient [-]
TC_{APP}	Approach thrust coefficient [-]
TC_{LD}	Landing thrust coefficient [-]
M_{DS}	Descent Mach Number [-]
$V_{D,CAS}$	Descent Calibrated Airspeed [kt]

Air density and calibrated airspeed are computed as follows,

$$\rho(h) = \frac{\gamma \cdot P(h)}{(\gamma - 1) \cdot C_p \cdot T(h)} \qquad \textbf{Eq. 16}$$

$$V_{CAS} = \sqrt{\frac{2 \cdot P_{ISA,0}}{\frac{\gamma - 1}{\gamma} \cdot \rho} \cdot \left(\left(1 + \frac{P(h)}{P_{ISA,0}} \cdot \left(1 + \frac{\gamma - 1}{\gamma} \cdot \frac{\rho(h) \cdot V_{TAS}{}^2}{2 \cdot P_0(h)} \right)^{\frac{1}{\mu}} \right)^{\mu} - 1 \right)} \qquad \textbf{Eq. 17}$$

where $P_{ISA,0} = 101.325\ [kPA]$, $\gamma = 1.4$, and $C_p = 1004.0$.

TASOpt

Mission	Segment	AEDT		TASOpt
[1:100]	[14]	h_{DES}		$\mathbb{E}_M\left[\mathbb{E}_S[\mathbf{B}(:,2)]\right]$
[1:100]	[11:14]	M_{DES}		$\mathbb{E}_M\left[\mathbb{E}_S[\mathbf{B}(:,4)]\right]$
[1:100]	[12:14]	$V_{D,CAS}$		$\mathbb{E}_M\left[\mathbb{E}_S[V_{CAS}]\right] \cdot kt\_ms^{-1}$
[1:100]	[12:13]	F_{mD}	$TC_{D,HI}$	$\mathbf{B}(M * 15 + S, 8) \cdot n_{eng} \cdot N\_kN$
[1:100]	[14]	F_{mD}	$TC_{D,LO}$	$\mathbf{B}(M * 15 + S, 8) \cdot n_{eng} \cdot N\_kN$
[1:100]	[15]	F_{mD}	TC_{APP}	$\mathbf{B}(M * 15 + S, 8) \cdot n_{eng} \cdot N\_kN$
[1:100]	[15]	F_{mD}	TC_{LD}	$\mathbf{B}(M * 15 + S, 8) \cdot n_{eng} \cdot N\_kN$

FLT_BADA_ACFT

UPDATE [FLEET].[dbo].[FLT_BADA_ACFT] SET
[MASS_REF] = $\boldsymbol{M_{ref}}$, [MASS_MIN] = $\boldsymbol{M_{min}}$,
[MASS_MAX] = $\boldsymbol{M_{max}}$, [MASS_PAYLD] = $\boldsymbol{M_{pay}}$,
[MASS_GRAD] = $\boldsymbol{G_w}$, [FENV_VMO] = $\boldsymbol{V_{MO}}$,
[FENV_MMO] = $\boldsymbol{M_{MO}}$, [FENV_ALT] = $\boldsymbol{h_{MO}}$,
[FENV_HMAX] = $\boldsymbol{h_{max}}$, [FENV_TEMP] = $\boldsymbol{G_t}$,
[WING_AREA] = $\boldsymbol{A(4)}$, [COEFF_CLBO] = $\boldsymbol{C_{Lbo(M=0)}}$,
[BUFF_GRAD] = $\boldsymbol{k}$, [COEFF_CM16] = **0** ,
[NUM_ENGS] = $\boldsymbol{n_{eng}}$
WHERE [BADA_ID] = **'ZZ001'**

AEDT

M_{ref}	Reference Aircraft Mass
M_{min}	Minimum Aircraft Mass
M_{max}	Maximum Aircraft Mass
M_{pay}	Maximum Payload Mass
V_{MO}	Maximum Operational Speed
M_{MO}	Maximum Operational Mach Number
h_{MO}	Maximum operational height above sea level
h_{max}	Maximum altitude at MTOW under ISA conditions for max mass

TASOpt

Mission	Segment	AEDT	TASOpt
[1:100]	[1:15]	M_{ref}	$\boldsymbol{A}(1) \cdot \mathbb{E}_M\left[\mathbb{E}_S[\mathbf{B}(M * 15 + S, 7)]\right] \cdot lb\_ton$
-	-	M_{min}	$\boldsymbol{A}(2) \cdot lb\_ton$
-	-	M_{max}	$\boldsymbol{A}(1) \cdot lb\_ton$
-	-	M_{pay}	$215 \cdot 180 = 37{,}800 \cdot lb\_ton$
[1:100]	[1:15]	V_{MO}	$max_M\left[max_S[\mathrm{V}_{CAS}]\right] \cdot kt\_ms^{-1}$
[1:100]	[1:15]	M_{MO}	$max_M\left[max_S[\mathbf{B}(M * 15 + S, 4)]\right]$
[1:100]	[1:15]	h_{MO}	$max_M\left[max_S[\mathbf{B}(M * 15 + S, 2)]\right]$
[1]	[9]	h_{max}	$\mathbf{B}(M * 15 + S, 2)$

AEDT: 3.6.3.1.5

The maximum altitude achievable by the aircraft h_m [ft] is given by:

$$h_m = \min\left[h_{Mo}, h_{max} + \left(\Delta T_{ISA} - C_{T_{C4}}\right) \cdot G_t + (m_{max} - m) \cdot G_w\right] \qquad \text{Eq. 18}$$

where

G_w	Mass gradient on maximum altitude [ft]
G_t	Temperature gradient on maximum altitude [ft K^{-1}]
m	Aircraft mass [kg]
m_{max}	Maximum Mass [kg]

TASOpt

Mission	Segment	AEDT	TASOpt
-	-	m_{max}	$\mathbf{A}(1) \cdot lb\_kg$
[1:100]	[8:10]	m	$\mathbf{A}(1) \cdot \mathbf{B}(M * 15 + S, 7) \cdot lb\_kg$
[1:100]	[8:10]	ΔT_{ISA}	$\mathbf{B}(M * 15 + S, 10) - T_{ISA}(h)$

BADA: 3.6.2 (BADA Tech. Manual)

For jet aircraft a low speed buffeting limit has been introduced. This buffeting limit is expressed as a Mach number and can be determined using the following equation:

$$k \cdot M^3 - C_{Lbo(M=0)} \cdot M^2 + \frac{W}{S \cdot p \cdot 0.583} = 0 \qquad \textbf{Eq. 19}$$

where

k	Lift coefficient gradient
$C_{Lbo(M=0)}$	Initial buffet onset lift coefficient for $M = 0$
p	Actual pressure [Pa]
M	Mach Number
S	Wing Reference Area $[m^3]$
W	Aircraft Weight [N]

TASOpt

Mission	Segment	AEDT	TASOpt
[1:100]	[3 4]	W	$\mathbf{A}(1) \cdot \mathbf{B}(M * 15 + S, 7) \cdot lb\_N$
[1:100]	[3 4]	M	$\mathbf{B}(M * 15 + S, 4)$
-	-	S	$\mathbf{A}(4) \cdot ft^2\_m^2$
[1:100]	[3 4]	p	$\mathbf{B}(M * 15 + S, 11)$

FLT_BADA_CONFIG

UPDATE [FLEET].[dbo].[FLT_BADA_CONFIG] SET [VSTALL] = $\boldsymbol{V_{stall_{AP}}}$, [COEFF_CD0] = $\boldsymbol{C_{D0,AP}}$, [COEFF_CD2] = $\boldsymbol{C_{D2,AP}}$ WHERE [BADA_ID] = **'ZZ001'** AND [PHASE] = **'AP'** UPDATE [FLEET].[dbo].[FLT_BADA_CONFIG] SET [VSTALL] = $\boldsymbol{V_{stall_{CR}}}$, [COEFF_CD0] = $\boldsymbol{C_{D0,CR}}$, [COEFF_CD2] = $\boldsymbol{C_{D2,CR}}$ WHERE [BADA_ID] = **'ZZ001'** AND [PHASE] = **'CR'** UPDATE [FLEET].[dbo].[FLT_BADA_CONFIG] SET [VSTALL] = $\boldsymbol{V_{stall_{IC}}}$, [COEFF_CD0] = $\boldsymbol{C_{D0,IC}}$, [COEFF_CD2] = $\boldsymbol{C_{D2,IC}}$ WHERE [BADA_ID] = **'ZZ001'** AND [PHASE] = **'IC'** UPDATE [FLEET].[dbo].[FLT_BADA_CONFIG] SET [VSTALL] = $\boldsymbol{V_{stall_{LD}}}$, [COEFF_CD0] = $\boldsymbol{C_{D0,LD}}$, [COEFF_CD2] = $\boldsymbol{C_{D2,LD}}$ WHERE [BADA_ID] = **'ZZ001'** AND [PHASE] = **'LD'** UPDATE [FLEET].[dbo].[FLT_BADA_CONFIG] SET [VSTALL] = $\boldsymbol{V_{stall_{TO}}}$, [COEFF_CD0] = $\boldsymbol{C_{D0,TO}}$, [COEFF_CD2] = $\boldsymbol{C_{D2,TO}}$ WHERE [BADA_ID] = **'ZZ001'** AND [PHASE] = **'TO'**

AEDT: 3.6.3.1.3

Coefficient of Drag C_D (N) is calculated from:

$$C_D = C_{D0,X} + C_{D2,X} \cdot \left(\frac{W}{\frac{1}{2} \cdot \rho \cdot S \cdot {V_{TAS}}^2} \right)^2 = C_{D0,X} + C_{D2,X} \cdot (C_L)^2 \qquad \textbf{Eq. 20}$$

where

$C_{D0,X}$	Parasitic drag coefficient in X condifiguration [-]
$C_{D2,X}$	Induced drag coefficient in X condifiguration [-]
C_L	Coefficient of Lift [-]
ρ	Atmospheric Density [kg m^{-3}]
V_{TAS}	Aircraft True Airspeed [m s^{-1}]
S	Wing Reference Area [m^3]
W	Aircraft Weight [N]

TASOpt

Mission	Segment	AEDT		TASOpt
[1:100]	[2 3]	C_D	$X = TO$	$\mathbf{B}(M * 15 + S, 6)/\mathbf{B}(M * 15 + S, 5)$
[1:100]	[2 3]	C_L	$X = TO$	$\mathbf{B}(M * 15 + S, 5)$
[1:100]	[4:7]	C_D	$X = CL$	$\mathbf{B}(M * 15 + S, 6)/\mathbf{B}(M * 15 + S, 5)$
[1:100]	[4:7]	C_L	$X = CL$	$\mathbf{B}(M * 15 + S, 5)$
[1:100]	[9 10]	C_D	$X = CR$	$\mathbf{B}(M * 15 + S, 6)/\mathbf{B}(M * 15 + S, 5)$
[1:100]	[9 10]	C_L	$X = CR$	$\mathbf{B}(M * 15 + S, 5)$
[1:100]	[12:13]	C_D	$X = AP$	$\mathbf{B}(M * 15 + S, 6)/\mathbf{B}(M * 15 + S, 5)$
[1:100]	[12:13]	C_L	$X = AP$	$\mathbf{B}(M * 15 + S, 5)$
[1:100]	[15]	C_D	$X = LD$	$\mathbf{B}(M * 15 + S, 6)/\mathbf{B}(M * 15 + S, 5)$
[1:100]	[15]	C_L	$X = LD$	$\mathbf{B}(M * 15 + S, 5)$

BADA: 3.5b (BADA Tech. Manual)

The minimum calibrated airspeed in X configuration is calculated from

$$V_{\min_X} = C_{V_{min}} \cdot V_{stall_X} \qquad \text{Eq. 21}$$

where

$C_{V_{min}}$	Minimum speed coefficient in non-take-off configuration [-]
V_{stall_X}	Aircraft's stall calibrated air speed in X configuration [kt]

where the stall speed is compute as

$$V_{TAS,stall} = \sqrt{\frac{2 \cdot W}{\rho \cdot S \cdot C_{L,max}}} \qquad \text{Eq. 22}$$

TASOpt

Mission	Segment	AEDT		TASOpt
[1:100]	[2]	V_{stall_X}	$X = TO$	Eq. 22
[1:100]	[4]	V_{stall_X}	$X = IC$	Eq. 22
[1:100]	[9 10]	V_{stall_X}	$X = CR$	Eq. 22
[1:100]	[14]	V_{stall_X}	$X = AP$	Eq. 22
[1:100]	[15]	V_{stall_X}	$X = LD$	Eq. 22

FLT_BADA_FUEL

UPDATE [FLEET].[dbo].[FLT_BADA_FUEL] SET [COEFF_CF1] = $\boldsymbol{C_{f_1}}$, [COEFF_CF2] = $\boldsymbol{C_{f_2}}$, [COEFF_CF3] = $\boldsymbol{C_{f_3}}$, [COEFF_CF4] = $\boldsymbol{C_{f_4}}$, [COEFF_CFCR] = $\boldsymbol{C_{f_{CR}}}$ WHERE [BADA_ID] = **'ZZ001'**

AEDT: 3.4.1

The nominal total rate of fuel flow f_{nom} [kg min^{-1}] for an aircraft, which is applicable for all situations where the aircraft is neither in the cruise phase of flight nor operating at an idle thrust setting, is given by:

$$f_{nom} = \left(1 + \frac{V_{TAS}}{C_{f_2}}\right) \cdot C_{f_1} \cdot F \qquad \textbf{Eq. 23}$$

where

- F Aircraft total net thrust from its engine [nK]
- C_{f_1} Aircraft-specific 1st thrust specific fuel consumption coefficient [kg min^{-1} kN^{-1}]
- C_{f_2} Aircraft-specific 2nd thrust specific fuel consumption coefficient [kt]

TASOpt

Mission	Segment	AEDT	TASOpt
[1:100]	[4:8]	f_{nom}	$\mathbf{B}(M * 15 + S, 9) \cdot min\_sec$
[1:100]	[4:8]	F	$\mathbf{B}(M * 15 + S, 8) \cdot n_{eng}$
[1:100]	[4:8]	V_{TAS}	$\mathbf{B}(M * 15 + S, 3) \cdot kt\_ms^{-1}$

AEDT: 3.4.1

The BADA total fuel flow rate f_{min} [kg min^{-1}] for an aircraft in an idle state is given by:

$$f_{min} = \left(1 - \frac{h}{C_{f_4}}\right) \cdot C_{f_3} \qquad \textbf{Eq. 24}$$

where

- C_{f_3} Aircraft-specific 1st descent fuel flow coefficient [kg min^{-1}]
- C_{f_4} Aircraft-specific 2nd descent fuel flow coefficient [ft]
- h Altitude above MSL [ft]

TASOpt

Mission	Segment	AEDT	TASOpt
[1:100]	[11:14]	f_{min}	$\mathbf{B}(M * 15 + S, 9) \cdot min\_sec$
[1:100]	[11:14]	h	$\mathbf{B}(M * 15 + S, 2)$

AEDT: 3.4.1

The BADA total fuel flow rate f_{CR} [kg min^{-1}] for an aircraft in a cruise state is calculated by scaling the nominal flow rate:

$$f_{CR} = C_{f_{CR}} \cdot f_{nom} \qquad \textbf{Eq. 25}$$

where

$C_{f_{CR}}$ Aircraft-specific cruise flue flow correction coefficient [-]

TASOpt

Mission	Segment	AEDT	TASOpt
[1:100]	[9:10]	f_{CR}	$\mathbf{B}(M * 15 + S, 9) \cdot min\_sec$

FLT_BADA_APF

UPDATE [FLEET].[dbo].[FLT_BADA_APF] SET
[CL_CAS_1] = $\boldsymbol{V_{cl,1,AV}}$, [CL_CAS_2] = $\boldsymbol{V_{cl,2,AV}}$, [CL_MACH] = $\boldsymbol{M_{cl,AV}}$,
[CR_CAS_1] = $\boldsymbol{V_{cr,1,AV}}$, [CR_CAS_2] = $\boldsymbol{V_{cr,2,AV}}$, [CR_MACH] = $\boldsymbol{M_{cr,AV}}$,
[DE_CAS_1] = $\boldsymbol{V_{de,1,AV}}$, [DE_CAS_2] = $\boldsymbol{V_{de,2,AV}}$, [DE_MACH] = $\boldsymbol{M_{de,AV}}$
WHERE [BADA_ID] = **'ZZ001'** AND [MASS_RANGE] = **'AV'**
UPDATE [FLEET].[dbo].[FLT_BADA_APF] SET
[CL_CAS_1] = $\boldsymbol{V_{cl,1,HI}}$, [CL_CAS_2] = $\boldsymbol{V_{cl,2,HI}}$, [CL_MACH] = $\boldsymbol{M_{cl,HI}}$,
[CR_CAS_1] = $\boldsymbol{V_{cr,1,HI}}$, [CR_CAS_2] = $\boldsymbol{V_{cr,2,HI}}$, [CR_MACH] = $\boldsymbol{M_{cr,HI}}$,
[DE_CAS_1] = $\boldsymbol{V_{de,1,HI}}$, [DE_CAS_2] = $\boldsymbol{V_{de,2,HI}}$, [DE_MACH] = $\boldsymbol{M_{de,HI}}$
WHERE [BADA_ID] = **'ZZ001'** AND [MASS_RANGE] = **'HI'**
UPDATE [FLEET].[dbo].[FLT_BADA_APF] SET
[CL_CAS_1] = $\boldsymbol{V_{cl,1,LO}}$, [CL_CAS_2] = $\boldsymbol{V_{cl,2,LO}}$, [CL_MACH] = $\boldsymbol{M_{cl,LO}}$,
[CR_CAS_1] = $\boldsymbol{V_{cr,1,LO}}$, [CR_CAS_2] = $\boldsymbol{V_{cr,2,LO}}$, [CR_MACH] = $\boldsymbol{M_{cr,LO}}$,
[DE_CAS_1] = $\boldsymbol{V_{de,1,LO}}$, [DE_CAS_2] = $\boldsymbol{V_{de,2,LO}}$, [DE_MACH] = $\boldsymbol{M_{de,LO}}$
WHERE [BADA_ID] = **'ZZ001'** AND [MASS_RANGE] = **'LO'**

BADA: 4 (BADA Tech. Manual)

The following parameters are defined for each aircraft type to characterize the climb phase:

$$V_{cl,1} = Standard\ Climb\ CAS\ [kt]\ between\ 1{,}500/6{,}000\ [ft]\ and\ 10{,}000\ [ft] \quad \textbf{Eq. 26}$$

$$V_{cl,2} = Standard\ Climb\ CAS\ [kt]\ between\ 10{,}000\ [ft]\ and\ Mach\ transition\ altitude \quad \textbf{Eq. 27}$$

$$M_{cl} = Standard\ climb\ Mach\ number\ above\ Mach\ transition\ altitude \quad \textbf{Eq. 28}$$

where

AV Average mission flight range
HI High mission flight range
LO Low mission flight range

TASOpt

Mission	Segment	AEDT		TASOpt
[1:100]	[4:8]	LO_1		$\begin{pmatrix} \mathbf{B}(M*15+S,1) = LO \\ \mathbf{B}(M*15+S,2) < 10{,}000\ [ft] \end{pmatrix}$
[1:100]	[4:8]	LO_2		$\begin{pmatrix} \mathbf{B}(M*15+S,1) = LO \\ \mathbf{B}(M*15+S,2) > 10{,}000\ [ft] \end{pmatrix}$
[1:100]	[4:8]	$V_{cl,1}$	LO	$\mathbb{E}_M\left[\mathbb{E}_S[\mathbf{B}(M*15+S,3) \mid LO_1]\right] \cdot kt\_ms^{-1}$
[1:100]	[4:8]	$V_{cl,2}$	LO	$\mathbb{E}_M\left[\mathbb{E}_S[\mathbf{B}(M*15+S,3) \mid LO_2]\right] \cdot kt\_ms^{-1}$
[1:100]	[4:8]	M_{cl}	LO	$\mathbb{E}_M\left[\mathbb{E}_S[\mathbf{B}(M*15+S,4)\ ]\right]$
[1:100]	[4:8]	AV_1		$\begin{pmatrix} \mathbf{B}(M*15+S,1) = AV \\ \mathbf{B}(M*15+S,2) < 10{,}000\ [ft] \end{pmatrix}$
[1:100]	[4:8]	AV_2		$\begin{pmatrix} \mathbf{B}(M*15+S,1) = AV \\ \mathbf{B}(M*15+S,2) > 10{,}000\ \ [ft] \end{pmatrix}$
[1:100]	[4:8]	$V_{cl,1}$	AV	$\mathbb{E}_M\left[\mathbb{E}_S[\mathbf{B}(M*15+S,3) \mid AV_1]\right] \cdot kt\_ms^{-1}$
[1:100]	[4:8]	$V_{cl,2}$	AV	$\mathbb{E}_M\left[\mathbb{E}_S[\mathbf{B}(M*15+S,3) \mid AV_2]\right] \cdot kt\_ms^{-1}$
[1:100]	[4:8]	M_{cl}	AV	$\mathbb{E}_M\left[\mathbb{E}_S[\mathbf{B}(M*15+S,4)\ ]\right]$
[1:100]	[4:8]	HI_1		$\begin{pmatrix} \mathbf{B}(M*15+S,1) = HI \\ \mathbf{B}(M*15+S,2) < 10{,}000\ [ft] \end{pmatrix}$
[1:100]	[4:8]	HI_2		$\begin{pmatrix} \mathbf{B}(M*15+S,1) = HI \\ \mathbf{B}(M*15+S,2) > 10{,}000\ \ [ft] \end{pmatrix}$
[1:100]	[4:8]	$V_{cl,1}$	HI	$\mathbb{E}_M\left[\mathbb{E}_S[\mathbf{B}(M*15+S,3) \mid HI_1]\right] \cdot kt\_ms^{-1}$
[1:100]	[4:8]	$V_{cl,2}$	HI	$\mathbb{E}_M\left[\mathbb{E}_S[\mathbf{B}(M*15+S,3) \mid HI_2]\right] \cdot kt\_ms^{-1}$
[1:100]	[4:8]	M_{cl}	HI	$\mathbb{E}_M\left[\mathbb{E}_S[\mathbf{B}(M*15+S,4)\ ]\right]$

BADA: 4 (BADA Tech. Manual)

The following parameters are defined for each aircraft type to characterize the descent phase:

$V_{de,1} = Standard\ descent\ CAS\ [kt]\ between\ 1{,}500/6{,}000\ [ft]\ and\ 10{,}000\ [ft]$ **Eq. 29**

$V_{de,2} = Standard\ descent\ CAS\ [kt]\ between\ 10{,}000\ [ft]\ and\ Mach\ transition\ altitude$ **Eq. 30**

$M_{de} = Standard\ descent\ Mach\ number\ above\ Mach\ transition\ altitude$ **Eq. 31**

where

AV Average mission flight range

HI High mission flight range

LO Low mission flight range

TASOpt

Mission	Segment	AEDT		TASOpt
[1:100]	[11:15]	LO_1		$\begin{pmatrix} \mathbf{B}(M*15+S,1) = LO \\ \mathbf{B}(M*15+S,2) < 10{,}000\ [ft] \end{pmatrix}$
[1:100]	[11:15]	LO_2		$\begin{pmatrix} \mathbf{B}(M*15+S,1) = LO \\ \mathbf{B}(M*15+S,2) > 10{,}000\ [ft] \end{pmatrix}$
[1:100]	[11:15]	$V_{de,1}$	LO	$\mathbb{E}_M\left[\mathbb{E}_S[\mathbf{B}(M*15+S,3) \mid LO_1]\right] \cdot kt\_ms^{-1}$
[1:100]	[11:15]	$V_{de,2}$	LO	$\mathbb{E}_M\left[\mathbb{E}_S[\mathbf{B}(M*15+S,3) \mid LO_2]\right] \cdot kt\_ms^{-1}$
[1:100]	[11:15]	M_{de}	LO	$\mathbb{E}_M\left[\mathbb{E}_S[\mathbf{B}(M*15+S,4)\ ]\right]$
[1:100]	[11:15]	AV_1		$\begin{pmatrix} \mathbf{B}(M*15+S,1) = AV \\ \mathbf{B}(M*15+S,2) < 10{,}000\ [ft] \end{pmatrix}$
[1:100]	[11:15]	AV_2		$\begin{pmatrix} \mathbf{B}(M*15+S,1) = AV \\ \mathbf{B}(M*15+S,2) > 10{,}000\ \ [ft] \end{pmatrix}$
[1:100]	[11:15]	$V_{de,1}$	AV	$\mathbb{E}_M\left[\mathbb{E}_S[\mathbf{B}(M*15+S,3) \mid AV_1]\right] \cdot kt\_ms^{-1}$
[1:100]	[11:15]	$V_{de,2}$	AV	$\mathbb{E}_M\left[\mathbb{E}_S[\mathbf{B}(M*15+S,3) \mid AV_2]\right] \cdot kt\_ms^{-1}$
[1:100]	[11:15]	M_{de}	AV	$\mathbb{E}_M\left[\mathbb{E}_S[\mathbf{B}(M*15+S,4)\ ]\right]$
[1:100]	[11:15]	HI_1		$\begin{pmatrix} \mathbf{B}(M*15+S,1) = HI \\ \mathbf{B}(M*15+S,2) < 10{,}000\ [ft] \end{pmatrix}$
[1:100]	[11:15]	HI_2		$\begin{pmatrix} \mathbf{B}(M*15+S,1) = HI \\ \mathbf{B}(M*15+S,2) > 10{,}000\ \ [ft] \end{pmatrix}$
[1:100]	[11:15]	$V_{de,1}$	HI	$\mathbb{E}_M\left[\mathbb{E}_S[\mathbf{B}(M*15+S,3) \mid HI_1]\right] \cdot kt\_ms^{-1}$
[1:100]	[11:15]	$V_{de,2}$	HI	$\mathbb{E}_M\left[\mathbb{E}_S[\mathbf{B}(M*15+S,3) \mid HI_2]\right] \cdot kt\_ms^{-1}$
[1:100]	[11:15]	M_{de}	HI	$\mathbb{E}_M\left[\mathbb{E}_S[\mathbf{B}(M*15+S,4)\ ]\right]$

BADA: 4 (BADA Tech. Manual)

The following parameters are defined for each aircraft type to characterize the cruise phase:

$V_{cr,1} = Standard\ cruise\ CAS\ [kt]\ between\ 1{,}500/6{,}000\ [ft]\ and\ 10{,}000\ [ft]$ **Eq. 32**

$V_{cr,2} = Standard\ cruise\ CAS\ [kt]\ between\ 10{,}000\ [ft]\ and\ Mach\ transition\ altitude$ **Eq. 33**

$M_{cr} = Standard\ cruise\ Mach\ number\ above\ Mach\ transition\ altitude$ **Eq. 34**

where

AV Average mission flight range

HI High mission flight range

LO Low mission flight range

TASOpt

Mission	Segment	AEDT		TASOpt
[1:100]	[9 10]	LO		$\begin{pmatrix} \mathbf{B}(M*15+S,1) = LO \\ \mathbf{B}(M*15+S,2) > 10{,}000\ [ft] \end{pmatrix}$
[1:100]	[9 10]	$V_{cr,1}$	LO	$\mathbb{E}_M\left[\mathbb{E}_S[\mathbf{B}(M*15+S,3) \mid LO]\right] \cdot kt\_ms^{-1}$
[1:100]	[9 10]	$V_{cr,2}$	LO	$\mathbb{E}_M\left[\mathbb{E}_S[\mathbf{B}(M*15+S,3) \mid LO]\right] \cdot kt\_ms^{-1}$
[1:100]	[9 10]	M_{cr}	LO	$\mathbb{E}_M\left[\mathbb{E}_S[\mathbf{B}(M*15+S,4)\ ]\right]$
[1:100]	[9 10]	AV		$\begin{pmatrix} \mathbf{B}(M*15+S,1) = AV \\ \mathbf{B}(M*15+S,2) > 10{,}000\ [ft] \end{pmatrix}$
[1:100]	[9 10]	$V_{cr,1}$	AV	$\mathbb{E}_M\left[\mathbb{E}_S[\mathbf{B}(M*15+S,3) \mid AV]\right] \cdot kt\_ms^{-1}$
[1:100]	[9 10]	$V_{cr,2}$	AV	$\mathbb{E}_M\left[\mathbb{E}_S[\mathbf{B}(M*15+S,3) \mid AV]\right] \cdot kt\_ms^{-1}$
[1:100]	[9 10]	M_{cr}	AV	$\mathbb{E}_M\left[\mathbb{E}_S[\mathbf{B}(M*15+S,4)\ ]\right]$
[1:100]	[9 10]	HI		$\begin{pmatrix} \mathbf{B}(M*15+S,1) = HI \\ \mathbf{B}(M*15+S,2) > 10{,}000\ [ft] \end{pmatrix}$
[1:100]	[9 10]	$V_{cr,1}$	HI	$\mathbb{E}_M\left[\mathbb{E}_S[\mathbf{B}(M*15+S,3) \mid HI]\right] \cdot kt\_ms^{-1}$
[1:100]	[9 10]	$V_{cr,2}$	HI	$\mathbb{E}_M\left[\mathbb{E}_S[\mathbf{B}(M*15+S,3) \mid HI]\right] \cdot kt\_ms^{-1}$
[1:100]	[9 10]	M_{cr}	HI	$\mathbb{E}_M\left[\mathbb{E}_S[\mathbf{B}(M*15+S,4)\ ]\right]$

FLT_ANP_AIRPLANES

UPDATE [FLEET].[dbo].[FLT_ANP_AIRPLANES] SET
[MX_GW_TKO] = **Var1**, [MX_GW_LND] = **Var2**,
[THR_STATIC] = **Var3**, [MIN_BURN] = **Var4**,
[NUMB_ENG] = $\boldsymbol{n_{eng}}$
WHERE [ACFT_ID] = **'MIT1'**

AEDT:

Name	Description	Unit	TASOpt
Var1	WMTO	[lb]	$\mathbf{A}(1)$
Var2	Maximum Landing Weight	[lb]	$(\mathbf{A}(1) - \mathbf{A}(3) \cdot 0.85)$
Var3	100% Static Thrust	[lbf]	$\mathbf{A}(5) \cdot kN\_lbf$
Var4	Minimum Fuel Burn	[kg sec^{-1}]	$max_M\left[max_S[\mathbf{B}(M * 15 + S, 9)]\right] \cdot lb\_kg/n_{eng}$

FLT_ANP_AIRPLANE_THRUST_JET

UPDATE [FLEET].[dbo].[FLT_ANP_AIRPLANE_THRUST_JET] SET
[COEFF_E] = $\boldsymbol{E_{climb}}$, [COEFF_F] = $\boldsymbol{F_{climb}}$, [COEFF_GA] = $\boldsymbol{G_{A_{climb}}}$,
[COEFF_GB] = $\boldsymbol{G_{B_{climb}}}$, [COEFF_H] = $\mathbf{0}$
WHERE [ACFT_ID] = **'MIT1'** AND [THRUST_TYPE] = **'C'**
UPDATE [FLEET].[dbo].[FLT_ANP_AIRPLANE_THRUST_JET] SET
[COEFF_E] = $\boldsymbol{E_{takeoff}}$, [COEFF_F] = $\boldsymbol{F_{takeoff}}$, [COEFF_GA] = $\boldsymbol{G_{A_{takeoff}}}$,
[COEFF_GB] = $\boldsymbol{G_{B_{takeoff}}}$, [COEFF_H] = $\mathbf{0}$
WHERE [ACFT_ID] = **'MIT1'** AND [THRUST_TYPE] = **'T'**

AEDT:

Jet aircraft corrected net thrust per engine is calculated by using a modified version of SAE-AIR-1845 equation (A1):

$$\frac{F_n}{\delta} = E + F \cdot v + G_A \cdot h + G_B \cdot h^2 + H \cdot T_C \qquad \textbf{Eq. 35}$$

where

$\frac{F_n}{\delta}$	Corrected net thrust per engine [lbf]
v	Equivalent/calibrated airspeed [kt]
h	Pressure altitude [ft] MSL
T_C	Temperature (°C) at the aircraft
E, F, G_A, G_B, H	Regression coefficients that depend on power state (max take off and max climb) and temperature state (below and above engine break point temperature) [lbf, lbf/kt, lbf/ft, lbf/ft^2, lbf/°C] respectively

TASOpt

Mission	Segment	AEDT		TASOpt
[1:50]	[4:7]	v	Climb	V_{CAS}
[1:50]	[4:7]	h	Climb	$\mathbf{B}(M * 15 + S, 2)$
[1:50]	[4:7]	F_n	Climb	$\mathbf{B}(M * 15 + S, 8)$
[1:50]	[4:7]	δ	Climb	$\mathbf{B}(M * 15 + S, 12)/P_{ISA}(h)$
[1:50]	[2]	v	Climb	V_{CAS}
[1:50]	[2]	h	Climb	$\mathbf{B}(M * 15 + S, 2)$
[1:50]	[2]	F_n	Climb	$\mathbf{B}(M * 15 + S, 8)$
[1:50]	[2]	δ	Climb	$\mathbf{B}(M * 15 + S, 12)/P_{ISA}(h)$

FLT_ANP_AIRPLANE_TSFC_COEFFICIENTS

```
UPDATE [FLEET].[dbo].[FLT_ANP_AIRPLANE_TSFC_COEFFICIENTS] SET
[COEFF1]      = C1_arr,      [COEFF2]      = C2_arr,
[COEFF3]      = C3_arr,      [COEFF4]      = C4_arr
WHERE [ACFT_ID] = 'MIT1' AND [MODE] = 'A'
UPDATE [FLEET].[dbo].[FLT_ANP_AIRPLANE_TSFC_COEFFICIENTS] SET
[COEFF1]      = C1_dep,      [COEFF2]      = C2_dep,
[COEFF3]      = C3_dep,      [COEFF4]      = C4_dep
WHERE [ACFT_ID] = 'MIT1' AND [MODE] = 'D'
```

AEDT (3.4.2):

In the Senzig-Fleming-Lovinelli method, operation type and terminal area specific fuel burn methods developed by the Volpe National Transportation System Center are used. For this method, fuel flow rate per engine during departure $f_{n_{dep}}$ [kg min] is calculated as:

$$\frac{f_{n_{dep}}}{\sqrt{\theta}} = F_n \cdot \left(C_1 + C_2 \cdot M + C_3 \cdot h_{MSL} + C_4 \cdot \frac{F_n}{\delta}\right) \quad \textbf{Eq. 36}$$

where

- C_1 Aircraft-specific 1st terminal-area departure TSFC coefficient [kg min^{-1} kN^{-1}]
- C_2 Aircraft-specific 2nd terminal-area departure TSFC coefficient [kg min^{-1} kN^{-1}]
- C_3 Aircraft-specific 3rd terminal-area departure TSFC coefficient [kg min^{-1} kN^{-1}]
- C_4 Aircraft-specific 3rd terminal-area departure TSFC coefficient [kg min^{-1} kN^{-1}]
- h_{MSL} Aircraft altitude with respect to MSL [ft]
- M Aircraft Mach number [-]

θ	Ratio of temperature at aircraft altitude to seal level temperature [-]
F_n/δ	Aircraft corrected net thrust per engine [lbf]
F_n	Aircraft net thrust per engine [kN]

TASOpt

Mission	Segment	AEDT		TASOpt
[1:100]	[4:8]	$f_{n_{dep}}$	Depart	$\mathbf{B}(M * 15 + S, 9)$
[1:100]	[4:8]	M	Depart	$\mathbf{B}(M * 15 + S, 4)$
[1:100]	[4:8]	h_{MSL}	Depart	$\mathbf{B}(M * 15 + S, 2)$
[1:100]	[4:8]	F_n	Depart	$\mathbf{B}(M * 15 + S, 8)$
[1:100]	[4:8]	δ	Depart	$\mathbf{B}(M * 15 + S, 12)/P_0$
[1:100]	[4:8]	θ	Depart	$\mathbf{B}(M * 15 + S, 12)/T_0$

AEDT:

Fuel flow rate per engine during approach $f_{n_{arr}}$ [kg min^{-1}] is calculated as:

$$\frac{f_{n_{arr}}}{\sqrt{\theta}} = F_n \cdot \left(C_1 + C_2 \cdot M + C_3 \cdot e\left(\frac{-C_4 \cdot F_n/\delta}{F_{n_o}} \right) \right) \quad \textbf{Eq. 37}$$

where

F_{n_o}	ISA sea-level static thrust [lbf]
C_1	Aircraft-specific 1st terminal-area arrival TSFC coefficient [kg min^{-1} kN^{-1}]
C_2	Aircraft-specific 2nd terminal-area arrival TSFC coefficient [kg min^{-1} kN^{-1}]
C_3	Aircraft-specific 3rd terminal-area arrival TSFC coefficient [kg min^{-1} kN^{-1}]
C_4	Aircraft-specific 3rd terminal-area arrival TSFC coefficient [kg min^{-1} kN^{-1}]
M	Aircraft Mach number [-]
θ	Ratio of temperature at aircraft altitude to seal level temperature [-]
F_n/δ	Aircraft corrected net thrust per engine [lbf]
F_n	Aircraft net thrust per engine [kN]

TASOpt

Mission	Segment	AEDT		TASOpt
[1:100]	[11:14]	$f_{n_{arr}}$	Arrival	$\mathbf{B}(M * 15 + S, 9)$
[1:100]	[11:14]	M	Arrival	$\mathbf{B}(M * 15 + S, 4)$
[1:100]	[11:14]	h_{MSL}	Arrival	$\mathbf{B}(M * 15 + S, 2)$
[1:100]	[11:14]	F_n	Arrival	$\mathbf{B}(M * 15 + S, 8)$
[1:100]	[11:14]	δ	Depart	$\mathbf{B}(M * 15 + S, 12)/P_0$
[1:100]	[11:14]	θ	Depart	$\mathbf{B}(M * 15 + S, 12)/T_0$

FLT_ANP_AIRPLANE_FLAPS

```
UPDATE [FLEET].[dbo].[FLT_ANP_AIRPLANE_FLAPS] SET
[COEFF_R]    = R_{f,S=4},     [COEFF_C_D]  = C_{d,S=4},     [COEFF_B]    = B_{f,S=4}
WHERE [ACFT_ID] = 'MIT1' AND [FLAP_ID] = 'T_00'

UPDATE [FLEET].[dbo].[FLT_ANP_AIRPLANE_FLAPS] SET
[COEFF_R]    = R_{f,S=3},     [COEFF_C_D]  = C_{d,S=3},     [COEFF_B]    = B_{f,S=3}
WHERE [ACFT_ID] = 'MIT1' AND [FLAP_ID] = 'T_01'

UPDATE [FLEET].[dbo].[FLT_ANP_AIRPLANE_FLAPS] SET
[COEFF_R]    = R_{f,S=2},     [COEFF_C_D]  = C_{d,S=2},     [COEFF_B]    = B_{f,S=2}
WHERE [ACFT_ID] = 'MIT1' AND [FLAP_ID] = 'T_05'

UPDATE [FLEET].[dbo].[FLT_ANP_AIRPLANE_FLAPS] SET
[COEFF_R]    = R_{f,S=14},    [COEFF_C_D]  = C_{d,S=14}
WHERE [ACFT_ID] = 'MIT1' AND [FLAP_ID] = 'A_40'

UPDATE [FLEET].[dbo].[FLT_ANP_AIRPLANE_FLAPS] SET
[COEFF_R]    = R_{f,S=15},    [COEFF_C_D]  = C_{d,S=15}
WHERE [ACFT_ID] = 'MIT1' AND [FLAP_ID] = 'A_15'
```

AEDT (3.6.2.1.4.2):

The calibrated airspeed at the rotation point, which is used in the thrust equation, is calculated by using SAE-AIR-1845 equation (A7):

$$v_2 = C_f \cdot \sqrt{W} \qquad \textbf{Eq. 38}$$

where

v_2 Calibrated airspeed [kts] at takeoff rotation
C_f Takeoff speed coefficient that depends on flaps setting [kts $lbf^{-0.5}$]
W Departure profile weight [lbf]; weight is assumed to remain constant for the entire departure profile.

TASOpt

Mission	Segment	AEDT		TASOpt
[1:100]	[2:4]	v_2	Depart	V_{CAS}
[1:100]	[2:4]	W	Depart	$\mathbf{A}(1) \cdot \mathbf{B}(M * 15 + S, 7)$
[1:100]	[2:4]	C_f	Depart	$\mathbb{E}_M[v_2/W]$

AEDT:

Takeoff ground-roll distance is calculated by using SAD-AIR-1845 equation (A6):

$$S_g = \frac{B_f \cdot \theta \cdot \left(\frac{W}{\delta}\right)^2}{N \cdot \left(\frac{F_n}{\delta}\right)_2} \qquad \text{Eq. 39}$$

where

S_g Ground-roll distance [ft]
B_f Ground-roll coefficient, which depends on the flaps setting [ft lbf^{-1}]
θ Temperature ratio at the airport elevation [-]
δ Pressure ratio at the airport [-]
$\left(\frac{F_n}{\delta}\right)_2$ Corrected net thrust per engine [lbf] at takeoff rotation

where the ground roll distance is,

$$S_g = 1.21 \cdot \frac{\frac{W}{S}}{\rho \cdot C_l \cdot \frac{F_n \cdot n_{eng}}{W}}. \qquad \text{Eq. 40}$$

TASOpt

Mission	Segment	AEDT		TASOpt
[1:100]	[2]	S_g	Depart	Eq. 42

AEDT:

The average climb angle is calculated by using SAE-AIR-1845 equation (A8):

$$\gamma = \sin^{-1}\left(K \cdot \left[\frac{N \cdot \left(\frac{F_n}{\delta}\right)}{\frac{W}{\delta}}\right] - R_f\right) \qquad \textbf{Eq. 41}$$

where

γ	Average climb angle [radians]
K	Speed-dependent constant [-] K = 1.01 when climb speed ≤ 200 [kt]; K = 0.95 otherwise.
N	Number of enginers [-]
$\left(\frac{F_n}{\delta}\right)$	Nominal value of corrected net thrust per engine [lbf]
δ	Pressure ratio at the airport [-]
W	Departure profile weight [lbf]
R_f	Drag-over-lift coefficient that depends on the flaps on the setting [-]

TASOpt

Mission	Segment	AEDT		TASOpt
[1:100]	[2]	γ	Depart 1	$\mathbf{B}(M * 15 + S, 10)$
[1:100]	[4]	γ	Depart 2	$\mathbf{B}(M * 15 + S, 10)$
[1:100]	[5]	γ	Depart 3	$\mathbf{B}(M * 15 + S, 10)$

AEDT:

R_f is used to calculate the thrust needed, assuming a known value for descend angle γ.

$$\left(\frac{F_n}{\delta}\right)_2 = \frac{\left(\frac{W}{\delta_2}\right) \cdot \left(R_f - \frac{sin(\gamma)}{1.03}\right)}{N} \qquad \textbf{Eq. 42}$$

where

$\left(\frac{F_n}{\delta}\right)_2$	Corrected net thrust per engine [lbf] at altitude A_2
γ	Average descent angle (a positive value)

TASOpt

Mission	Segment	AEDT		TASOpt
[1:100]	[14]	γ	Arrival 15	$\mathbf{B}(M * 15 + S, 10)$
[1:100]	[15]	γ	Arrival 40	$\mathbf{B}(M * 15 + S, 10)$

AEDT:

D_f is a coefficient used by AEDT to calculate the landing speed. For a landing segment in AEDT the following equation is used:

$$D_f = \frac{V_1}{\sqrt{W}} \qquad \text{Eq. 43}$$

where

V_1 Calibrated airspeed [kt] just before landing

TASOpt

Mission	Segment	AEDT		TASOpt
[1:100]	[14]	V_1	Arrival 15	V_{CAS}
[1:100]	[15]	V_1	Arrival 40	V_{CAS}

FLT_ANP_AIRPLANE_PROFILES

```
UPDATE [FLEET].[dbo].[FLT_ANP_AIRPLANE_PROFILES]  SET
[WEIGHT]= W_A
WHERE [ACFT_ID] = 'MIT1' AND [OP_TYPE] = 'A' AND
[PROF_ID1] = 'STANDARD' AND [PROF_ID2] = 1

UPDATE [FLEET].[dbo].[FLT_ANP_AIRPLANE_PROFILES]  SET
[WEIGHT]= W_1,D
WHERE [ACFT_ID] = 'MIT1' AND [OP_TYPE] = 'D' AND
[PROF_ID1] = 'STANDARD' AND [PROF_ID2] = 1

UPDATE [FLEET].[dbo].[FLT_ANP_AIRPLANE_PROFILES]  SET
[WEIGHT]= W_2,D
WHERE [ACFT_ID] = 'MIT1' AND [OP_TYPE] = 'D' AND
```

```
[PROF_ID1] = 'STANDARD' AND [PROF_ID2] = 2

UPDATE [FLEET].[dbo].[FLT_ANP_AIRPLANE_PROFILES]  SET
[WEIGHT]= W_{3,D}
WHERE [ACFT_ID] = 'MIT1' AND [OP_TYPE] = 'D' AND
[PROF_ID1] = 'STANDARD' AND [PROF_ID2] = 3

UPDATE [FLEET].[dbo].[FLT_ANP_AIRPLANE_PROFILES]  SET
[WEIGHT]= W_{4,D}
WHERE [ACFT_ID] = 'MIT1' AND [OP_TYPE] = 'D' AND
[PROF_ID1] = 'STANDARD' AND [PROF_ID2] = 4

UPDATE [FLEET].[dbo].[FLT_ANP_AIRPLANE_PROFILES]  SET
[WEIGHT]= W_{5,D}
WHERE [ACFT_ID] = 'MIT1' AND [OP_TYPE] = 'D' AND
[PROF_ID1] = 'STANDARD' AND [PROF_ID2] = 5

UPDATE [FLEET].[dbo].[FLT_ANP_AIRPLANE_PROFILES]  SET
[WEIGHT]= W_{6,D}
WHERE [ACFT_ID] = 'MIT1' AND [OP_TYPE] = 'D' AND
[PROF_ID1] = 'STANDARD' AND [PROF_ID2] = 6
```

AEDT:

The airplane profiles define the aircraft's takeoff weight which is a function of flight range. We will assume for a flight range less than 450 [nmi] the aircraft weight is,

$$W_{min} = W_{empty} + W_{pax}, \qquad \textbf{Eq. 44}$$

for a flight range equal to 3000 [nmi] the aircraft weight is the $MTOW$. The remaining flight ranges are compute using linear interpolation from the minimum flight range to the maximum flight range. The AEDT input file uses 6 profile steps which represent the takeoff weight assuming the mission ranges are 0 – 449 [nmi], 450 – 999 [nmi] , 1000 – 1499 [nmi] , 1500 – 2499 [nmi] , 2500 – 3499 [nmi] , 3500 – 999 [nmi]. For this study, since the 20 flight trajectories are between 500 [nmi] and 2200 [nmi] the applicable profiles are 2, 3, and 4. Therefore, their respective interpolations are set to capture their maximum weight in the profile step.

TASOpt

AEDT		TASOpt
W_A		$\mathbf{A}(2) + 40{,}500 + (\mathbf{A}(1) - \mathbf{A}(3) \cdot 0.85)/10$
$W_{1,D}$	0 – 449 [nmi]	$\mathbf{A}(5) + \mathbf{A}(2)$ at 0 [nmi]
$W_{2,D}$	450 – 999 [nmi]	Interpolation using 999 [nmi]
$W_{3,D}$	1000 – 1499[nmi]	Interpolation using 1499 [nmi]
$W_{4,D}$	1500 – 2499 [nmi]	Interpolation using 2100 [nmi]
$W_{5,D}$	2500 – 3499 [nmi]	$\mathbf{A}(1)$ at 3000 [nmi]
$W_{6,D}$	3500 – 4499 [nmi]	Interpolation using 4499 [nmi]

FLT_AIRFRAMES

AEDT:

UPDATE [FLEET].[dbo].[FLT_AIRFRAMES] SET
[ENGINE_COUNT] = $\boldsymbol{n_{eng}}$
WHERE [AIRFRAME_ID] =**1001**

FLT_REF_ICAO_ACTYPES

AEDT:

UPDATE [FLEET].[dbo].[FLT_REF_ICAO_ACTYPES] SET
[ENGINE_COUNT] = $\boldsymbol{n_{eng}}$
WHERE [ICAO_ACTYPE] = **'ZZ001'**

Validation

The validation study compares the fuel burn between an aircraft in TASOpt and the same aircraft imported and flown in AEDT over the three flight scenarios shown in **Error! Reference source not found.**. The flight scenarios are great circle flights from Boston to Atlanta, Boston to Denver, and Boston to Los Angeles.

Figure 13: Validation trajectory for TASOpt & AEDT

To generate the AEDT sensor path the TASOpt module flew a total of 7 missions with each of the three aircraft configuration. The first mission sizes the aircraft to the optimal configuration, while the even and odd missions flew with different airport altitudes. For example, missions 2 and 3 in TASOpt flew Boston to Atlanta using the departure airport altitude (mission 2) and arrival airport altitude (mission 3). This way we could generate the flight trajectory (e.g., Boston to Atlanta) by splitting the TASOpt output in midflight therefore having the correct airport departure altitude (e.g., Boston mission 2) and correct arrival altitude (e.g., Atlanta mission 3). The flight trajectory data (e.g., latitude, longitude, altitude, and true airspeed) shown in **Error! Reference source not found.** is used to generate sensor path and populate the ASIF and the procedure discussed in the previous section is used to generate an AEDT version of the aircraft.

Error! Reference source not found. compares the fuel burn and net corrected thrust between the TASOpt and AEDT modules for the Boston to Atlanta flight. The results show the fuel burn and net corrected thrust match well between the two modules indicating the mapping from TASOpt to AEDT was successful. The arrival discrepancy is due to the difference between how

AEDT 2a and TASOpt pull out of the cruise segment. AEDT 2s assumes the aircraft is idle whereas TASOpt does not.

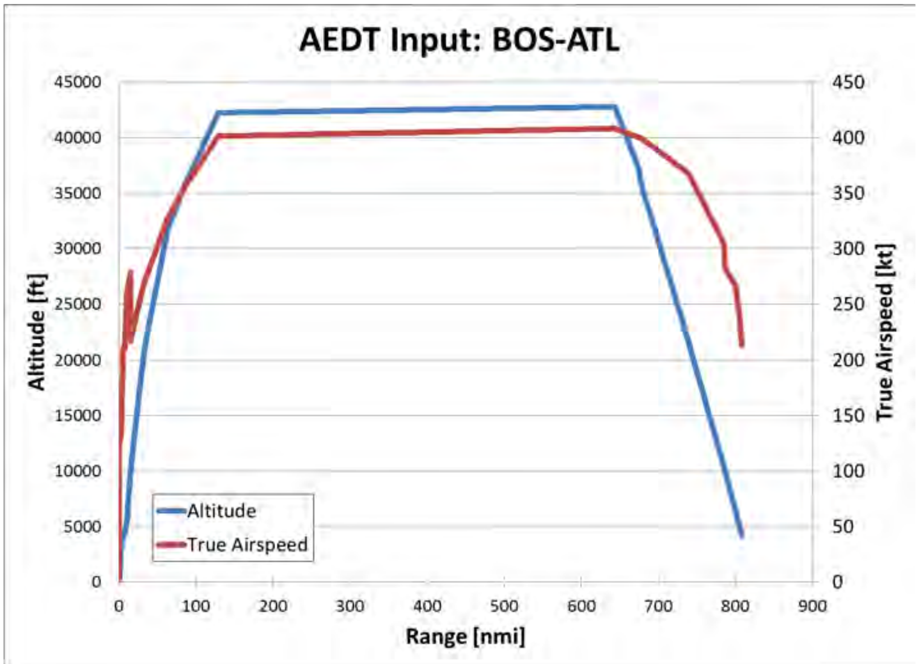

Figure 14: D8 with standard technology BOS-ATL flight sensor path altitude and true airspeed.

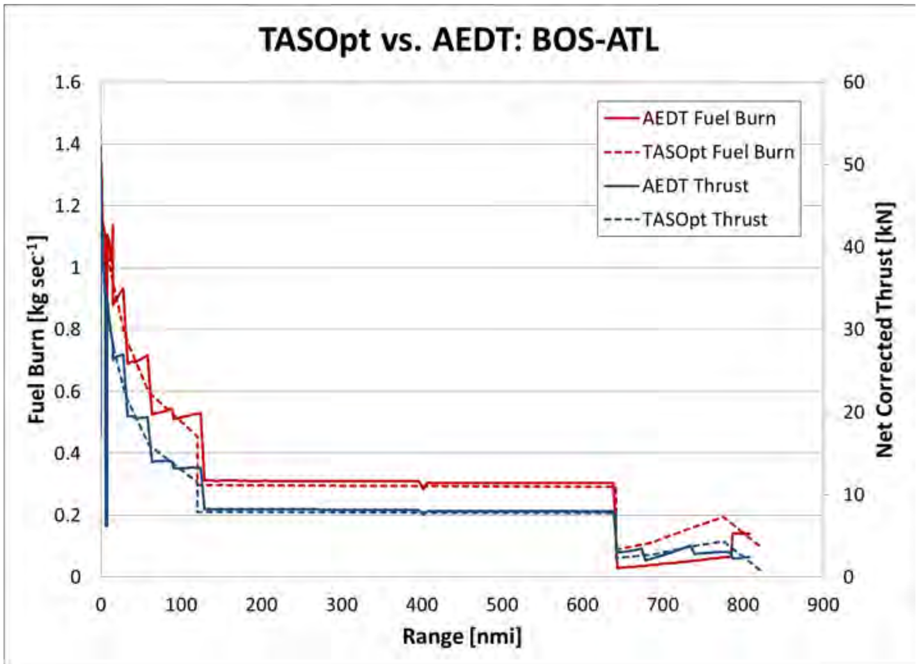

Figure 15: D8 with standard technology AEDT vs TASOpt BOS-ATL Fuel Burn and Net Correct Thrust Results.

The total fuel burn associated to a given flight segment is given in Table 17. The relative percent uncertainty is given in **Error! Reference source not found.**. The results show a good comparison between TASOpt and AEDT for the flight segments above 1,000 ft. We now discuss the discrepancies and possible sources of differences between modules. The flight from Boston to Denver performed worse then the other two flights due to the flight paths range. The Boston to Denver flight range is 1520 [nmi] which is in the lower range of the AEDT standard profile 3 (i.e., 1500 – 2499 [nmi]). The AEDT standard profile 3 takeoff weight was set to the TASOpt takeoff weight at 2499 [nmi]. As a result, the AEDT uses a takeoff weight which is significantly larger than the TASOpt takeoff weight resulting in a larger fuel burn by AEDT. The Atlanta and Los Angles flights had ranges of 850 [nmi] and 2300 [nmi] respectively which put the AEDT takeoff weight closer to the TASOpt takeoff weight. This resulted in a fairer agreement between the modules fuel burns. Further, AEDT assumes the aircraft is carrying 65% load capacity which when accounted for in TASOpt resulted in significant improvements between the modules results. Also, the flight segments which TASOpt and AEDT flew are slightly different (i.e.., +/- 1000 [ft]) due to AEDTs modification of the flight paths contained in the ASIF. Finally, we aware that there exists an unknown source of uncertainty which results in a 7% shift between AEDT and TASOpt-AEDT total fuel burn.

Table 17: (Data Not Final) Total fuel burn comparison between TASOpt and AEDT over three flight scenarios and five flight segments.

Segment Altitude [ft]	TASOpt BOS-ATL	AEDT BOS-ATL	TASOpt BOS-DEN	AEDT BOS-DEN	TASOpt BOS-LAX	AEDT BOS-LAX
Depart $\leq$ 1000	40.6	62.9	42.5	77.7	45.5	77.7
Depart $\leq$ 10000	298.9	314.5	310.9	328.3	324.6	328.7
Cruise $\geq$ 10000	2389.7	2315.3	4317.5	4441.8	6449.9	6422.6
Arrival $\leq$ 10000	96.1	114.2	82.2	98.8	98.9	115.6
Arrival $\leq$ 1000	9.3	24.9	8.2	15.8	9.5	25.7
$Total$	2784.7	2744.0	4710.6	4868.9	6873.4	6866.9

Table 18: TASOpt and AEDT comparison; total fuel burn and relative percent uncertainty.

	BOS-ATL		BOS-DEN		BOS-LAX	
	Total Fuel [lb]	% Difference	Total Fuel [lb]	% Difference	Total Fuel [lb]	% Difference
TASOpt	5015.6	-	8715.3	-	13186.4	-
AEDT	4885.1	-2.60%	9014.5	2.37%	12524.3	-5.02%
TASOpt-AEDT	5284.7	5.37%	9737.4	9.62%	13594.4	3.09%

Section 5

System-Level MCS Uncertainty Quantification

The uncertainty quantification results investigate the fuel energy consumption per payload range (PFEI) given as,

$$F = \frac{\sum_k W_{fuel_k} h_{fuel_k}}{\sum_k W_{pay_k} R_{total_k}}, \quad \text{Eq. 45}$$

where W_{fuel}^k is the total fuel burn, h_{fuel}^k is the fuel specific heat value, W_{pay}^k is the aircraft payload weight, R_{total}^k is the flight range, and k is the mission number. The fuel specific heat value for this analysis is considered deterministic and equal to the fuel specific heat value of Kerosene, 46.0 MJ/kg. The payload weight is assumed to be the aircraft takeoff weight minus the aircraft empty weight and fuel burn weight. The summation in Eq. 45 is taken over the 20 flight scenarios discussed in Section 4.

The uncertainty analysis is performed using 10,000 Monte Carlo simulations. The global sensitivity analysis is performed using 1,000 Monte Carlo simulations for each individual input. The results will examine the distribution of PFEI and the sensitivity of PFEI to the system inputs for all three aircraft configurations.

B738 Standard Technology

The uncertainty analysis result for the B738 is shown in Figure 16. The expectation and standard deviation of PFEI are 3.12 kJ/kg/km and 0.064 kJ/kg/km respectively. The global sensitivity analysis results are shown in Figure 17. The sensitivity analysis indicates the important factors are cruise altitude and wing cap yield stress followed by operating pressure ratio, gas temperature at turbine inlet in cruise conditions, and metal temperature. The Monte Carlo simulation results for PFEI plotted against the aircraft technology parameters are shown in Figure 18.

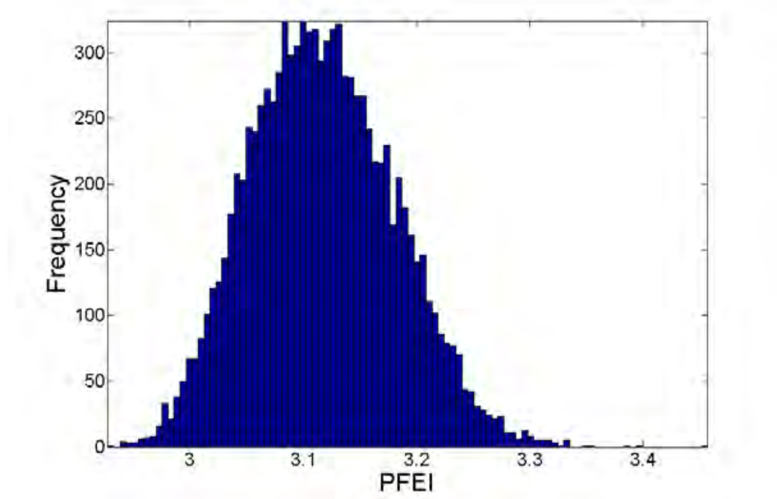

Figure 16: B738 total fuel energy per payload range distribution.

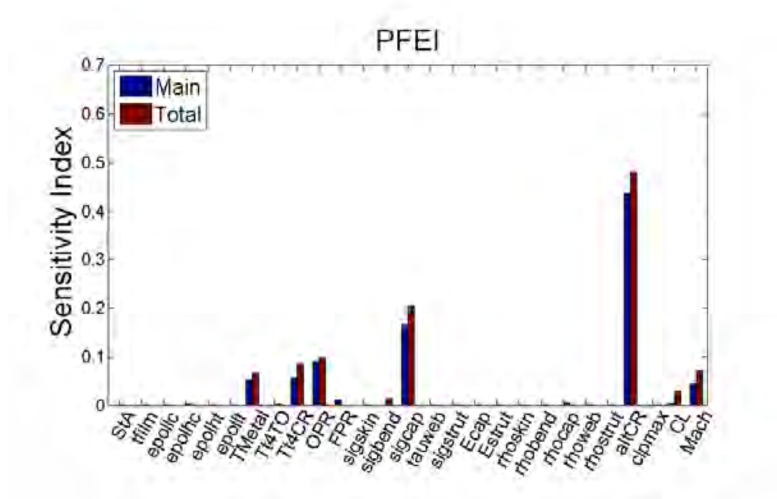

Figure 17: B738 fuel energy per payload range sensitivity index.

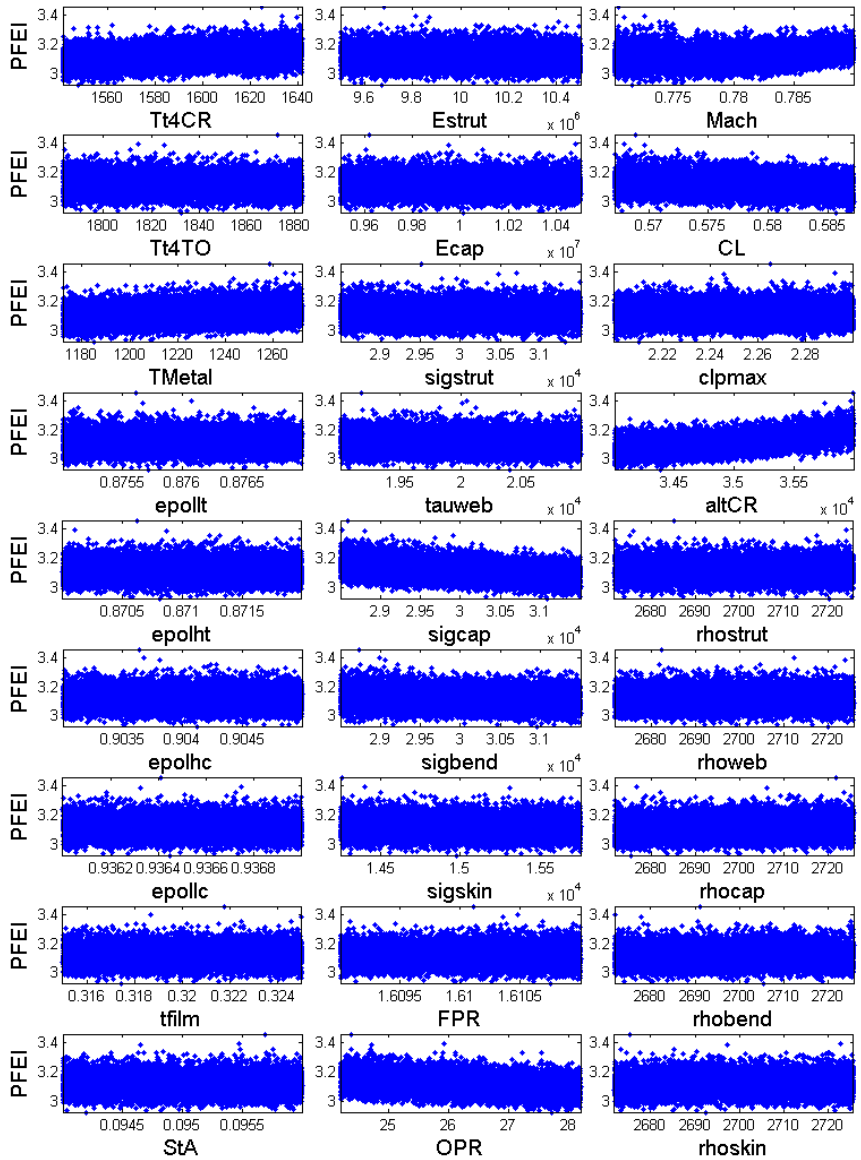

Figure 18: B738 MCS results of PFEI against the aircraft technology parameters.

The results show that B738 aircraft configuration PFEI is sensitive to the cruise design altitude. That is, uncertainty in the operation of the B738 fleet will have a detrimental impact on our predictability of aviation environmental impacts. The second largest impact factor is the wing cap yield stress which has a direct impact on the wing structural performance shown in Figure 19. The reason cruise altitude and wing cap yield stress uncertainties are important factors in the uncertainty of PFEI is because they are also significant factors in the Boeing 737-800 aircraft's empty weight as shown in Figure 20. Uncertainty in the aircraft's empty weight will have a significant impact on the aircraft's PFEI since it increases uncertainty associated to the amount of payload the aircraft may carry aboard.

The turbine inlet gas temperature, metal temperature, and operational pressure ratio are significant contributors to uncertainty in nominal total rate of fuel flow and maximum total net thrust as shown in Figure 21.

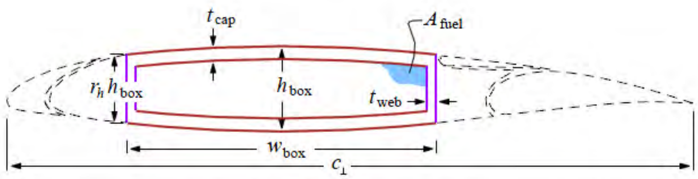

Figure 19: Wing or Tail Section (Drela, Simultaneous Optimization of the Airframe, Powerplant, and Operation of Transport Aircraft., 2010)

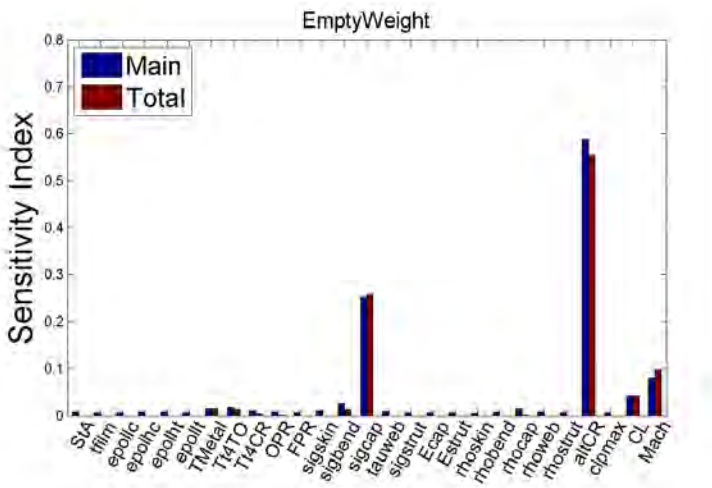

Figure 20: B738 Aircraft Empty Weight Sensitivity Analysis.

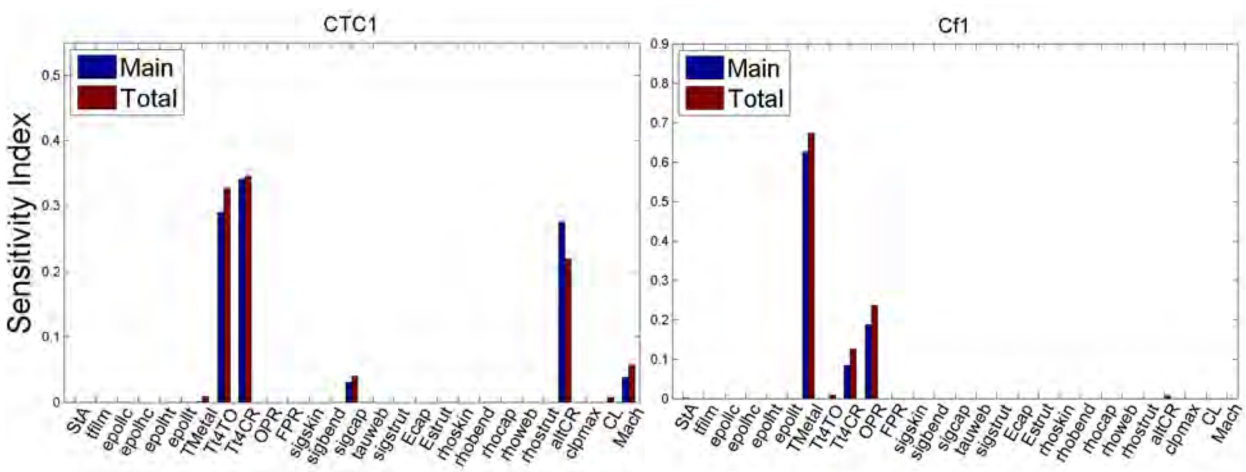

Figure 21: Global sensitivity index for TC_1 and C_{f1}

D8 Standard Technology

The uncertainty analysis result for the D8 standard technology is shown in Figure 22. The expectation and standard deviation of PFEI are 1.81 kJ/kg/km and 0.033 kJ/kg/km respectively. The global sensitivity analysis results are shown in Figure 23. The sensitivity analysis indicates the important factors are cruise Mach number, turbine inlet temperature at cruise conditions, turbine inlet temperature at takeoff conditions, metal temperature, wing caps yield stress, and cruise altitude. The Monte Carlo simulation results for PFEI plotted against the aircraft technology parameters are shown in Figure 24. The D8 standard technology PFEI has a lower variance than the B738 standard technology PFEI, which indicates the D8 aircraft configuration potentially, improves our ability to quantify PFEI. However, the drawback is that the D8 standard technology important factors are spread across multiple input uncertainties.

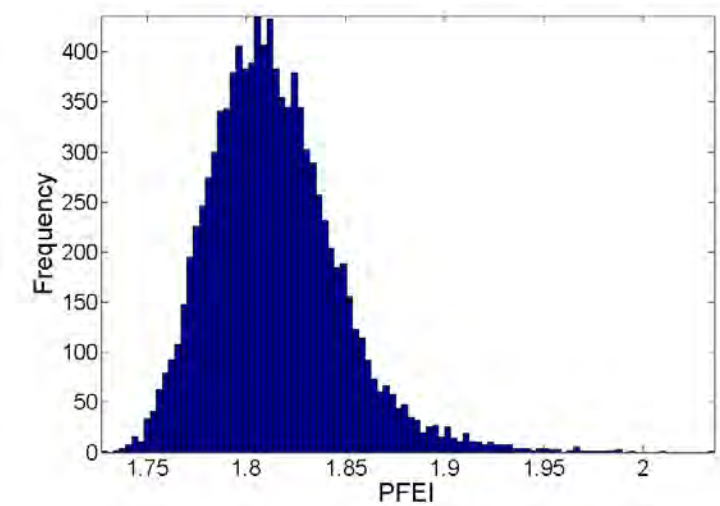

Figure 22: D8 Standard Technology PFEI distribution.

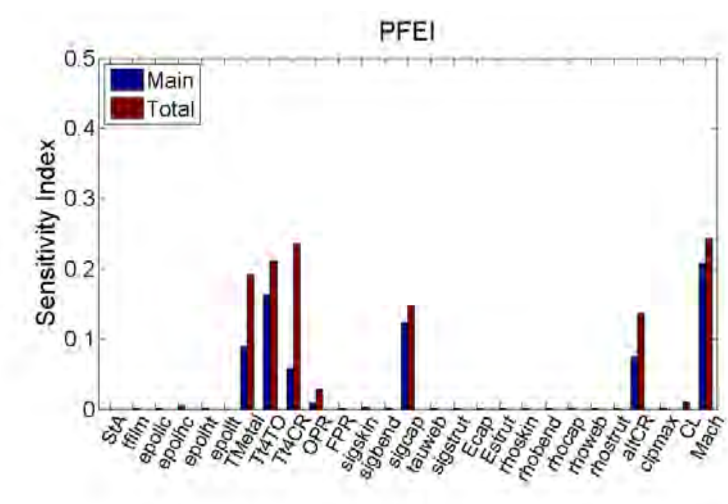

Figure 23: D8 Standard Technology PFEI sensitivity analysis.

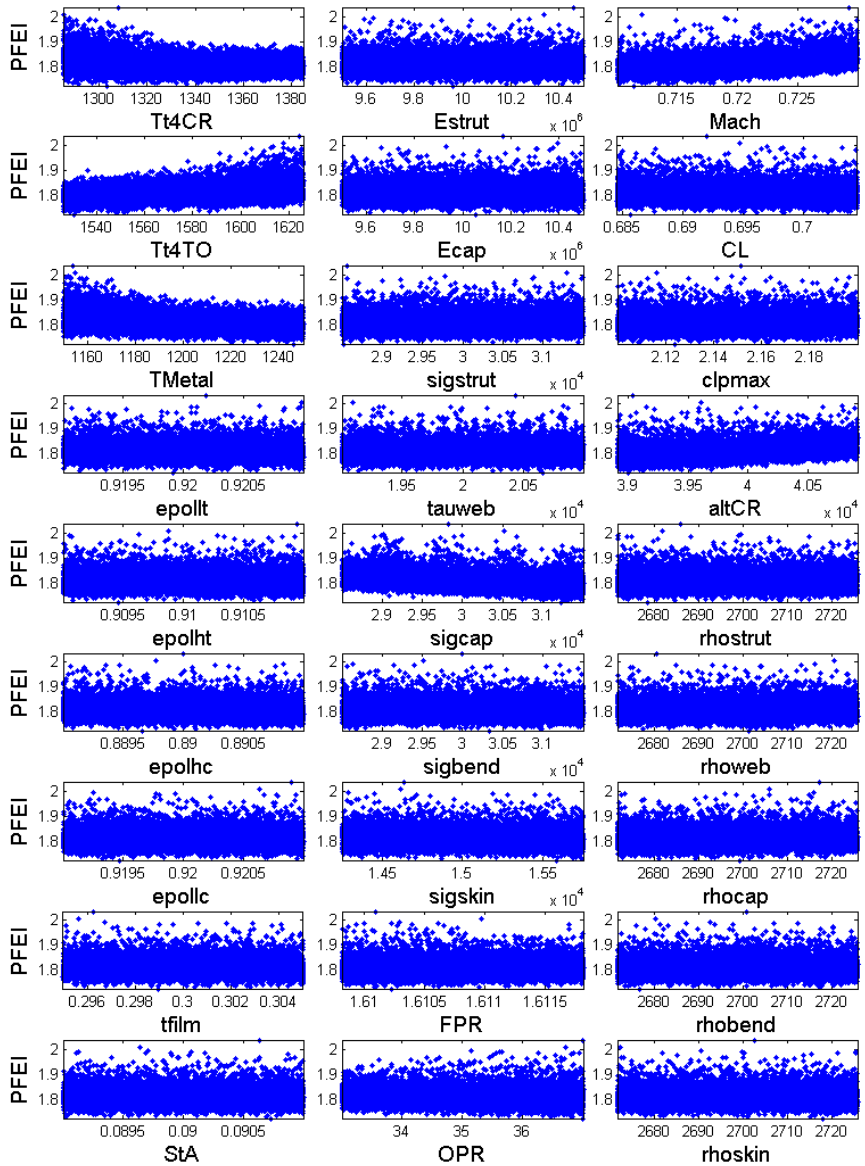

Figure 24: D8 Standard Technology MCS results of PFEI against the aircraft technology parameters.

The D8 standard technology aircraft PFEI is more sensitive to the uncertainty in the aircraft engines technology whereas the B738 PFEI is more sensitive to uncertainty in both the aircraft's technology and its operations. The D8 standard technology aircraft's empty weight sensitivity indices have contributions from the turbine inlet gas temperature and metal temperature shown in Figure 25. These engine parameters also play a significant role in the aircraft's fuel burn rate and thrust sensitivities shown in Figure 26. Finally, the Mach number has the biggest contributing factor to the D8 standard technology induced drag and parasitic drag sensitivities shown in Figure 27.

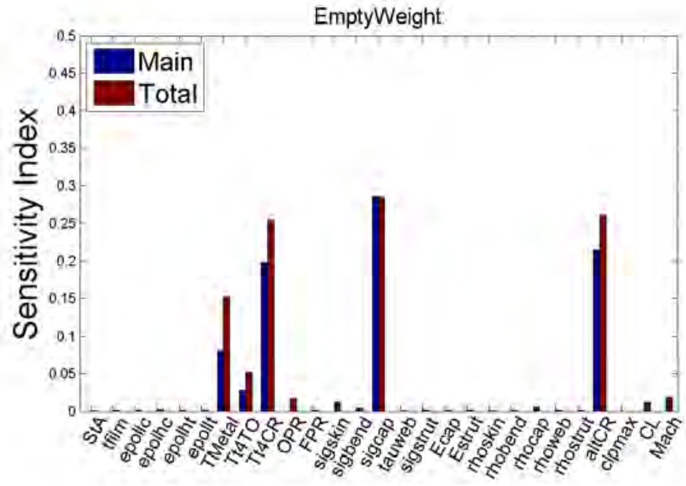

Figure 25: D8 Standard Technology Aircraft Empty Weight Sensitivity Analysis.

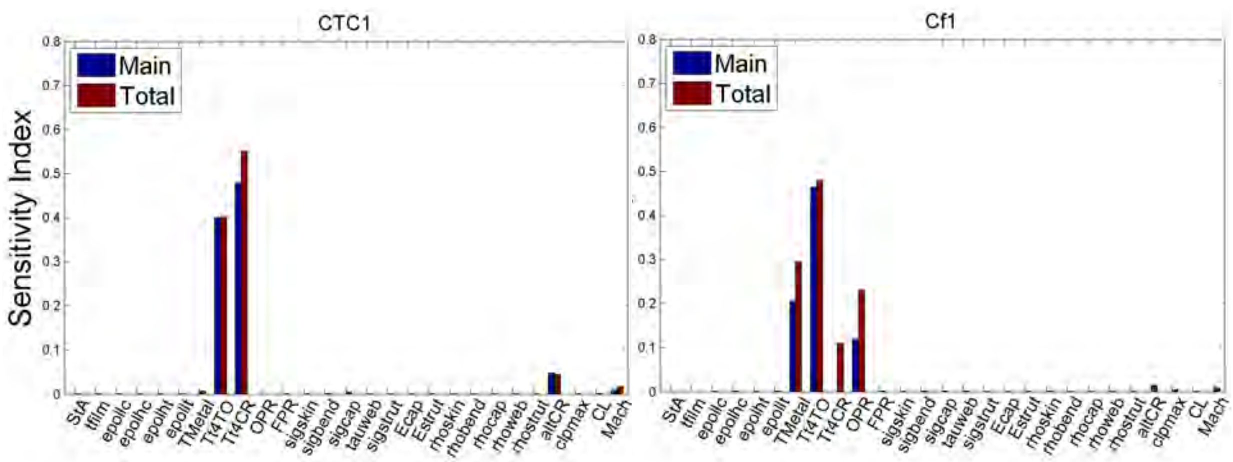

Figure 26: D8 Standard Technology Global sensitivity index for $C_{TC,1}$ and C_{f1}

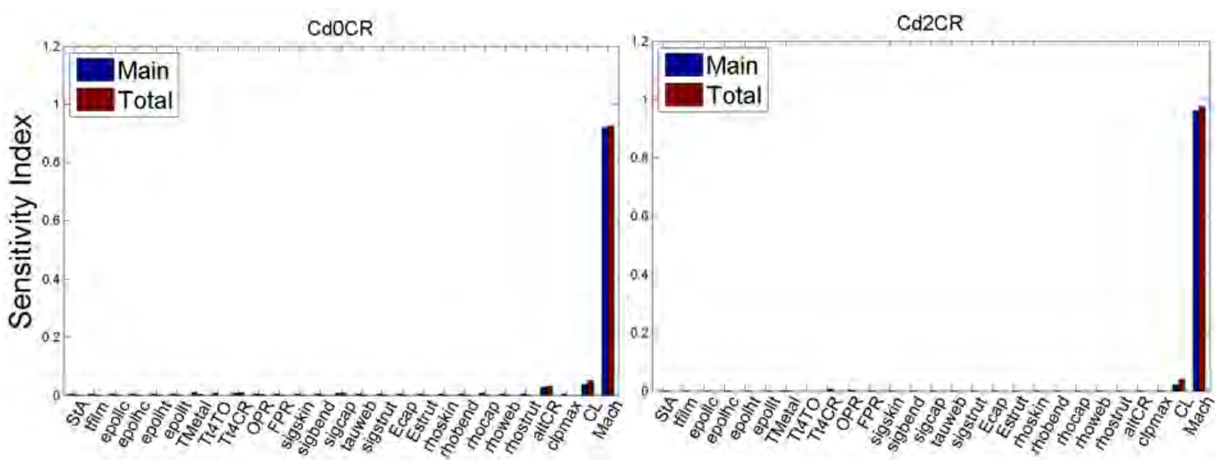

Figure 27: D8 Standard Technology Global sensitivity index for C0,CR and C2,CR

D8 Advanced Technology

The uncertainty analysis result for the D8 advanced technology is shown in Figure 28. The expectation and standard deviation of PFEI are 1.10 kJ/kg/km and 0.015 kJ/kg/km respectively. The global sensitivity analysis results are shown in Figure 29Figure 23. The sensitivity analysis indicates the important factors are cruise Mach number and turbine inlet temperature at cruise conditions. The Monte Carlo simulation results for PFEI plotted against the aircraft technology parameters are shown in Figure 30. The D8 PFEI with advanced technologies shows an improved ability to quantify the aircraft's PFEI (with lower variability). The D8 advanced technology has only two significant contributing factors to PFEI variance, compared to the D8 standard technology which had six contributing factors.

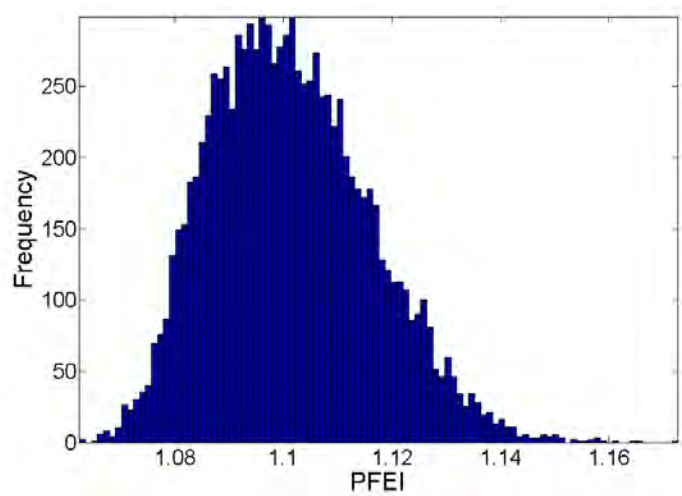

Figure 28: D8 Advanced Technology PFEI distribution.

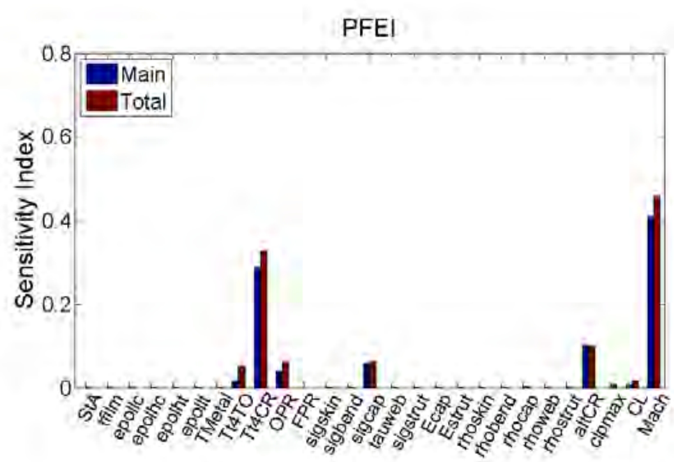

Figure 29: D8 Advanced Technology PFEI sensitivity analysis.

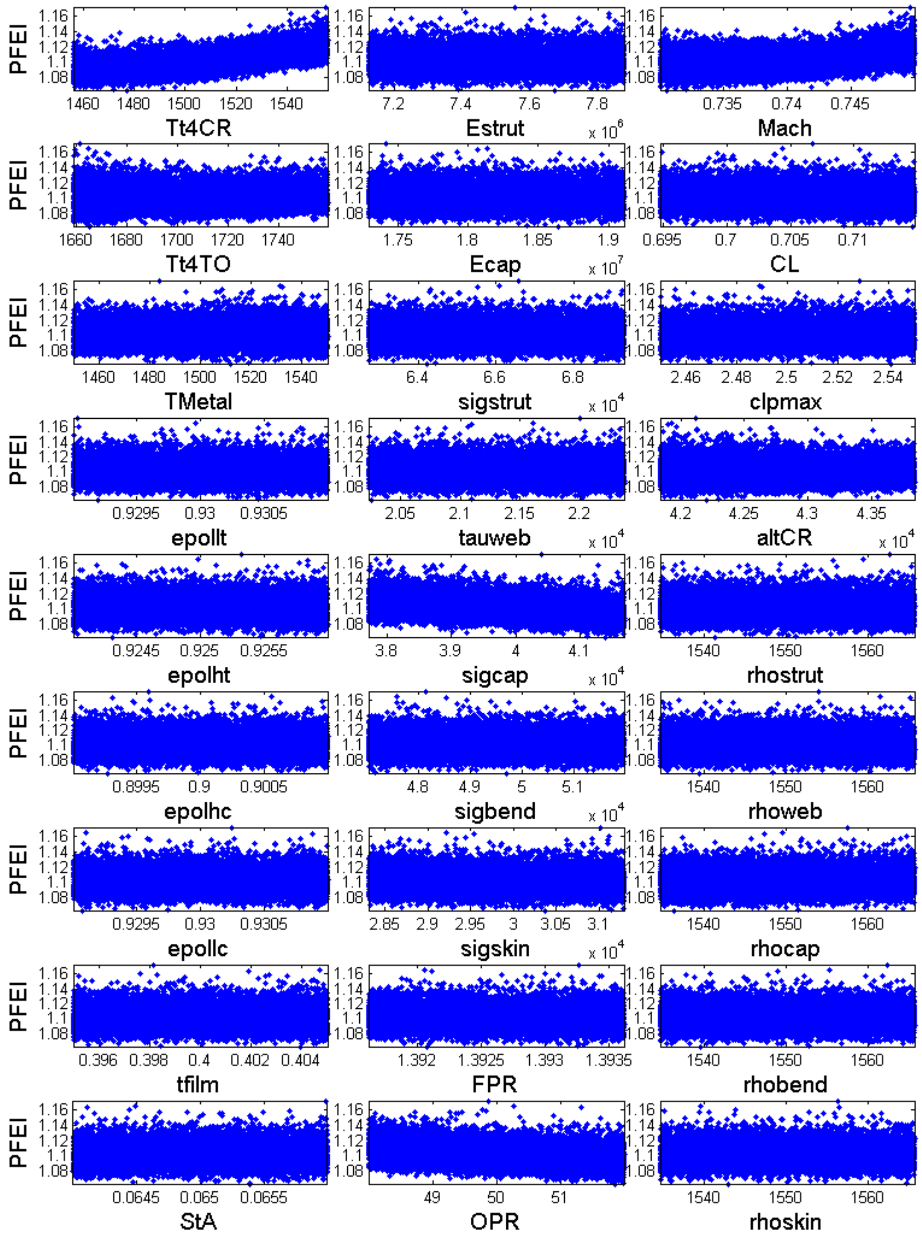

Figure 30: D8 Advanced technology MCS results of PFEI against the aircraft technology parameters.

The turbine inlet gas temperature at cruise conditions is a large contributing factor to the aircraft's net thrust as shown in Figure 31. The Mach number is a significant contributing factor to the aircraft's induced and parasitic drag as shown in Figure 32. The D8 advanced technology has high sensitivity to turbine inlet gas temperature at cruise conditions, which may be relatively simpler to research and control than the combined uncertainties of the six important factors for the D8 standard technology aircraft.

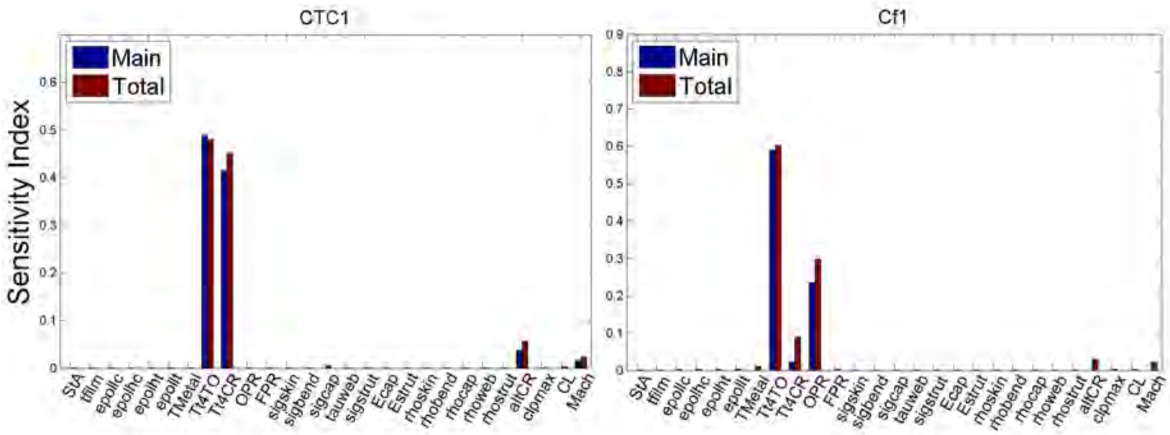

Figure 31: D8 advanced technology Global sensitivity index for CTC,1 and Cf1

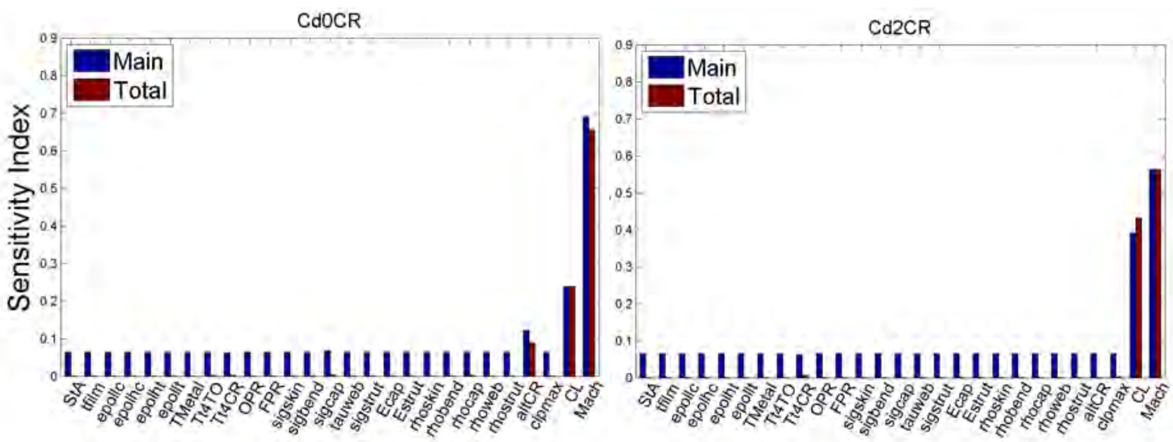

Figure 32: D8 advanced technology Global sensitivity index for C0,CR and C2,CR

Section 6

Decomposition-Based Uncertainty Quantification

Decomposition-based uncertainty quantification performs the uncertainty analysis and global sensitivity analysis using a divide-and-conquer methodology motivated by multidisciplinary design and optimization algorithm architectures. Decomposing the uncertainty quantification process provides a variety of benefits which include performing the UQ on the manageable components, using local resources, and by experts in the specific field. The uncertainty analysis results are presented in this report and the global sensitivity analysis results are still under investigation.

TASOpt-AEDT Interface Challenge

The challenge with the decomposition-based uncertainty analysis approach is in managing the interfaces between components. This challenge is exacerbated if the information being transferred between components is high dimensional (e.g., > 10). In this report, the information transferred between TASOpt and AEDT is on the O(100) variables making this problem very challenging. Furthermore, the O(100) variables are highly dependent which adds to the difficulty of characterizing the underlying probability distribution. Because of the dependencies among these variables, the global sensitivity analysis of the AEDT module would require advanced methods which are under development and beyond the scope of this work.

Here we will present a best practices for decomposition-based uncertainty quantification when the information being transferred between components is high dimensional. Our recommended approach is to reduce the dimensions to the important variables, selecting a good proposal distribution, and performing the global compatibility satisfaction step efficiently.

Dimension Reduction

The challenging aspect of the TASOpt-AEDT interface is the number of interface variables (i.e., O(100)) and the high dependency among variables. The objective here is to reduce the number of interface variables to a moderate size which still contains all the necessary information. This means the reduced set should contain the input variables to AEDT which are of greatest importance to the output of interest variance. These variables can be identified by the largest total sensitivity indices based on a global sensitivity analysis. However, global sensitivity analysis assumes the inputs are independent. Therefore, we will make two significant assumptions in this work. The first assumption is that variables with the largest total sensitivity indices in the independent space are also the same variables in the dependent space with the largest impact on the output of interest variance. The second assumption is that the number of important variables are moderate (i.e., O(10)). This assumption is necessary since we will use Quasi-Monte Carlo simulation to evaluate the integrals required by the global sensitivity analysis. We now focus on how to select the importance variables.

Jansen Winding Stairs

The Jansen winding stairs method is a sensitivity analysis approach based on screening methods which were developed for large scale applications. A screening method is a qualitative sensitivity analysis approach while a variance based method is considered a quantitative sensitivity analysis approach. The Jansen winding stairs method samples the high dimensional space by modifying one dimension at a time. This is illustrated in Figure 33 for a three dimensional problem. For our problem, we coupled this approach with engineering judgment in order to select 17 important variables of the O(100) interface variables. The 17 important variables are listed in Table 19.

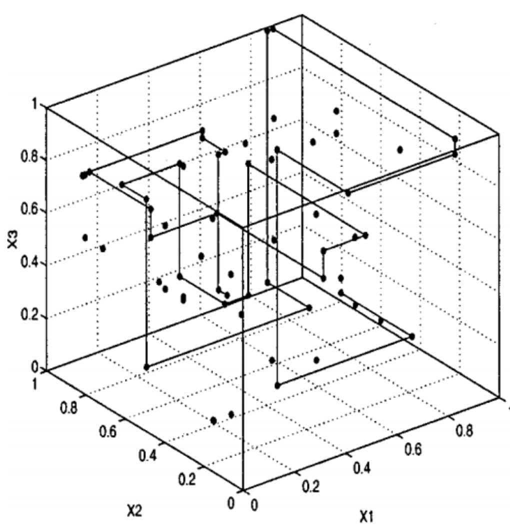

Figure 33: Jansen winding stairs sampling method.

Table 19: The 17 important interface variables selected from the O(100) variables.

Variable	Description
CtC1	Thrust Coefficient 1
MTOW	Maximum TO Weight
CtC3	Thrust Coefficient 1
CtC2	Thrust Coefficient 1
Cd2CR	Parasitic Drag
Cd0CR	Induced Drag
S	Wing Area
Hmax	Maximum Altitude
Wmt	Aircraft Empty Weight
Cf1	Fuel Coefficient 1
VstCR	Cruise Stall Velocity
Cf2	Fuel Coefficient 2
Cf3	Fuel Coefficient 3
CfCR	Fuel Coef. Cruise
HiCR_1	Hi Cruise CAS 1
HiCR_2	Hi Cruise CAS 2
HiCR_M	Hi Cruise Mach

Proposal Distribution

The decomposition-based uncertainty analysis approach relies heavily on selecting a good proposal distribution. A proposal distribution is a distribution we select to perform the AEDT uncertainty analysis. Upon receiving the target distribution from TASOpt, we adjust the results from the proposal uncertainty analysis to estimate the target uncertainty analysis. However, to accomplish this task we require that the proposal distribution encompasses the target distribution. As an example, in a one dimension scenario, if the target distribution is U[0,1] then an adequate proposal could be U[-0.5,1.5]. However, an inadequate proposal would be U[0.5, 2.5]. Here the problem of selecting an good proposal distribution is challenging since we are dealing with an O(100) dimensional distribution. To accomplish this task we recommend performing a small uncertainty analysis (e.g., 1000 samples) of the system-level MCS to obtain an estimate of the mean and variance of the interface distributions. We then increase the variance to encapsulate the non observable target distribution. Next we use for our proposal distribution a multivariate Gaussian with the estimated mean and enlarged variance. This approach coupled with expert opinion would assist in selecting adequate proposal distributions as illustrated in Figure 34.

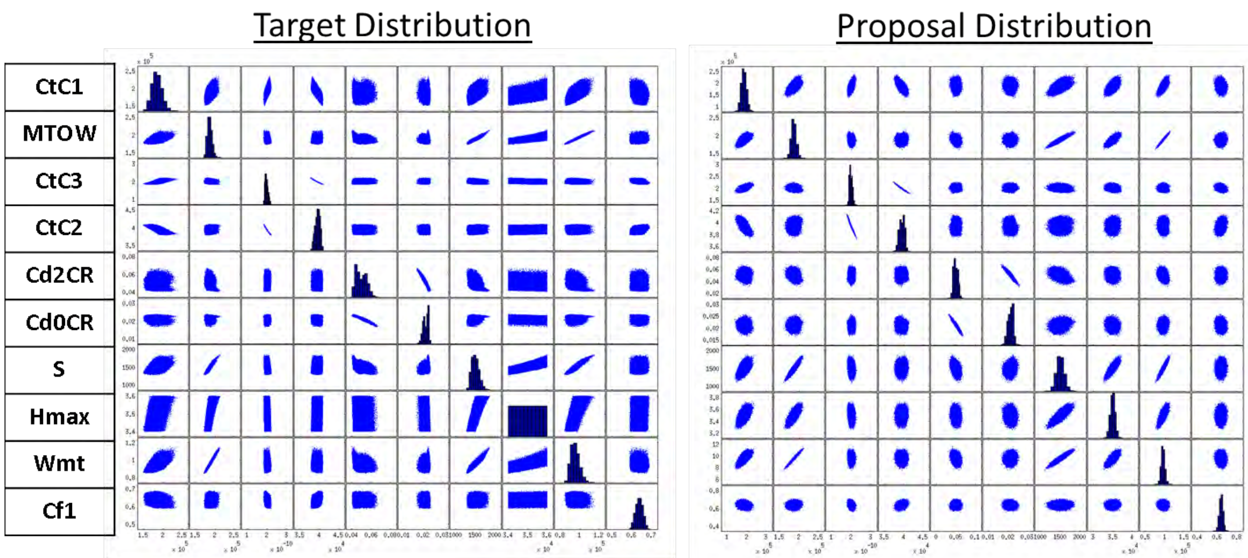

Figure 34: Example selection of an adequate proposal distribution (WORK IN PROGRES: Increase Font Size).

Proposal-to-Target Transformation

The final challenge requires transforming the proposal distribution into the target distribution in order to estimate the module statistics under the target distribution. This step is encompassed in the global compatibility satisfaction step. The method requires adjusting the weights associated to the proposal samples such that the statistics approximate the target distribution. The typical approach to computing these weights requires density estimation which does not scale well with dimensions. Instead we have formulated this problem as an optimization problem that operates directly on the samples; the optimization problem has lots of structure so we can handle large scale (i.e., large number of proposal samples) applications. The proposed method to computing the importance weight minimizes the L2–norm, with respect to the importance weights, between the proposal empirical distribution function and the target empirical distribution function as shown in Figure 35.

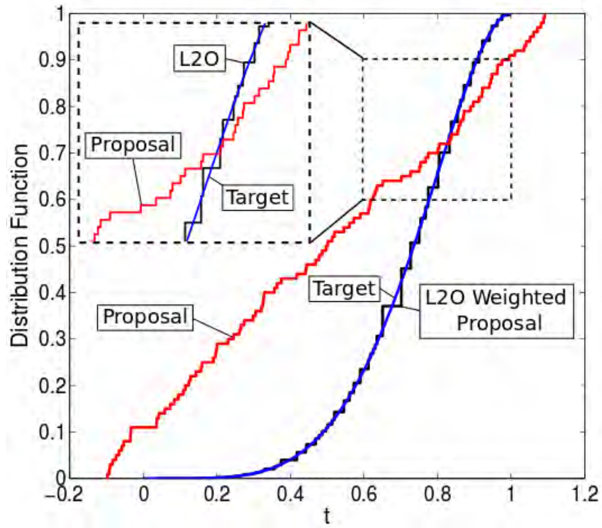

Figure 35: Proposed approach to transform the proposal distribution (U[0,1])into the target distribution (Beta(0.5,0.5)) adjusts the proposal samples such that the weight proposal distribution (L2O weighted) matches the target distribution.

Uncertainty Analysis

Here we only consider the Boeing 737-800 decomposition-based uncertainty analysis. The approach, as described previously, relies on preforming the uncertainty analysis of each module concurrently. The proposal distribution for the AEDT module is selected based on the previous discussion using 1,000 samples randomly selected from the system-level MCS uncertainty analysis. The TASOpt proposal distribution is the system-level MCS uncertainty analysis; that is to say it is the target distribution. Upon completing both local uncertainty analyses the global compatibility satisfaction step is performed. However, instead of using all O(100) interface variables we use the 17 important variables in Table 19. The procedure uses the optimization algorithm shown in Figure 35 on the 17 dimensional distributions (e.g., see Figure 34 as an example of 10 dimensions). The result is the AEDT modules output which was originally distributed with respect to the proposal distribution now is adjusted to represent the target distribution. This is illustrated in Figure 36. These results show that our decomposition-based uncertainty analysis results visually matches the system-level MCS results.

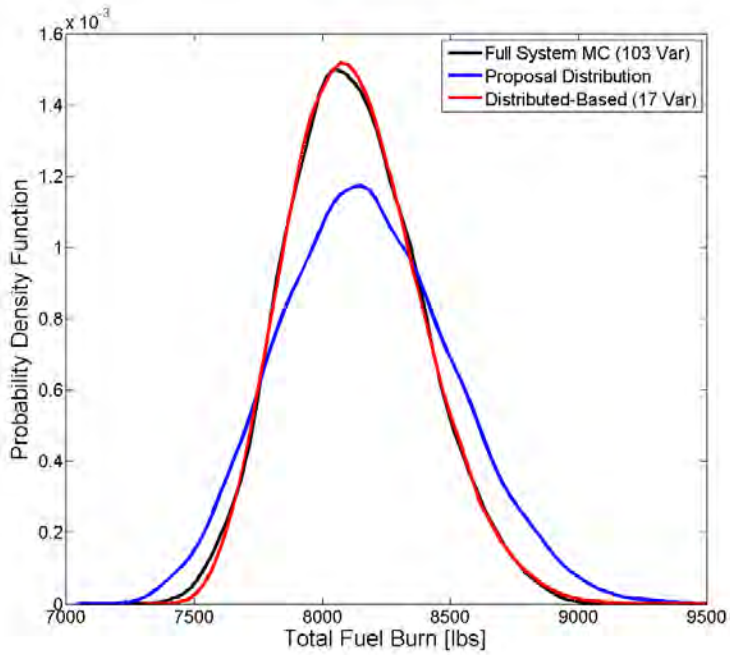

Figure 36: Total fuel burn using the decomposition-based uncertainty analysis method on the Boeing 737-800.

Section 7

Conclusion

Quantifying an aircraft's fuel burn performance is important for aviation policy analyses. However, our lack of knowledge in aircraft technologies and design operations result in an uncertain aircraft fuel burn performance, which must be quantified through an uncertainty analysis. This report studied the impact on aircraft fuel burn performance of varying aircraft configurations and aviation technological enhancements. The aircraft's fuel burn performance methodology is based on a system-level tool composed of a conceptual-level aircraft performance tool and an aviation environmental consequence tool. The uncertainty quantification methodology is based on an all-at-once system-level approach and a new decomposition-based approach.

The system-level integration coupled a conceptual level aircraft performance tool, TASOpt, to the aviation environmental design tool, AEDT 2a. The coupling of these two tools required propagating approximately one hundred variables from the TASOpt module to the AEDT module. The results of this coupling showed good agreement over similar flight scenarios with respect to fuel burn for the climb above 10,000 [ft] and cruise segment. With these results, we have drawn comparisons between TASOpt and AEDT fuel burn calculations which can drive software developers to investigate and improve upon their respective tools. The study revealed a drawback, of which the AEDT developers are aware, in AEDT's calculation of fuel burn during the descent out of cruise. In the descent out of cruise segment, AEDT assumes the aircraft is descending with the engines idling, which is not a typical flight procedure. The analysis also revealed that it is possible to incur at worst case fuel burn absolute error of approximately 3.0% in assuming a step change in takeoff aircraft weight versus range instead of a continuous change in takeoff aircraft weight versus range. Finally, the fuel burn in the AEDT climb segment does not seem realistic and the author attributes this discrepancy to possible interpolation effects in AEDT.

The system-level uncertainty quantification offered multiple insights into the impacts of uncertainty in aircraft technologies and design operations on quantifying an aircraft's fuel burn performance. The Boeing 737-800 uncertainty quantification revealed that the conventional aircraft configuration incurs a significant variation in PFEI which can be attributed to uncertainties in design cruise altitude and wing cap yield stress. The lack of knowledge for design cruise altitude and wing cap yield stress have a significant impact on the uncertainty associated to the aircraft empty weight which in turn directly impacts the aircraft's PFEI. The D8 with standard technology aircraft configuration had approximately half the variation in PFEI than the Boeing 737-800. The drawback with the D8 standard technology is that the PFEI uncertainty is attributed to multiple aircraft technologies and design operations uncertainty. This makes it difficult to determine which factor to prioritize for future research endeavors. The D8 with advanced technology had approximately half the variation in PFEI than the D8 with standard technology. Also, the uncertainty in PFEI is mainly attributed to a single aircraft technology, turbine inlet gas temperature at cruise conditions, and a single design operation, cruise Mach number.

These results have offered a meaningful conclusion: uncertainty in PFEI is dependent on aircraft configurations and aviation technological enhancements. Furthermore, uncertainty in PFEI across varying aircraft configurations and aviation technological enhancements is significantly affected by different aircraft technologies and design operations.

The report also investigated the implementation of our decomposition-based uncertainty quantification method on a large-scale application problem. The results show our decomposition-based uncertainty analysis approach coupled with the best practices matched the system-level MCS results. We have provided evidence that even in high dimensional interfaces our method can still be applied assuming the information being transferred lives in a low dimensional subspace. We have also demonstrated that our optimization based approach to the transport of distributions problem works in relatively large dimensions. However, future research is required to improve our decomposition-based uncertainty quantification approach. A method which systematically identifies the variables of importance when the input distributions are dependent would assist our method by reducing the interface dimensions.

References

2010a, I. (2010). *Report of the committee on aviation enviornmental protection, Eighth Meeting.* Montreal, 1 - 12 : Doc 9938 CAEP/8.

2010b, I. (2010). *37th Session of the ICAO Assembly, Resolution A37-19: Consolidated statement of continuing ICAO policies and practices related to enviornmental protection climate change.*

Administration, F. A. (2013). *Aviation Enviornmental Design Tool (AEDT) 2a Uncertianty Quantification Report.* U.S. Department of Transportation.

Allaire, D. (2009). *Uncertainty Assessment of Complex Models with Application to Aviation Environmental Systems.* Massachusetts Institute of Technology.

Amaral, S., Allaire, D., & Willcox, K. (2012). A Decomposition Approach to Uncertainty Analysis of Multidisciplinary Systems. *12th AIAA Aviation Technology, Integration, and Operations (ATIO) Conference and 14th AIAA/ISSM*, (pp. 1-18). Indianapolis, Indiana.

Andrea Saltelli, M. R. (2008). *Global sensitivity analysis: the primer.* Wiley.

BADA. (2012). *User Manual for the Base of Aircraft Data (BADA) Revision 3.10.* EEC Technical/Scientific Report No. 12/04/10-45.

Cumpsty, N., Alonso, J., Eury, S., Maurice, L., Nas, B., Ralph, M., & Sawyer, R. (2010). *Report of the Independent Experts on Fuel Burn Reduction Technology.* CAEP-SG/20101-WP/11 Doc 9963.

Dons, J., Mariens, J., & O'Callaghan, G. (2011). *Use of Third-party Aircraft Performance Tools in the Development of the Aviation Enviornmental Design Tool (AEDT).* DOT-VNTSC-FAA-11-08.

Drela, M. (2010). Development of the D8 Transport Configuration. *AIAA Transport Aircraft*.

Drela, M. (2010). *Simultaneous Optimization of the Airframe, Powerplant, and Operation of Transport Aircraft.* Hamilton Place.

Greitzer, E., Bonnefoy, P., Blanco, E. d., Dorbian, C., Drela, M., Hall, D., . . . et, a. (2010). N+3 Aircraft Concept Designs and Trade Studies. *NASA/CR-2010-216794/Vol2*.

Gunston, B. (1998). *Jane's Aero-Engines.* Jane's Information Group.

Kyprianidis, K. (2011). *Future Aero Engine Designs: An Evolving Vision.*

Lee, D., Fahey, D., Forster, P. M., Newton, P. J., Wit, R. C., Lim, L. L., . . . Sausen, R. (2009). Aviation and global climate change in the 21st century. *Atmospheric Enviornment 43 no. 22*, 3520-3537.

Manual, A. T. (2012). *Aviation Enviornmental Design Tool (AEDT) 2a: Technical Manual.* DOT-VNTSC-FAA-12-09.

Niederreiter, H. (1992). *Random Number Generation and Quasi-Monte Carlo Methods.* Society for Industrial and Applied Mathematics.

Roof, C., Hansen, A., Fleming, G., Thrasher, T., Nguyen, A., Hall, C., . . . Hollingsworth, P. (2007). *Aviation environmental design tool (AEDT) system architecture.* Doc# AEDT-AD-01 .

Rutherford, D., & Mazyar, Z. (2009). *Efficiency trends for new commerical jet aircraft 1960 to 2008.* International Council on Clean Transportation.

Appendix A

Global Sensitivity Analysis

To perform GSA, the Sobol' method which utilizes the Monte-Carlo Simulations is applied. The algorithm to solve the GSA analysis is shown below. [Saltelli (2008)]

$$\mathrm{A} = \text{Input Vector} = \begin{bmatrix} X_1^{(1)} & X_2^{(1)} & \cdots & X_i^{(1)} & \cdots & X_k^{(1)} \\ X_1^{(2)} & X_2^{(2)} & \cdots & X_i^{(2)} & \cdots & X_k^{(2)} \\ \cdots & \cdots & \cdots & \cdots & \cdots & \cdots \\ X_1^{(N)} & X_2^{(N)} & \cdots & X_i^{(N)} & \cdots & X_k^{(N)} \end{bmatrix}$$

$$\mathrm{A} = \text{Input Vector} = \begin{bmatrix} X_{k+1}^{(1)} & X_{k+2}^{(1)} & \cdots & X_{k+i}^{(1)} & \cdots & X_{k+k}^{(1)} \\ X_{k+1}^{(2)} & X_{k+2}^{(2)} & \cdots & X_{k+i}^{(2)} & \cdots & X_{k+k}^{(2)} \\ \cdots & \cdots & \cdots & \cdots & \cdots & \cdots \\ X_{k+1}^{(N)} & X_{k+2}^{(N)} & \cdots & X_{k+i}^{(N)} & \cdots & X_{k+k}^{(N)} \end{bmatrix}$$

$$A = \text{Input Vector} = \begin{bmatrix} X_{k+1}^{(1)} & X_{k+2}^{(1)} & \cdots & X_{i}^{(1)} & \cdots & X_{k+k}^{(1)} \\ X_{k+1}^{(2)} & X_{k+2}^{(2)} & \cdots & X_{i}^{(2)} & \cdots & X_{k+k}^{(2)} \\ \cdots & \cdots & \cdots & \cdots & \cdots & \cdots \\ X_{k+1}^{(N)} & X_{k+2}^{(N)} & \cdots & X_{i}^{(N)} & \cdots & X_{k+k}^{(N)} \end{bmatrix}$$

$$Module\ (x) = f(x): \quad y_A = f(A), \quad y_B = f(B), \quad y_C = f(C)$$

$$f_0 = \frac{\left(\frac{1}{N}\sum_{j=1}^{N} y_A^j\right) + \left(\frac{1}{N}\sum_{j=1}^{N} y_B^j\right)}{2}$$

$$y_A = y_A - f_0\ , y_B = y_B - f_0, y_C = y_C - f_0$$

$$V(Y) = y_A \cdot y_B - f_0^2 = \frac{1}{N}\sum_{j=1}^{N} y_A^j \cdot y_B^j - f_0^2$$

$$S_i = Main\ Effect = \frac{V(E[Y|X_i])}{V(Y)} = \frac{y_A \cdot y_{C_i} - f_0^2}{y_A \cdot y_B - f_0^2} = \frac{\frac{1}{N}\sum_{j=1}^{N} y_A^j \cdot y_{C_i}^j - f_0^2}{\frac{1}{N}\sum_{j=1}^{N} y_A^j \cdot y_B^j - f_0^2}$$

$$S_{Ti} = Total\ Effect = 1 - \frac{V(E[Y|X_{\sim i}])}{V(Y)} = 1 - \frac{y_B \cdot y_{C_i} - f_0^2}{y_A \cdot y_B - f_0^2} = \frac{\frac{1}{N}\sum_{j=1}^{N} y_B^j \cdot y_{C_i}^j - f_0^2}{\frac{1}{N}\sum_{j=1}^{N} y_A^j \cdot y_B^j - f_0^2}$$

Appendix B

TASOpt Input Files (*.tas)

Appendix C

AEDT SQL Fleet Database Import (*.sql)

```
Insert Into [FLEET].[dbo].[FLT_REF_ICAO_ACTYPES]

select * from OpenRowset('MSDASQL', 'Driver={Microsoft Access Text Driver
(*.txt, *.csv)}; DefaultDir=D:\TASOpt\AEDT_Aircraft\CSV\;Extended
properties="ColNameHeader=True;Format=Delimited (,);"','select * from
FLT_REF_ICAO_ACTYPES.csv')

Insert Into [FLEET].[dbo].[FLT_ACTYPES]

select * from OpenRowset('MSDASQL', 'Driver={Microsoft Access Text Driver
(*.txt, *.csv)}; DefaultDir=D:\TASOpt\AEDT_Aircraft\CSV\;Extended
properties="ColNameHeader=True;Format=Delimited(,);"','select * from
FLT_ACTYPES.csv')

SET IDENTITY_INSERT FLEET.dbo.FLT_AIRFRAMES ON

Insert Into [FLEET].[dbo].[FLT_AIRFRAMES] ([AIRFRAME_ID]
      ,[MODEL],[ENGINE_COUNT],[ENGINE_LOCATION],[DESIGNATION_CODE]
      ,[EURO_GROUP_CODE],[MAX_RANGE],[INTRO_YEAR],[USAGE_CODE]
      ,[SIZE_CODE],[ENGINE_TYPE])
select [AIRFRAME_ID],[MODEL],[ENGINE_COUNT],[ENGINE_LOCATION]
      ,[DESIGNATION_CODE],[EURO_GROUP_CODE],[MAX_RANGE],[INTRO_YEAR]
      ,[USAGE_CODE],[SIZE_CODE]
      ,[ENGINE_TYPE] from OpenRowset('MSDASQL', 'Driver={Microsoft Access
Text Driver (*.txt, *.csv)};
DefaultDir=D:\TASOpt\AEDT_Aircraft\CSV\;Extended
properties="ColNameHeader=True;Format=Delimited(,);"','select * from
FLT_AIRFRAMES.csv')

SET IDENTITY_INSERT FLEET.dbo.FLT_AIRFRAMES OFF

Insert Into [FLEET].[dbo].[FLT_REF_ACCODES]

select * from OpenRowset('MSDASQL', 'Driver={Microsoft Access Text Driver
(*.txt, *.csv)}; DefaultDir=D:\TASOpt\AEDT_Aircraft\CSV\;Extended
properties="ColNameHeader=True;Format=Delimited(,);"','select * from
FLT_REF_ACCODES.csv')

Insert Into [FLEET].[dbo].[FLT_AIRFRAME_ACTYPE_MAP]

select * from OpenRowset('MSDASQL', 'Driver={Microsoft Access Text Driver
(*.txt, *.csv)}; DefaultDir=D:\TASOpt\AEDT_Aircraft\CSV\;Extended
properties="ColNameHeader=True;Format=Delimited(,);"','select * from
FLT_AIRFRAME_ACTYPE_MAP.csv')

Insert Into [FLEET].[dbo].[FLT_BADA_ACFT]
```

```
select * from OpenRowset('MSDASQL', 'Driver={Microsoft Access Text Driver
(*.txt, *.csv)}; DefaultDir=D:\TASOpt\AEDT_Aircraft\CSV\;Extended
properties="ColNameHeader=True;Format=Delimited(,);"','select * from
FLT_BADA_ACFT.csv')

Insert Into [FLEET].[dbo].[FLT_ANP_AIRPLANES]

select * from OpenRowset('MSDASQL', 'Driver={Microsoft Access Text Driver
(*.txt, *.csv)}; DefaultDir=D:\TASOpt\AEDT_Aircraft\CSV\;Extended
properties="ColNameHeader=True;Format=Delimited(,);"','select * from
FLT_ANP_AIRPLANES.csv')

SET IDENTITY_INSERT [FLEET].[dbo].[FLT_EQUIPMENT] ON

Insert Into [FLEET].[dbo].[FLT_EQUIPMENT] ([EQUIP_ID]
      ,[AIRFRAME_ID],[ENGINE_ID],[ENGINE_MOD_ID]
      ,[ANP_AIRPLANE_ID],[ANP_HELICOPTER_ID],[BADA_ID])
select [EQUIP_ID],[AIRFRAME_ID],[ENGINE_ID],[ENGINE_MOD_ID]
      ,[ANP_AIRPLANE_ID],[ANP_HELICOPTER_ID]
      ,[BADA_ID] from OpenRowset('MSDASQL', 'Driver={Microsoft Access Text
Driver (*.txt, *.csv)}; DefaultDir=D:\TASOpt\AEDT_Aircraft\CSV\;Extended
properties="ColNameHeader=True;Format=Delimited(,);"','select * from
FLT_EQUIPMENT.csv')

SET IDENTITY_INSERT [FLEET].[dbo].[FLT_EQUIPMENT] OFF

SET IDENTITY_INSERT [FLEET].[dbo].[FLT_DEFAULT_ENGINES] ON

Insert Into [FLEET].[dbo].[FLT_DEFAULT_ENGINES] ([DEF_ENG_ID]
      ,[ENG_ID],[AIRFRAME_ID],[REGION_CODE],[SOURCE])
select [DEF_ENG_ID],[ENG_ID],[AIRFRAME_ID],[REGION_CODE]
      ,[SOURCE] from OpenRowset('MSDASQL', 'Driver={Microsoft Access Text
Driver (*.txt, *.csv)}; DefaultDir=D:\TASOpt\AEDT_Aircraft\CSV\;Extended
properties="ColNameHeader=True;Format=Delimited(,);"','select * from
FLT_DEFAULT_ENGINES.csv')

SET IDENTITY_INSERT [FLEET].[dbo].[FLT_DEFAULT_ENGINES] OFF

SET IDENTITY_INSERT [FLEET].[dbo].[FLT_FLEET] ON

Insert Into [FLEET].[dbo].[FLT_FLEET] ([FLEET_ID]
      ,[AIRFRAME_ID],[ENGINE_ID],[ENGINE_MOD_ID],[DATE_START]
      ,[DATE_END],[REF_ACCODE],[REF_ENG_CODE],[REF_ENG_MOD_CODE]
      ,[EQGROUP],[SERIAL_NO],[REG_NO],[AC_TYPE_DESC],[ENG_TYPE],[WINGLETS]
      ,[HUSH_TYPE],[HUSH_TYPE_CODE],[COMBUSTOR],[ROLE],[DELDATE]
      ,[OPERATOR],[COUNTRY_CD],[MAX_TAKEOFF_WGT],[MAX_TAKEOFF_WGT_LK]
      ,[MAX_LANDING_WGT],[MAX_LANDING_WGT_LK],[CERT_NOISE_LEVEL_TAKEOFF]
      ,[CERT_NOISE_LEVEL_SIDELINE],[CERT_NOISE_LEVEL_APPROACH]
      ,[STG3_TRADE_MARGIN_CUM],[NOX_CHAR],[CAEP_4_NOX_MARGIN]
      ,[ENG_PRESSURE_RATIO],[ENG_MAX_RATED_THRUST],[SOURCE_TYPE]
      ,[SOURCE],[AEDT_SEATS],[AEDT_SEATS_SOURCE]
      ,[AEDT_OPERATING_EMPTY_WEIGHT_LBS]
      ,[AEDT_OPERATING_EMPTY_WEIGHT_LBS_SOURCE]
```

```
      ,[AGE],[FESG_RETIREMENT_CURVE_ID],[OEW],[OEW_SOURCE],[MAX_PAYLOAD]
      ,[EQCAT],[OPERATOR_ICAO_DEPRECATED],[OPERATOR_IATA_DEPRECATED]
      ,[COUNTRY_LAR],[COUNTRY_OAG],[AEDT_CARRIER_CODE]
      ,[FUEL_CAPACITY_US_GALS_FLOAT] select
([FLEET_ID],[AIRFRAME_ID],[ENGINE_ID],[ENGINE_MOD_ID],[DATE_START]
      ,[DATE_END],[REF_ACCODE],[REF_ENG_CODE],[REF_ENG_MOD_CODE]
      ,[EQGROUP],[SERIAL_NO],[REG_NO],[AC_TYPE_DESC],[ENG_TYPE],[WINGLETS]
      ,[HUSH_TYPE],[HUSH_TYPE_CODE],[COMBUSTOR],[ROLE],[DELDATE]
      ,[OPERATOR],[COUNTRY_CD],[MAX_TAKEOFF_WGT],[MAX_TAKEOFF_WGT_LK]
      ,[MAX_LANDING_WGT],[MAX_LANDING_WGT_LK],[CERT_NOISE_LEVEL_TAKEOFF]
      ,[CERT_NOISE_LEVEL_SIDELINE],[CERT_NOISE_LEVEL_APPROACH]
      ,[STG3_TRADE_MARGIN_CUM],[NOX_CHAR],[CAEP_4_NOX_MARGIN]
      ,[ENG_PRESSURE_RATIO],[ENG_MAX_RATED_THRUST],[SOURCE_TYPE]
      ,[SOURCE],[AEDT_SEATS],[AEDT_SEATS_SOURCE]
      ,[AEDT_OPERATING_EMPTY_WEIGHT_LBS]
      ,[AEDT_OPERATING_EMPTY_WEIGHT_LBS_SOURCE]
      ,[AGE],[FESG_RETIREMENT_CURVE_ID],[OEW],[OEW_SOURCE],[MAX_PAYLOAD]
      ,[EQCAT],[OPERATOR_ICAO_DEPRECATED],[OPERATOR_IATA_DEPRECATED]
      ,[COUNTRY_LAR],[COUNTRY_OAG],[AEDT_CARRIER_CODE]
      ,[FUEL_CAPACITY_US_GALS_FLOAT] from OpenRowset('MSDASQL',
'Driver={Microsoft Access Text Driver (*.txt, *.csv)};
DefaultDir=D:\TASOpt\AEDT_Aircraft\CSV\;Extended
properties="ColNameHeader=True;Format=Delimited(,);"','select * from
FLT_FLEET.csv')

SET IDENTITY_INSERT [FLEET].[dbo].[FLT_FLEET] OFF

SET IDENTITY_INSERT [FLEET].[dbo].[FLT_DISPERSION] ON

Insert Into [FLEET].[dbo].[FLT_DISPERSION] ([DISPERSION_ID]
      ,[REL_HEIGHT],[SIGMAZ0],[AIRFRAME_ID])
select [DISPERSION_ID],[REL_HEIGHT],[SIGMAZ0]
      ,[AIRFRAME_ID] from OpenRowset('MSDASQL', 'Driver={Microsoft Access
Text Driver (*.txt, *.csv)};
DefaultDir=D:\TASOpt\AEDT_Aircraft\CSV\;Extended
properties="ColNameHeader=True;Format=Delimited(,);"','select * from
FLT_DISPERSION.csv')

SET IDENTITY_INSERT [FLEET].[dbo].[FLT_DISPERSION] OFF

Insert Into [FLEET].[dbo].[FLT_BADA_CONFIG]

select * from OpenRowset('MSDASQL', 'Driver={Microsoft Access Text Driver
(*.txt, *.csv)}; DefaultDir=D:\TASOpt\AEDT_Aircraft\CSV\;Extended
properties="ColNameHeader=True;Format=Delimited(,);"','select * from
FLT_BADA_CONFIG.csv')

Insert Into [FLEET].[dbo].[FLT_BADA_FUEL]

select * from OpenRowset('MSDASQL', 'Driver={Microsoft Access Text Driver
(*.txt, *.csv)}; DefaultDir=D:\TASOpt\AEDT_Aircraft\CSV\;Extended
properties="ColNameHeader=True;Format=Delimited(,);"','select * from
FLT_BADA_FUEL.csv')
```

```
Insert Into [FLEET].[dbo].[FLT_BADA_APF]

select * from OpenRowset('MSDASQL', 'Driver={Microsoft Access Text Driver
(*.txt, *.csv)}; DefaultDir=D:\TASOpt\AEDT_Aircraft\CSV\;Extended
properties="ColNameHeader=True;Format=Delimited(,);"','select * from
FLT_BADA_APF.csv')

Insert Into [FLEET].[dbo].[FLT_BADA_ALTITUDE_DISTRIBUTION]

select * from OpenRowset('MSDASQL', 'Driver={Microsoft Access Text Driver
(*.txt, *.csv)}; DefaultDir=D:\TASOpt\AEDT_Aircraft\CSV\;Extended
properties="ColNameHeader=True;Format=Delimited(,);"','select * from
FLT_BADA_ALTITUDE_DISTRIBUTION.csv')

Insert Into [FLEET].[dbo].[FLT_BADA_THRUST]

select * from OpenRowset('MSDASQL', 'Driver={Microsoft Access Text Driver
(*.txt, *.csv)}; DefaultDir=D:\TASOpt\AEDT_Aircraft\CSV\;Extended
properties="ColNameHeader=True;Format=Delimited(,);"','select * from
FLT_BADA_THRUST.csv')

Insert Into [FLEET].[dbo].[FLT_ANP_AIRPLANE_FLAPS]

select * from OpenRowset('MSDASQL', 'Driver={Microsoft Access Text Driver
(*.txt, *.csv)}; DefaultDir=D:\TASOpt\AEDT_Aircraft\CSV\;Extended
properties="ColNameHeader=True;Format=Delimited(,);"','select * from
FLT_ANP_AIRPLANE_FLAPS.csv')

SET IDENTITY_INSERT [FLEET].[dbo].[FLT_ANP_AIRPLANE_PROFILES] ON

Insert Into [FLEET].[dbo].[FLT_ANP_AIRPLANE_PROFILES] ([ACFT_ID]
      ,[OP_TYPE],[PROF_ID1],[PROF_ID2],[PROFILE_ID],[WEIGHT])
select [ACFT_ID],[OP_TYPE],[PROF_ID1],[PROF_ID2],[PROFILE_ID]
      ,[WEIGHT] from OpenRowset('MSDASQL', 'Driver={Microsoft Access Text
Driver (*.txt, *.csv)}; DefaultDir=D:\TASOpt\AEDT_Aircraft\CSV\;Extended
properties="ColNameHeader=True;Format=Delimited(,);"','select * from
FLT_ANP_AIRPLANE_PROFILES.csv')

SET IDENTITY_INSERT [FLEET].[dbo].[FLT_ANP_AIRPLANE_PROFILES] OFF

Insert Into [FLEET].[dbo].[FLT_ANP_AIRPLANE_PROCEDURES]

select * from OpenRowset('MSDASQL', 'Driver={Microsoft Access Text Driver
(*.txt, *.csv)}; DefaultDir=D:\TASOpt\AEDT_Aircraft\CSV\;Extended
properties="ColNameHeader=True;Format=Delimited(,);"','select * from
FLT_ANP_AIRPLANE_PROCEDURES.csv')

Insert Into [FLEET].[dbo].[FLT_ANP_AIRPLANE_PROCEDURES_EXT]

select * from OpenRowset('MSDASQL', 'Driver={Microsoft Access Text Driver
(*.txt, *.csv)}; DefaultDir=D:\TASOpt\AEDT_Aircraft\CSV\;Extended
properties="ColNameHeader=True;Format=Delimited(,);"','select * from
FLT_ANP_AIRPLANE_PROCEDURES.csv')
```

```
%%%%% NOT USED BY 737700 AIRCRAFT %%%%%

Insert Into [FLEET].[dbo].[FLT_ANP_AIRPLANE_PROFILE_POINTS]
select * from OpenRowset('MSDASQL', 'Driver={Microsoft Access Text Driver
(*.txt, *.csv)}; DefaultDir=D:\TASOpt\AEDT_Aircraft\CSV\;Extended
properties="ColNameHeader=True;Format=Delimited(,);"','select * from
FLT_ANP_AIRPLANE_PROFILE_POINTS.csv')
Insert Into [FLEET].[dbo].[FLT_ANP_AIRPLANE_PROFILE_POINTS_EXT]
select * from OpenRowset('MSDASQL', 'Driver={Microsoft Access Text Driver
(*.txt, *.csv)}; DefaultDir=D:\TASOpt\AEDT_Aircraft\CSV\;Extended
properties="ColNameHeader=True;Format=Delimited(,);"','select * from
FLT_ANP_AIRPLANE_PROFILE_POINTS.csv')

%%%%% NOT USED BY 737700 AIRCRAFT %%%%%

Insert Into [FLEET].[dbo].[FLT_ANP_AIRPLANE_THRUST_JET]

select * from OpenRowset('MSDASQL', 'Driver={Microsoft Access Text Driver
(*.txt, *.csv)}; DefaultDir=D:\TASOpt\AEDT_Aircraft\CSV\;Extended
properties="ColNameHeader=True;Format=Delimited(,);"','select * from
FLT_ANP_AIRPLANE_THRUST_JET.csv')

Insert Into [FLEET].[dbo].[FLT_ANP_AIRPLANE_TSFC_COEFFICIENTS]

select * from OpenRowset('MSDASQL', 'Driver={Microsoft Access Text Driver
(*.txt, *.csv)}; DefaultDir=D:\TASOpt\AEDT_Aircraft\CSV\;Extended
properties="ColNameHeader=True;Format=Delimited(,);"','select * from
FLT_ANP_AIRPLANE_TSFC_COEFFICIENTS.csv')

Insert Into [FLEET].[dbo].[FLT_ACTYPE_CARRIER]

select * from OpenRowset('MSDASQL', 'Driver={Microsoft Access Text Driver
(*.txt, *.csv)}; DefaultDir=D:\TASOpt\AEDT_Aircraft\CSV\;Extended
properties="ColNameHeader=True;Format=Delimited(,);"','select * from
FLT_ACTYPE_CARRIER.csv')

Insert Into [FLEET].[dbo].[FLT_REF_ANP_EQUIPMENT_DEFAULT]

select * from OpenRowset('MSDASQL', 'Driver={Microsoft Access Text Driver
(*.txt, *.csv)}; DefaultDir=D:\TASOpt\AEDT_Aircraft\CSV\;Extended
properties="ColNameHeader=True;Format=Delimited(,);"','select * from
FLT_REF_ANP_EQUIPMENT_DEFAULT.csv')

Insert Into [FLEET].[dbo].[FLT_ANP_BADA_ENERGYSHARE]

select * from OpenRowset('MSDASQL', 'Driver={Microsoft Access Text Driver
(*.txt, *.csv)}; DefaultDir=D:\TASOpt\AEDT_Aircraft\CSV\;Extended
properties="ColNameHeader=True;Format=Delimited(,);"','select * from
FLT_ANP_BADA_ENERGYSHARE.csv')
```

Appendix D

SQL Script to Duplicate Operations

Duplicate [AIR_OPERATION_AIRCRAFT]

```
SET IDENTITY_INSERT [TEST].[dbo].[AIR_OPERATION_AIRCRAFT] ON

INSERT INTO [TEST].[dbo].[AIR_OPERATION_AIRCRAFT] ([AIRCRAFT_ID]
,[NAME],[EQUIPMENT_ID],[AIRCRAFT_SOURCE],[DESCRIPTION])
VALUES (2,'MIT1',5001,0,'MIT1')

INSERT INTO [TEST].[dbo].[AIR_OPERATION_AIRCRAFT] ([AIRCRAFT_ID]
,[NAME],[EQUIPMENT_ID],[AIRCRAFT_SOURCE],[DESCRIPTION])
VALUES (3,'MIT2',5002,0,'MIT2')

.
.
.

INSERT INTO [TEST].[dbo].[AIR_OPERATION_AIRCRAFT] ([AIRCRAFT_ID]
,[NAME],[EQUIPMENT_ID],[AIRCRAFT_SOURCE],[DESCRIPTION])
VALUES (1000,'MIT999',5999,0,'MIT999')

SET IDENTITY_INSERT [TEST].[dbo].[AIR_OPERATION_AIRCRAFT] OFF
```

Duplicate [AIR_OPERATION]

```
INSERT INTO [TEST].[dbo].[AIR_OPERATION]
([AIRCRAFT_ID],[CASE_ID],[USER_ID],[OPERATION_TYPE],[OP_COUNT],[OPERATION_
TIME],[DEPARTURE_AIRPORT_LAYOUT_ID],[DEPARTURE_RUNWAY_END_ID],[ARRIVAL_AIR
PORT_LAYOUT_ID],[ARRIVAL_RUNWAY_END_ID],[SENSOR_PATH_ID])
SELECT
2,[CASE_ID],[USER_ID],[OPERATION_TYPE],[OP_COUNT],[OPERATION_TIME],[DEPART
URE_AIRPORT_LAYOUT_ID],[DEPARTURE_RUNWAY_END_ID],[ARRIVAL_AIRPORT_LAYOUT_I
D],[ARRIVAL_RUNWAY_END_ID],[SENSOR_PATH_ID] from
[TEST].[dbo].[AIR_OPERATION] WHERE [AIRCRAFT_ID] = 1

INSERT INTO [TEST].[dbo].[AIR_OPERATION]
([AIRCRAFT_ID],[CASE_ID],[USER_ID],[OPERATION_TYPE],[OP_COUNT],[OPERATION_
TIME],[DEPARTURE_AIRPORT_LAYOUT_ID],[DEPARTURE_RUNWAY_END_ID],[ARRIVAL_AIR
PORT_LAYOUT_ID],[ARRIVAL_RUNWAY_END_ID],[SENSOR_PATH_ID])
SELECT
3,[CASE_ID],[USER_ID],[OPERATION_TYPE],[OP_COUNT],[OPERATION_TIME],[DEPART
URE_AIRPORT_LAYOUT_ID],[DEPARTURE_RUNWAY_END_ID],[ARRIVAL_AIRPORT_LAYOUT_I
D],[ARRIVAL_RUNWAY_END_ID],[SENSOR_PATH_ID] from
[TEST].[dbo].[AIR_OPERATION] WHERE [AIRCRAFT_ID] = 1

.
.
.

INSERT INTO [TEST].[dbo].[AIR_OPERATION]
([AIRCRAFT_ID],[CASE_ID],[USER_ID],[OPERATION_TYPE],[OP_COUNT],[OPERATION_
TIME],[DEPARTURE_AIRPORT_LAYOUT_ID],[DEPARTURE_RUNWAY_END_ID],[ARRIVAL_AIR
PORT_LAYOUT_ID],[ARRIVAL_RUNWAY_END_ID],[SENSOR_PATH_ID]) SELECT
1000,[CASE_ID],[USER_ID],[OPERATION_TYPE],[OP_COUNT],[OPERATION_TIME],[DEP
ARTURE_AIRPORT_LAYOUT_ID],[DEPARTURE_RUNWAY_END_ID],[ARRIVAL_AIRPORT_LAYOU
T_ID],[ARRIVAL_RUNWAY_END_ID],[SENSOR_PATH_ID] from
[TEST].[dbo].[AIR_OPERATION] WHERE [AIRCRAFT_ID] = 1
```